



Ricerca di Sistema elettrico

# Assessment of PWR cores behavior and estimate of confidence level got with the use of mechanistic and/or integral codes calculations of accident sequences with reference to TMI-2 reactor

G. Bandini, S. Ederli, M. Di Giuli, M. Sumini, A. Manfredini,  
W. Ambrosini



ASSESSMENT OF PWR CORES BEHAVIOR AND ESTIMATE OF CONFIDENCE LEVEL GOT WITH THE USE OF  
MECHANISTIC AND/OR INTEGRAL CODES CALCULATIONS OF ACCIDENT SEQUENCES WITH REFERENCE TO  
TMI-2 REACTOR

G. Bandini, S. Ederli - ENEA, M. Di Giuli, M. Sumini - CIRTEN: CERSEUNIBO, A. Manfredini, W. Ambrosini  
CIRTEN: CERSE-UNUPI

Settembre 2015

Report Ricerca di Sistema Elettrico

Accordo di Programma Ministero dello Sviluppo Economico - ENEA

Piano Annuale di Realizzazione 2014

Area: Produzione di energia elettrica e protezione dell'ambiente

Progetto: Sviluppo competenze scientifiche nel campo della sicurezza nucleare e collaborazione ai programmi internazionali per il nucleare di IV Generazione

Linea: Sviluppo competenze scientifiche nel campo della sicurezza nucleare

Obiettivo: Valutazione degli incidenti e delle loro conseguenze

Responsabile del Progetto: Felice De Rosa, ENEA

Il presente documento descrive le attività di ricerca svolte all'interno dell'Accordo di collaborazione Sviluppo competenze scientifiche nel campo della sicurezza nucleare e collaborazione ai programmi internazionali per il nucleare di IV Generazione

Responsabile scientifico ENEA: Felice De Rosa

Responsabile scientifico CIRTEN: Giuseppe Forasassi

**Titolo**

**Assessment of PWR cores behavior and estimate of confidence level got with the use of mechanistic and / or integral codes calculations of accident sequences with reference to TMI-2 reactor**

**Descrittori**

**Tipologia del documento:** Rapporto Tecnico

**Collocazione contrattuale:** Accordo di programma ENEA-MSE: Piano Annuale di Realizzazione 2014, Linea Progettuale 1, Obiettivo B: Analisi Incidentale e Valutazioni di Sicurezza per Reattori BWR e PWR di Centrali Prossime ai Confini Nazionali, Task B1.2

**Argomenti trattati:** Sicurezza Nucleare

**Sommario**

This report presents the activity performed in the frame of LP1, Objective B (Valutazione del comportamento di noccioli PWR e del livello di confidenza dei risultati ottenuti con l'uso di codici meccanicistici e/o integrali mediante il calcolo di sequenze incidentali in reattori PWR con riferimento al reattore della centrale di TMI-2), Task B1.2 of PAR2014, ADP ENEA-MSE. In this study the integral codes ASTEC and MELCOR have been applied for the calculation of a reference severe accident sequence (SBLOCA) and some core reflooding scenarios on the TMI-2 plant (PWR of 900 MWe). Similar core degradation parameters/criteria have been used with the two codes to try to reduce the differences observed in previous analyses (PAR2013). Furthermore, sensitivity studies on important and uncertain core degradation parameters/criteria have been performed to investigate their influence on code results. Core reflooding scenarios starting from different core degradation conditions have highlighted the ability of emergency core cooling systems to stop the core degradation and prevent vessel failure in the late phase of a severe accident.

**Note:**

This document has been prepared by the following main contributors:

- G. Bandini, S. Ederli (ENEA)
- M. Di Giuli, M. Sumini (CIRTEN - Università di Bologna) <sup>(1)</sup>
- A. Manfredini, W. Ambrosini (CIRTEN - Università di Pisa) <sup>(1)</sup>


<sup>(1)</sup> Ref. doc. CERSE-UNIBO-UNIFI RL 1360 / 2015



2			NOME			
			FIRMA			
1			NOME			
			FIRMA			
0	EMISSIONE	18/09/15	NOME	G. Bandini	F. De Rosa	F. De Rosa
			FIRMA			
REV.	DESCRIZIONE	DATA	REDAZIONE	CONVALIDA	APPROVAZIONE	

## List of Contents

<b>1.</b>	<b>Introduction .....</b>	<b>4</b>
<b>2.</b>	<b>Accident scenario and plant data .....</b>	<b>7</b>
2.1	SBLOCA accident scenario .....	7
2.2	Boundary conditions .....	7
2.2.1	<i>Power</i> .....	7
2.2.2	<i>Steam generator pressure and level control</i> .....	9
2.2.3	<i>Hot leg break</i> .....	11
2.2.4	<i>Letdown/make-up flow and ECCS injections</i> .....	11
2.2.5	<i>Threshold set-point values</i> .....	11
2.3	TMI-2 plant data .....	11
2.3.1	<i>Free volumes</i> .....	11
2.3.2	<i>Heat transfer with secondary side</i> .....	12
2.3.3	<i>Intact core geometry</i> .....	12
2.3.4	<i>Vessel and internal structures</i> .....	12
2.3.5	<i>Vent valve operation</i> .....	12
2.4	Initial TMI-2 plant conditions .....	13
2.4.1	<i>Nominal TMI-2 steady-state</i> .....	13
2.4.2	<i>Primary coolant mass inventory</i> .....	13
2.5	Core reflooding scenarios .....	14
<b>3.</b>	<b>MELCOR calculations .....</b>	<b>16</b>
3.1	Brief description of the MELCOR code .....	16
3.2	Reference physical parameters of the code .....	17
3.3	Initial TMI-2 plant conditions .....	18
3.3.1	<i>Nominal TMI-2 steady-state</i> .....	18
3.3.2	<i>TMI-2 plant model</i> .....	19
3.3.3	<i>Primary mass inventory</i> .....	21
3.4	Parameters and results .....	22
3.4.1	<i>Reference case</i> .....	23
3.4.2	<i>Sensitivity case A</i> .....	35
3.4.3	<i>Sensitivity case B</i> .....	45
3.5	Final remarks .....	55
<b>4.</b>	<b>ASTEC calculations .....</b>	<b>57</b>
4.1	Brief description of the ASTEC code .....	57
4.2	TMI-2 reactor ASTEC model .....	58
4.3	Reference scenario and sensitivity analysis .....	61
4.3.1	<i>Calculation results</i> .....	62

 <b>Ricerca Sistema Elettrico</b>	<b>Sigla di identificazione</b>	<b>Rev.</b>	<b>Distrib.</b>	<b>Pag.</b>	<b>di</b>
	ADPFISS-LP1-054	0	L	3	106

4.4	Reflooding cases .....	70
4.4.1	<i>Calculation results</i> .....	72
4.5	Platform dependencies .....	81
4.6	Summary and conclusions .....	84
<b>5.</b>	<b>MELCOR and ASTEC result comparison .....</b>	<b>86</b>
5.1	TMI-2 steady-state conditions at nominal power .....	86
5.2	In-vessel core degradation parameters and modelling options .....	87
5.3	Chronology of main events .....	88
5.4	Evolution of main parameters .....	88
3.4.1	<i>Reference case without reflooding</i> .....	89
3.4.2	<i>Reflooding of a slightly degraded core</i> .....	95
3.4.3	<i>Reflooding of a highly degraded core</i> .....	100
<b>6.</b>	<b>Conclusions and recommendations .....</b>	<b>105</b>

## 1. Introduction

During a severe accident in a light water reactor, the core can melt and can be relocated to the lower plenum of the reactor pressure vessel (RPV). Due to the possible presence of water, the melt can form a particle debris bed (in-vessel scenario). An insufficient heat removal of decay heat in the debris bed may lead to a re-melting of the debris and to a failure of the RPV. On the other hand a reflooding (due to the intervention of safety systems) of hot (temperatures above 1500 K), but relatively intact, fuel rods may result in a sharp increase of temperature of the fuel rods and surrounding core regions, large production of hydrogen and steam, enhanced fission product release and core material melting. This sounds counterintuitive, but the increase of temperature is caused by the oxidation of the regions of the core that have not yet been quenched but are exposed to large quantities of hot steam produced by the quenching process.

Although this is still an area of active research, a large number of reflooding experimental data, as well as data from TMI-2, has demonstrated these characteristic trends. Nowadays, computer codes are essential tools for understanding how the reactor might respond under severe accident conditions. The codes are used as a tool to support engineering judgement, based on which specific measures to mitigate the effects of severe accidents are designed. They are also used to determine accident management strategies and for probabilistic safety assessment. It is very important to use these sophisticated tools in accordance with certain rules derived from knowledge accumulated worldwide. In the case of numerical simulation of severe accidents, generally is adopted a two-tier approach: integral codes or code systems that simulate the entire accident rapidly, from the initiating event to the possible release of radionuclides outside the containment and taking into account the main safety systems; detailed or mechanistic codes that provide a finer simulation of the phenomena involved a finer simulation of single phenomenon or group of phenomena (core degradation or FP release).

The integral codes are primarily not designed to perform best estimate simulations; the objective is rather to allow the user to bound important processes or phenomena by numerous user-defined parameters in a fast running manner. The fast running codes may contain best estimate models for some phenomena, but not necessarily for all of the relevant phenomena. It is, therefore, difficult to use them for a best estimate analysis because of large uncertainties in some of the models. After all, a completely conservative approach cannot be applied in the analysis of a severe accident because a conservative assumption for one parameter may lead to a non-conservative response for another parameter. For example, a low failure temperature (i.e. temperature for the onset of relocation of molten material) is conservative with respect to the time of vessel failure but not with respect to hydrogen production. On contrary, the aim of detailed or mechanistic codes is to represent the plant behavior as realistically as possible according to state of the art knowledge. It is important to point out that for the early phase of a severe accident up to the formation of large amounts of molten fuel in the core, the experimental database is sufficiently large, an understanding of the phenomena is good and




the models are adequately detailed and validated. For the late in-vessel phase of a severe accident, the experimental database is still poor (particularly with respect to the scale), the models have more modelling parameters, are less general and not well validated.

Since the Three Mile Island Unit 2 (TMI-2) reactor accident in 1979, there have been extensive research activities to try to understand the phenomena involved, and to develop accident management strategies to mitigate the consequences of core melt accidents. Given that a severe accident cannot be simulated at or near full scale, since all the experimental database on core heat up, melt progression and fission product release is limited to the results of small-scale experiments, which are only partially representative of what could occur in a real reactor. Therefore, integral codes are used to describe core degradation transients in nuclear reactors without a clear idea of their predictive capabilities. This is the reason why TMI-2 provides a unique opportunity to assess the capability of integral codes to simulate a severe accident in a full scale Pressurizer Water Reactor (PWR).

The TMI-2 reactor modeling used in computer codes for severe accidents as MELCOR, ASTEC, MAAP 4 and ATHLET-CD has improved significantly over the years due to better understanding, and the simulation results confirm these continuous improvements. In the frame of the current ADP LP1 Task B1.2 program, the activity of ENEA in collaboration with CIRTEN, is devoted to verify the progress and reliability of ASTEC and MELCOR codes through the result comparison for a representative severe accident sequence in a pressurized nuclear power plant of 900 MWe.

The comparison of MELCOR and ASTEC results for the SBLOCA scenario calculated in Ref. [1.1] has shown significant differences mainly regarding the core melt progression in the late transient phase. These differences may come from different core degradation parameters/criteria used by the two codes. In order to try to understand the reason of these differences some sensitivity analysis have been performed, and in an attempt to reduce them the same SBLOCA scenario has been calculated starting with the same core degradation parameters/criteria implemented in the two code calculations. Furthermore, starting from the new reference calculation without safety injection, two core reflooding scenarios have been calculated to investigate the impact of severe accident management measures that implement the delayed availability of emergency core cooling systems to stop the core degradation and the propagation of the severe accident.

In Section 2 of this report, the reference specifications for both code calculations are defined regarding: the SBLOCA accident scenario, the boundary conditions, the TMI-2 plant data, the steady-state conditions of the TMI-2 plant at transient initiation, and the specifications for the reflooding scenarios to be investigated. In Section 3, the results of the MELCOR calculation performed by the University of Pisa are presented in details, along with a short description of the code models used in the analysis to best represent the in-vessel core degradation phase. Similarly, in Section 4, the results of the ASTEC calculations performed by the University of Bologna and the code models used are presented in detail. In Section 5,


 <b>Ricerca Sistema Elettrico</b>	<b>Sigla di identificazione</b>	<b>Rev.</b>	<b>Distrib.</b>	<b>Pag.</b>	<b>di</b>
	ADPFISS-LP1-054	0	L	6	106

the main code results are compared and the main differences tentatively explained. Finally, main conclusions and recommendations are drawn in Section 6.

## References

- 1.1. G. Bandini, M. Di Giuli, M. Sumini, A. Manfredini, W. Ambrosini – Lessons Learned from the Result Comparison of a Reference Severe Accident Sequence on a TMI2-like Reactor of 900 MWe Power with the Integral Codes ASTEC and MELCOR – ENEA - ADPFISS - LP1 – 032 – Settembre 2014.



 <b>Ricerca Sistema Elettrico</b>	<b>Sigla di identificazione</b>	<b>Rev.</b>	<b>Distrib.</b>	<b>Pag.</b>	<b>di</b>
	ADPFISS-LP1-054	0	L	7	106

## 2. Accident scenario and plant data

### 2.1 SBLOCA accident scenario

The initial event is a small break (size = 0.0015 m<sup>2</sup>) in the hot leg A at  $t = 0$  s, with simultaneous loss of main feedwater on the secondary side of steam generators (SGs). The primary pressure begins to reduce along with the pressurizer level as soon as the break opens. After few seconds, the fast SG dryout with consequent loss of heat removal from the primary side results in sudden primary pressure increase. The opening of the pressurizer PORV is not enough to limit the pressure rise and, therefore, reactor scram occurs when the pressurizer pressure set-point of 16.3 MPa is reached. The further primary pressure increase after reactor scram might be attenuated by the pressurizer safety valve operation (valve pressure set-point at 17.0 MPa).

The auxiliary feedwater starts at  $t = 100$  s trying to restore 1 m water level in the SG secondary side. The primary pump stop occurs when the whole primary water mass (liquid + steam) inventory reduces below 85000 kg.

Then the accidental transient is let free to evolve towards core uncover and heatup, core melting and corium relocation in the lower plenum, until possible lower head vessel failure. In the reference accident scenario, no HPI or LPI injection are actuated during the transient phase. In this case, the transient calculation should be pursued until vessel failure using code model options and parameter values recommended by code Best Practice Guidelines. Conversely, HPI injection is taken into account in the calculation of core reflooding scenarios as specified in section 2.5.

### 2.2 Boundary conditions

The SBLOCA scenario is specified with very simple and well defined boundary conditions, in order to minimize the influence of uncertainty of these conditions on the variability of code results.

#### 2.2.1 Power

- Initial core power = 2772 MW.
- Thermal heat losses from primary system to containment atmosphere are not taken into account.
- Core residual power after reactor scram is given in Table 2.1 below.

Table 2.1: Core power evolution

Time (s)	Power (W)
0	2772.00e6
ts (scram time)	2772.00e6
ts + 1	167.94e6
ts + 4	147.96e6
ts + 10	130.14e6
ts + 40	103.14e6
ts + 100	86.13e6
ts + 400	65.34e6
ts + 800	52.92e6
ts + 1000	49.95e6
ts + 2000	42.39e6
ts + 4000	34.56e6
ts + 8000	28.35e6
ts + 10000	26.05e6
ts + 20000	21.46e6

- Radial core power profile (6 rings) is given in Table 2.2 below (according to the radial discretization and number of fuel rods defined in the ASTEC simulation by ENEA in ATMI Benchmark [2.1]).

Table 2.2: Radial profile of core power

Ring	Factor	Number of fuel rods	External radius (m)
1	1.2572	1040	0.27
2	1.2127	3120	0.54
3	1.1469	5200	0.81
4	1.0596	7072	1.08
5	0.951	9152	1.35
6	0.8198	11232	1.665

- Axial profile of core power is given in Table 2.3 below (same axial power profile in different rings).

Table 2.3: Axial profile of core power

Z (m)	Factor
0	0
0.15	0
0.302	0.675
0.607	0.857
0.912	1.037
1.217	1.153
1.522	1.202
1.826	1.231
2.131	1.241
2.436	1.209
2.893	1.102
3.503	0.595
3.81	0
4	0

The radial and axial profiles in Table 2.2 and Table 2.3 are valid for intact core geometry. The change in power distribution following core degradation and fuel relocation must be taken into account by the respective code models.

### 2.2.2 *Steam generator pressure and level control*

Boundary conditions for the SG secondary side are given by controlling the steam generator pressure and water level (in the riser) as follows:

- SG pressure at steady-state value in the first 100 s ( $P = 6.41$  MPa), then pressure rise up to 7.0 MPa in 100 s and constant value until the end of the transient, as shown in Figure 2.1.
- SG level reduces quickly down to 0 due to heat transfer from primary side (timing of SG dryout is calculated by the code), then linear increase from  $t = 100$  s, by startup of auxiliary feedwater, reaching the 1 m value at 200 s, and then constant until the end of the transient, as shown in Figure 2.2, by auxiliary feedwater flow rate control.

Regarding the feedwater control, we assume:

- Maximum feedwater flow rate = 50 kg/s per SG.
- Feedwater temperature = 295.15 K.

The linear increase of SG level up to 1 m, starting at 100 s by auxiliary feedwater injection, might be delayed because of strong evaporation inside the SG and due to the limit on maximum feedwater flow rate.

Also based on the experience of the ATMI Benchmark, it seems important to note that the SG pressure and level might deviate from the boundary values, when SG power removal reduces down close to 0, due to stop of natural circulation in the primary loops, after the initial boil-off phase. By this time, steam condensation in the secondary side of SG leads to slow progressive decrease of the SG pressure below 7.0 MPa and, at the same time, leads to slow progressive increase of the SG level above 1 m. In any case, and in particular in this situation, the pressure cannot be controlled by steam ingress into the SG dome, so as the level cannot be controlled by water draining from the SG bottom.

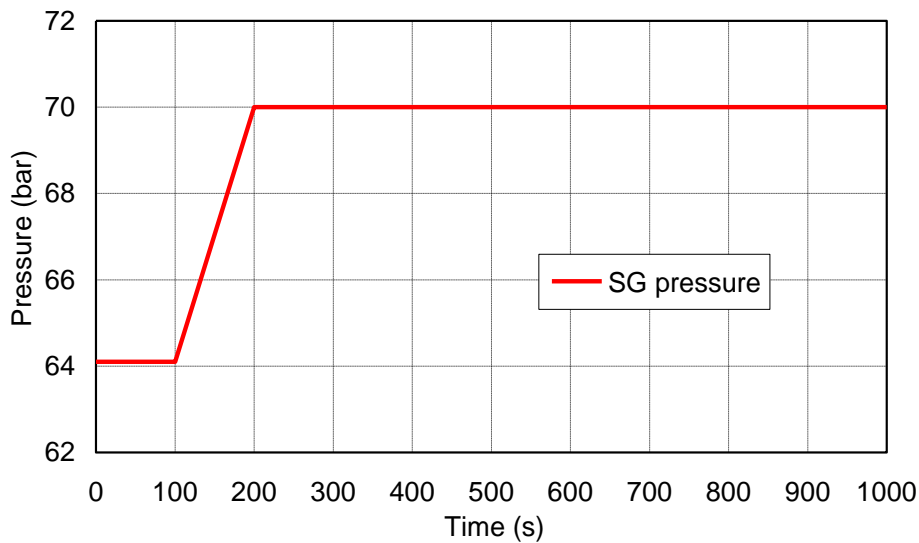


Figure 2.1: SG pressure control

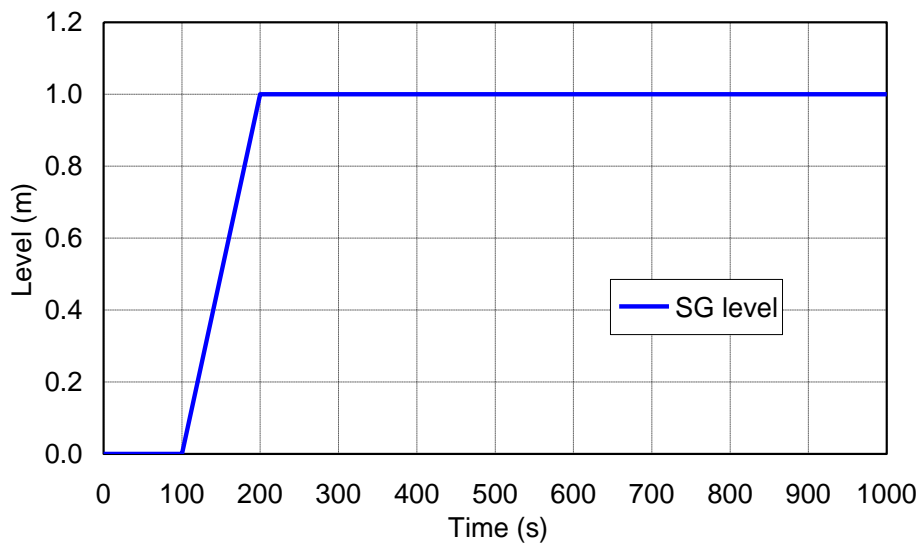



Figure 2.2: SG level control

 <b>Ricerca Sistema Elettrico</b>	<b>Sigla di identificazione</b>	<b>Rev.</b>	<b>Distrib.</b>	<b>Pag.</b>	<b>di</b>
	ADPFISS-LP1-054	0	L	11	106

### 2.2.3 Hot leg break

- Break size = 0.0015 m<sup>2</sup>
- Break position = 4 m along the hot leg of loop A, from vessel outlet nozzle
- Containment pressure = 0.1 MPa (pressurization of the containment atmosphere is not taken into account)
- No stratification in the hot leg during the boil-off phase before primary pump stop, which may significantly affect the break mass flow rate value.

### 2.2.4 Letdown/make-up flow and ECCS injections

- Letdown flow rate = 0
- Make-up flow rate = constant value of 2 kg/s during the all transient in cold leg 2B (water temperature = 315.15 K)
- No HPI injection
- No LPI injection

### 2.2.5 Threshold set-point values

- Pressurizer PORV opening → Pressurizer pressure > 15.56 MPa
- Pressurizer PORV closure → Pressurizer pressure < 14.96 MPa
- Reactor scram → Pressurizer pressure > 16.30 MPa
- Pressurizer safety valve set-point → 17.0 MPa (valve capacity = 86.9 kg/s)
- Primary pump stop → Primary mass (liquid + steam) < 85000 kg


## 2.3 TMI-2 plant data

General plant geometry is defined according to the Final Report of the OECD/ATMI Benchmark [2.1]. Plant data concerning free volumes of the primary system have been updated according to the Final Specifications of MSLB Benchmark Report [2.2]. Other details on the overall TMI-2 plant layout can be found in Ref. [2.2] if needed.

The radial and axial core discretization is left free to the code user, but the power distribution in the core must be consistent with the radial and axial power profiles given in Section 2.2.1.

### 2.3.1 Free volumes

- Primary system volume without the pressurizer = 288.29 m<sup>3</sup>
- Pressurizer volume = 42.5 m<sup>3</sup>
- Reactor pressure volume = 113.6 m<sup>3</sup>
- Secondary side free volume of one SG (up to the SG exit) = 34.4 m<sup>3</sup>

 <b>Ricerca Sistema Elettrico</b>	<b>Sigla di identificazione</b>	<b>Rev.</b>	<b>Distrib.</b>	<b>Pag.</b>	<b>di</b>
	ADPFISS-LP1-054	0	L	12	106

### 2.3.2 *Heat transfer with secondary side*

- SG tubes surface per SG (secondary side) = 12302.5 m<sup>2</sup>
- Number of tubes per SG = 15530

### 2.3.3 *Intact Core Geometry*

#### Main characteristics of the core

- Number of fuel bundles of type 15x15 = 177
- Active core length = 3.66 m
- Total core length = 4.0 m (from core bottom: 0.15 m + 3.66 m (active length) + 0.19 m)
- Type of fuel lattice = square, pitch = 0.01443 m
- Number of fuel rods per assembly = 208
- External diameter of fuel rod = 0.0109 m
- Fuel pellet radius = 0.0047 m
- Fuel rod cladding thickness = 0.000673 m

#### Initial core material inventory

- UO<sub>2</sub> mass = 93650 kg (over the 3.66 m of core active length)
- Zircaloy mass = 23050 kg
- H<sub>2</sub> total mass if converted from total zircaloy = 1011 kg (Zircaloy mass / 22.8)
- AIC mass (Ag + In + Cd) = 2750 kg

### 2.3.4 *Vessel and internal structures*

- Core baffle internal diameter = 3.28 m
- Core baffle external diameter = 3.33 m
- Core barrel internal diameter = 3.584 m
- Core barrel external diameter = 3.683 m
- Thermal shield internal diameter = 3.683 m
- Thermal shield external diameter = 3.753 m
- Vessel wall internal diameter = 4.36 m
- Vessel wall external diameter = 4.86 m

### 2.3.5 *Vent valve operation*

These valves, between the upper plenum and the top of the downcomer, are designed to avoid a direct loss of water by the hot leg. They should be modeled, as they were shown to have an influence on the transient. Simplified simulation of these valves is defined as follows:

- If  $\Delta P < 414$  Pa, the valves are closed.

- If  $\Delta P > 1724$  Pa, the valves are fully open, which corresponds to a total section of  $0.794 \text{ m}^2$ .
- If  $414 \text{ Pa} < \Delta P < 1724$  Pa, the valves are considered partly open, with a cross section area increasing linearly with  $\Delta P$ .

## 2.4 Initial TMI-2 plant conditions

### 2.4.1 Nominal TMI-2 steady-state

The nominal steady-state of the TMI-2 plant is the one defined in the “Pressurizer Water Reactor Main Steam Line Break (MSLB) Benchmark” Final Specifications [2.2]. The nominal values of the main TMI-2 plant parameters for both primary and secondary systems are listed in Table 2.4.

Table 2.4: Nominal TMI-2 steady-state conditions at transient initiation

Parameter	Unit	TMI-2 steady-state
Reactor core power	MW	2772
Pressurizer pressure (dome)	MPa	14.96
Temperature hot leg A & B	K	591.15
Temperature cold leg A & B	K	564.15
Mass flow rate loop A & B	kg/s	8800
Pressurizer collapsed level	m	5.588
Pressurizer water mass	kg	13710
Total primary mass	kg	222808 (**)
Steam pressure SG A & B (outlet nozzle)	MPa	6.41
Steam temperature SG A & B	K	572.15
Riser collapsed level SG A & B	m	3.28 – 4.03 (*)
Downcomer collapsed level SG A & B	m	5.1 – 5.6 (*)
Liquid mass SG A & B	kg	13140 – 19210 (*)
Feedwater flow rate SG A & B	kg/s	761.1
Feedwater Temperature SG A & B	K	511.15

(\*) Range of values used by participants in the ATMI Benchmark

(\*\*) According to primary volumes in Table 2.5

### 2.4.2 Primary coolant mass inventory

The coolant mass inventory in the primary system has been evaluated according to the primary component volumes defined in Ref. [2.2]. The calculation of the primary mass inventory is illustrated in Table 2.5 below.



Table 2.5: Coolant mass inventory in the primary system

Component	Vol. (m <sup>3</sup> )	N°	Tot. vol. (m <sup>3</sup> )	Temp. (K)	Density (kg/m <sup>3</sup> )	Mass (kg)
Pressurizer water volume	22.7	1	22.7	615.1	604.0	13710
Pressurizer steam volume	19.8	1	19.8	615.1	96.1	1903
Surge line	0.566	1	0.566	603.15 (*)	649.3	368
Cold leg (each)	6.73	4	26.92	564.15	744.1	20030
Reactor coolant pump (each)	1.59	4	6.36	564.25	744.1	4732
Hot leg (each)	13.3	2	26.6	591.15	684.6	18209
Reactor vessel water volume: - Lower plenum = 8.27 m <sup>3</sup> - Core = 20.4 m <sup>3</sup> - Downcomer = 34.69 m <sup>3</sup> - Upper plenum = 21.97 m <sup>3</sup> - Upper head = 14.4 m <sup>3</sup>	113.6	1	113.6	575.22 (*)	721.8	81992
SG primary side volume (each): - Upper plenum = 7.96 m <sup>3</sup> - Lower plenum = 7.84 m <sup>3</sup>	57.12	2	114.24	577.65 (*)	716.5	81858
Total			330.79			222808
Total without pressurizer			288.29			207189


(\*) Estimated average temperature values

## 2.5 Core reflooding scenarios

In order to evaluate the ability of emergency core cooling systems to stop the in-vessel core degradation during a severe accident and thus avoid the propagation of the accident through the vessel failure, two different reflooding scenarios have been calculated starting from different core degradation conditions.


The actuation of emergency core cooling system is simulated by starting the HPI injection at the constant flow rate of 30 kg/s of water (T = 40 °C) in the cold legs, which is equal to about 50% of full HPI capacity.

In the first reflooding scenario, the HPI injection is started at the beginning of the core degradation phase, from a slightly degraded core condition, when the core degraded mass is around five tons. In the second reflooding scenario, the HPI injection is started with a delay of 1000 s with respect to the initial scenario, from a highly degraded core condition, when the core degraded mass might amount to several tens of tons.

 <b>Ricerca Sistema Elettrico</b>	<b>Sigla di identificazione</b>	<b>Rev.</b>	<b>Distrib.</b>	<b>Pag.</b>	<b>di</b>
	ADPFISS-LP1-054	0	L	15	106

## References

- 2.1. F. Fichot, O. Marchand, G. Bandini, H. Austregesilo, M. Buck, M. Barnak, P. Matejovic, L. Humphries, K. Suh, S. Paci, “Ability of Current Advanced Codes to Predict Core Degradation, Melt Progression and Reflooding - Benchmark Exercise on an Alternative TMI-2 Accident Scenario”, NEA/CSNI/R(2009)3, July 2009.
- 2.2. K.N. Ivanov, T. M. Beam, A. J. Baratta, “Pressurised Water Reactor Main Steam Line Break (MSLB) Benchmark”, Volume 1: Final Specifications, NEA/NSC/DOC(99)8, April 1999.

 <b>Ricerca Sistema Elettrico</b>	<b>Sigla di identificazione</b>	<b>Rev.</b>	<b>Distrib.</b>	<b>Pag.</b>	<b>di</b>
	ADPFISS-LP1-054	0	L	16	106

### 3. MELCOR calculations

#### 3.1 Brief description of the MELCOR code

MELCOR is a fully integrated, engineering-level computer code able to model the progression of severe accidents in LWR nuclear power plants [3.1]. It is being developed at SNL for the U.S.N.R.C. as a second generation plant risk assessment tool and the successor to the Source Term Code Package. The spectrum of severe accident phenomena, including reactor coolant system and containment thermal-hydraulic response, core heat-up, degradation and relocation, and fission product release and transport, is treated in MELCOR in a unified framework for both BWR and PWR reactors. MELCOR has especially been designed to facilitate sensitivity and uncertainty analyses. The code has been under development since 1982 and the latest version is the 2.1, released in 2008.

Thermal-hydraulic behavior is modeled in MELCOR in terms of control volumes and flow paths. All hydrodynamic material (and its energy) resides in control volumes. Hydrodynamic material includes the coolant and non-condensable gases. These materials are assumed to separate under the influence of gravity within a control volume to form a pool beneath and an atmosphere above. Each control volume is characterized by a single pressure and two temperatures, one temperature for the pool and one for the atmosphere. The control volumes are connected by flow paths through which materials may move without residence time, driven by a momentum equation. Based on the elevations of the pool surfaces in the connected control volumes relative to the junctions with the flow paths, both pool and atmosphere may pass through each flow path. Appropriate hydrostatic head terms are included in the momentum equation for the flow paths, allowing calculation of natural circulation.

The MELCOR COR-package calculates the thermal response of the core and lower plenum structures, including the portion of the lower head directly beneath the core. In addition, the relocation of core materials during melting, slumping, and debris formation are modelled. Fuel pellets, cladding, grid spacers, canister walls, other core structures (e.g. control rods), and particulate debris are modelled separately with individual cells. Cells are the basic nodalization units in the COR-package. All the important heat transfer processes are modelled in each COR cell. Thermal radiation within a cell and between different cells in both axial and radial direction is accounted for, as well as radiation to boundary structures. Radiation to a liquid pool and to steam is also included. Radial conduction across the fuel cladding gap and axial conduction between cells is modelled. Convection to the control volume fluids is simulated for a wide range of fluid conditions and structure surface temperatures, including nucleate and film boiling. Oxidation of Zircaloy and steel is modelled for both the limiting cases of solid state diffusion of oxygen through the oxide layer and gaseous diffusion of steam or oxygen through the mixture. The core degradation model treats eutectic reactions, dissolution reactions, candling of molten core materials and the formation and relocation of particulate debris.

MELCOR calculates both the release and transport behavior of fission products and control rod materials. It tracks the masses of these materials by grouping them into classes. Each material class represents a group of one or more elements or compounds with similar physical properties. Each class has its own set of values of parameters, such as release coefficients and vapor pressure. Aerosols and vapors can deposit directly on surfaces such as heat structures and water pools. In addition, aerosols can agglomerate and settle.


### 3.2 Reference physical parameters of the code

Main core degradation physical parameters used in the reference calculation with MELCOR are summarized in the Table 3.1. The physical parameters used in the standard calculation of MELCOR in Ref. [3.2] where the default recommended values. In this reference calculation, the default values are modified according to the same values used in the ASTEC calculation.

Table 3.1: Main assumptions on main degradation models for the reference calculation

Parameter	MELCOR
Zircaloy oxidation kinetics	Urbanic-Heidrick
Cladding failure criteria ( <i>with molten material candling</i> )	ZrO <sub>2</sub> thickness < 100 μm and T <sub>clad</sub> > 2350 K or T <sub>clad</sub> > 2500 K
Melting point of UO <sub>2</sub> -ZrO <sub>2</sub> ceramic material	UO <sub>2</sub> T <sub>m</sub> = 2800 K ZrO <sub>2</sub> T <sub>m</sub> = 2800 K
Debris formation criteria	For other materials than fuel rods: thickness < 100 μm Fuel rod failure and debris formation when: T <sub>fuel</sub> > 2500 K
Molten core relocation into the lower plenum	After failure of grid-supported plate that can initially support fuel assemblies and particulate debris above it. Thus, everything resting on that ring of the plate will fall, but the plate will remain in place until it melts (1273 K). This event corresponds to failure of the plate portion with survival of the grid
Reactor pressure vessel failure	Failure of the lower head will occur if creep-rupture failure of a lower head segment occurs, in response to mechanical loading at elevated temperatures

For Zircaloy oxidation, the solid-state diffusion of oxygen through an oxide layer to unoxidized metal is represented by a parabolic rate equation, whose rate constant is evaluate using the Urbanic-Heidrick correlation. For very low oxidant concentrations, gaseous diffusion may limit the reaction rate, and a mass transfer coefficient is calculated via a heat-mass transfer analogy from the heat transfer correlations.

 <b>Ricerca Sistema Elettrico</b>	<b>Sigla di identificazione</b>	<b>Rev.</b>	<b>Distrib.</b>	<b>Pag.</b>	<b>di</b>
	ADPFISS-LP1-054	0	L	18	106

Candling, that is the downward flow of molten core materials and the subsequent refreezing of these materials as they transfer latent heat to cooler structures below, is addressed with a semi-mechanistic model, based on fundamental thermal/hydraulic principles. Relocation of core materials may result in a reduction of area and increase of flow resistance, or even total blocking of flow, within various parts of the core. A model is also implemented for an oxide shell to hold up molten material until the shell is breached. Molten material is held up within a component if the oxide thickness is greater than a critical value hold, if the component temperature is less than a critical value, and if no candling from the component in that cell has yet taken place.

MELCOR contains several simple models that consider the structural integrity and support of intact components, and convert them to particulate debris when either is lost. Most are logical models rather than structural models; no stress calculations are performed for any component other than supporting structure. All components other than fuel rods are immediately converted to particulate debris whenever the unoxidized metal thickness is reduced below a user defined minimum value. The thickness criterion is also used for cladding, which is assumed to support fuel pellets, but other criteria are also considered for fuel rods. Oxidized rods are assumed to retain their identity until they reaches 2500 K, after that they collapse unconditionally.

### **3.3 Initial TMI-2 plant conditions**

#### **3.3.1 Nominal TMI-2 steady-state**

The nominal steady-state of the TMI-2 plant is the one defined in the “Pressurizer Water Reactor Main Steam Line Break (MSLB) Benchmark” Final Specifications. The nominal values of the main TMI-2 plant parameters for both primary and secondary systems are listed in Table 3.2. The TMI2 initial conditions are obtained by a steady-state code run lasting 2000 s and starting from plant thermal-hydraulic parameter values close to the ones specified for TMI-2. During the steady-state calculation, some regulations in the primary and secondary sides are activated to facilitate the achievement of stable conditions.

The controlled parameters are:

- the pressurizer pressure by turning on the heaters when the pressure is lower than the nominal value;
- the pressurizer liquid mass, by water injection or draining, in order to obtain the precise liquid level;

These controls are deactivated during the last 600 s of the steady-state.

The TMI2 plant initial conditions calculated by the MELCOR code are compared with TMI-2 accident data at turbine trip in the table below. The primary circuit conditions are very well reproduced by the code, the larger mismatch being the mass core flowrate which resulted about 3% lower with respect to reference plant parameters.

Table 3.2: Nominal TMI-2 steady-state conditions at transient initiation

Parameter	Unit	TMI-2 steady-state	MELCOR
Reactor core power	MW	2772	2772
Pressurizer pressure (dome)	MPa	14.96	14.95
Temperature hot leg A & B	K	591.15	591.3
Temperature cold leg A & B	K	564.15	561.8
Mass flow rate loop A & B	kg/s	8800	8600
Pressurizer collapsed level	m	5.588	5.56
Pressurizer water mass	kg	13710	14200
Total primary mass	kg	222808	220300
Steam pressure SG A & B (outlet nozzle)	MPa	6.41	6.41
Steam temperature SG A & B	K	572.15	570.0
Riser collapsed level SG A & B	m	3.28 – 4.03	6.12
Downcomer collapsed level SG A & B	m	5.1 – 5.6	7.79
Liquid mass SG A & B	kg	13140 – 19210	25938
Feedwater flow rate SG A & B	kg/s	761.1	761.1
Feedwater Temperature SG A & B	K	511.15	511.15

### 3.3.2 TMI-2 plant model

The same nodalization used to simulate the first two phases of the TMI-2 accident has been used for these analyses, with proper boundary conditions. Moreover, minor changes were performed with respect to this benchmark, in order to reduce stratification in the primary side and improve heat transfer through steam generators.

The nodalization of the TMI-2 primary system for the MELCOR 1.8.6 code is presented in the Fig. 3.1. Both primary loops (A and B) have been modelled simulating each SGs and considering a single equivalent main pump and cold leg. The secondary system is modelled only up to the main feed and isolation valves, while the SGs were modelled with a high level of detail. The secondary side is connected to an imposed pressure control volume and to a “spill&feed” level control, which assure the desired imposed boundary conditions.

Particular care has also been devoted to core simulation (Fig. 3.2). The core schematization is constituted by five radial rings and twelve axial levels; four thermal-hydraulic levels are used in each ring of the core region, with three core cells axially in each thermal-hydraulic control volume. Radial and axial flow paths in the core region allow for the prediction of 2-D flow patterns. Heat structures representative of the control rod guide tubes and upper tie plate in the upper plenum have been added to the MELCOR model to permit condensation heat transfer and coolant recirculation inside the vessel. The input deck was developed using standard default MELCOR modeling parameters as far as possible, and allows for a complete description of an eventual severe progression of an accidental transient.

The VENT valves are also explicitly modeled between the cold and hot collectors. The plant geometry, the boundary conditions and the accident scenario have been strictly defined according to TMI-2 scenario benchmark specifications.

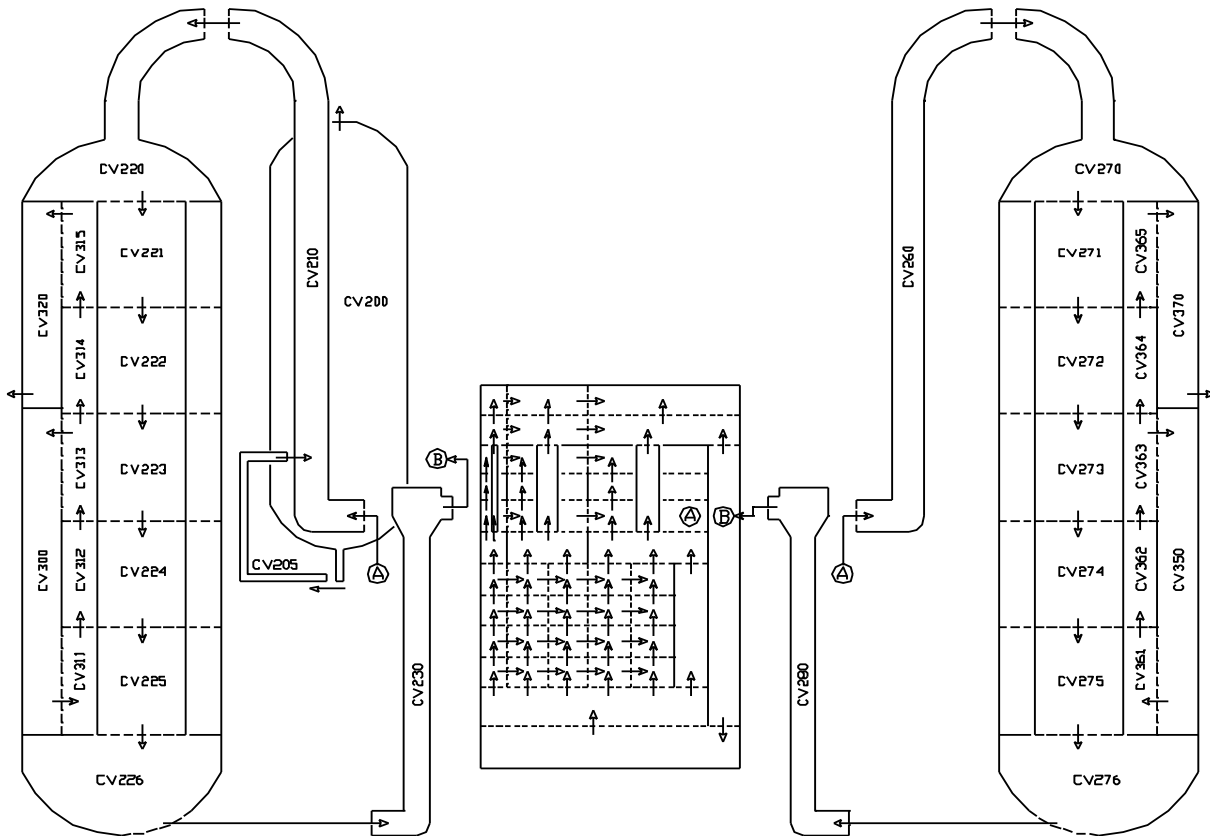


Figure 3.1: TMI-2 plant nodalization scheme



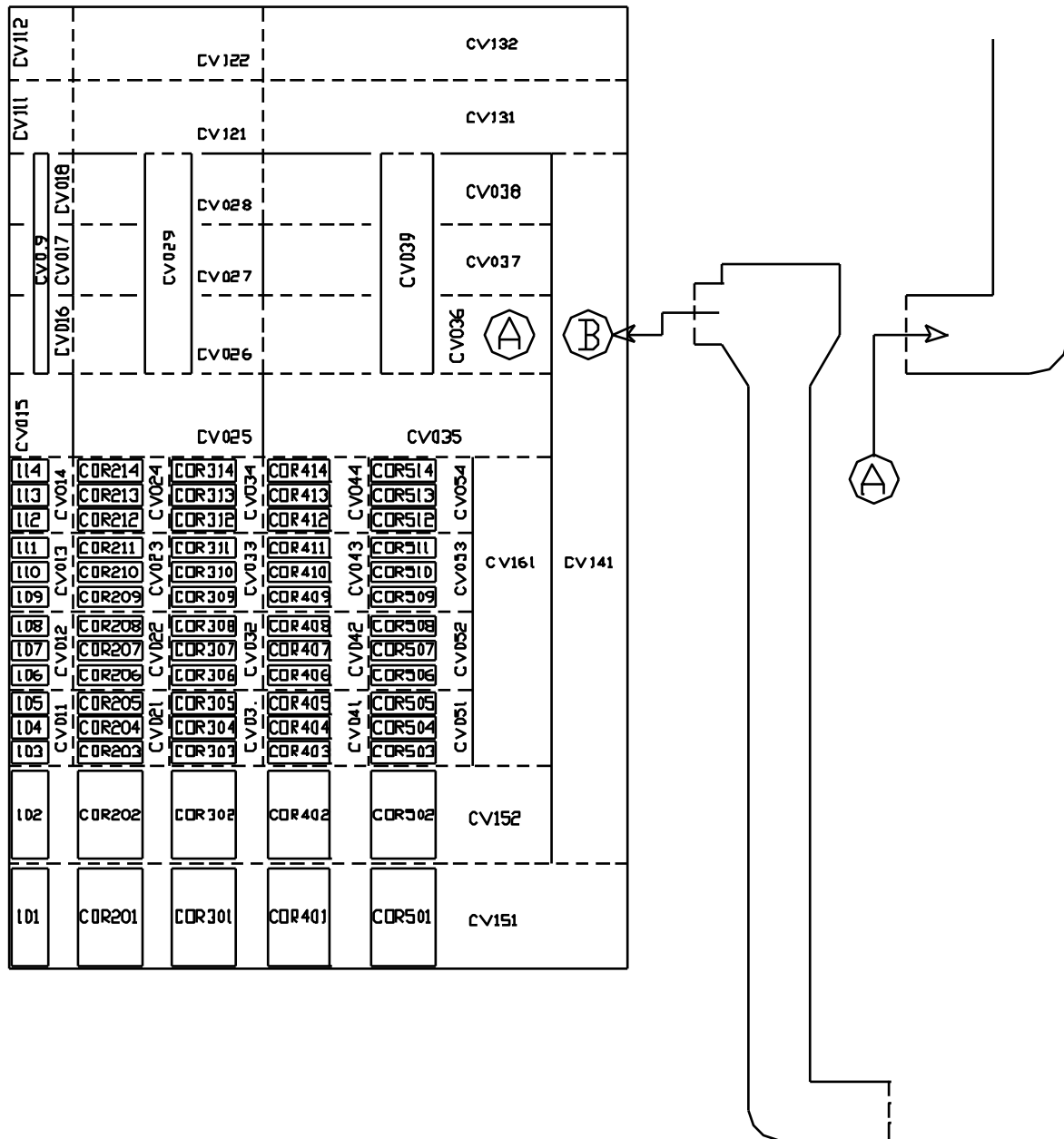


Figure 3.2: TMI-2 core simulation with MELCOR

### 3.3.3 Primary mass inventory

The coolant mass inventory in the primary system has been evaluated according to the primary component volumes defined in Ref. [3.3]. The calculation of the primary mass inventory is illustrated in Table 3.3.

Table 3.3: Coolant mass inventory in the primary system

Component	Vol. (m <sup>3</sup> )	MELCOR (m <sup>3</sup> )	Mass (kg)	MELCOR (kg)
Pressurizer water volume	22.7	22.7	13710	14347
Pressurizer steam volume	19.8	19.8	1903	1867
Surge line	0.566	0.9078	368	599
Cold leg	26.92	32.148	20030	24049
Reactor coolant pump	6.36		4732	
Hot leg	26.6	24.66	18209	16943
Reactor vessel water volume - Lower plenum = 16.23 m <sup>3</sup> - Core = 21.57 m <sup>3</sup> - Downcomer = 25.62 m <sup>3</sup> - Upper plenum = 30.16 m <sup>3</sup> - Upper head = 13.573 m <sup>3</sup>	113.6	107.16	81992	75746
SG primary side volume (each) - Upper plenum = 10.9 m <sup>3</sup> - Lower plenum = 10.9 m <sup>3</sup>	57.12	60.78	81858	86938
<b>Total</b>	<b>330.8</b>	<b>328.9</b>	<b>222808</b>	<b>220489</b>
<b>Total without pressurizer</b>		<b>281.6</b>	<b>207189</b>	<b>204275</b>

### 3.4 Parameters and results

The chronology of major events calculated by MELCOR is presented in Table 3.4 below and discussed in the following sections.

Table 3.4: Chronology of main events (code output)

Parameter	Time (s)
Break opening and total loss of main feedwater	0
Pressurizer PORV opens (P > 15.56 MPa)	14.00
Reactor scram (P > 16.30 MPa)	22.5
Pressurizer PORV closes (P < 14.96 MPa)	27.02
Full steam generator dryout	54.02
Startup of auxiliary feedwater	100.00
Pressurizer is empty	250.0
Stop of primary pumps (primary mass (liquid + steam) < 85000 kg)	2910

First fuel rod clad perforation/burst	(-)
First clad oxidation	4610
First clad melting and dislocation (also considering control rods)	5850
First molten material slumping in the lower plenum	5890
First ceramic melting and dislocation	6140
Vessel failure	13100

### 3.4.1 Reference case

Minor differences in the thermal-hydraulic behavior of the primary circuit were detected, with respect to the results obtained in the previous calculation of Ref. [3.2], due to a refinement of primary legs MELCOR model. This modification led to a much similar thermal hydraulic behavior, with respect to results obtained using the ASTEC code, during the earlier phase of the transient. This allowed obtaining a better agreement between MELCOR and ASTEC predictions up to the beginning of the core damage phase. As no injection of cooling fluid is considered during the Reference case, the calculation is stopped at vessel failure time.

Boundary conditions on the SGs secondary side (Figures 3.3 to 3.4) are maintained during the whole transient, by connecting each steam generator secondary side to a control volume with imposed pressure and using a “spill&feed” level control. So, changes in pressure and in liquid level due to steam evaporation/condensation which takes place during the transient are continuously corrected by injecting/spilling saturated steam and water from/to the two controlled source.

The initial feedwater trip and the consequent heat removal through the two steam generators causes the primary pressure to rapidly reach the opening PORV set-point and after about 22 s the SCRAM is actuated. The primary pressure (Fig. 3.5) rapidly approaches saturation as a consequence of the break on the hot leg and remains almost constant at a value of 7.6 MPa up to the trip of the pumps which takes place after 2910 s. Almost at the same time, the break uncovers and pressure starts increasing due to reduced removed power through the steam generators and the break. After 10 minutes the pressure decreases again, due to the beginning of core uncover, reaching a minimum value of about 6.8 MPa. Finally, primary pressure increases due to lower plate failure followed by a strong interaction of corium with water remained in the lower plenum and finally decreases up to the time of vessel failure.

Formation of void fraction is predicted in the primary system (Fig. 3.6) reaching almost 50% when the main pumps trip, due to the low primary mass. Heat transfer through the two steam generators (Fig. 3.7) is directly correlated to the primary system saturation temperature up to the trip of the main pumps, when heat removal steeply decreases to zero.

The mass of water in the primary system (Fig. 3.8) decreases with an almost constant rate during liquid flowrate through the break. The calculation of break mass flowrate (Fig. 3.9) is performed using RETRAN correlations for choked flow, that is the Moody model for saturated water and the Henry-Fauske model for the subcooled phase. After break uncovering the mass inventory decreases more slowly reaching a minimum value of about 34 tons at the end of the calculation.

The mass flowrate through the two primary loops (Fig. 3.10) is predicted to be rapidly reduced due to void formation inside the primary system. A void degradation factor has been also applied in order to simulate the decrease of pumps head as a function of the void fraction.

The core starts to uncover at 2600 s (Fig. 3.11) as a consequence of the break and pumps trip, while core heatup starts at 3000 s at the core top, because the core decay power is no more removed by natural circulation in the primary circuit. Core level is predicted to reach the bottom of the active fuel after 5700 s since the beginning of the transient and it remains to this level up to the vessel failure.

The temperature in the cold leg (Fig. 3.12) remains at saturation during the first part of the transient and undergoes a steep increase after steam generator emptying. The behavior of the temperature inside the hot leg (Fig. 3.13) is similar, even though higher values of steam superheating are evaluated during core heatup phase.

The fuel rod temperature in the central ring, as evaluated by MELCOR at three different core elevations (Figures from 3.14 to 3.16), shows a steep increase during the oxidation phase. At the bottom of the core, a weaker fuel rod heatup is anyway predicted during the phase where the core level goes to zero.

Fuel rod melting starts just before the main oxidation phase. Melting of control rods materials starts after 5400 s since the beginning of the transient, while Zircaloy starts melting at about 5700 s also causing a partial dissolution of the fuel. The total mass of molten metals is predicted to be about 25 tons (Fig. 3.17), while about 17 tons of debris is predicted to relocate towards the vessel bottom (Fig. 3.18) before the failure of lower supporting plate. Fig. 3.19 shows that most of initially degraded core material reaches the lower plenum; after the failure of lower plate at about 12000 s, almost the whole mass of the core falls into the lower plenum, eventually leading to final vessel failure.

The main oxidation phase takes place (Fig. 3.20) between 4600 s and 7300 s since the beginning of the transient. During this phase almost 417 kg of hydrogen are generated (Fig. 3.21), with a maximum rate of about 0.7 kg/s at 6300 s (Fig. 3.22).

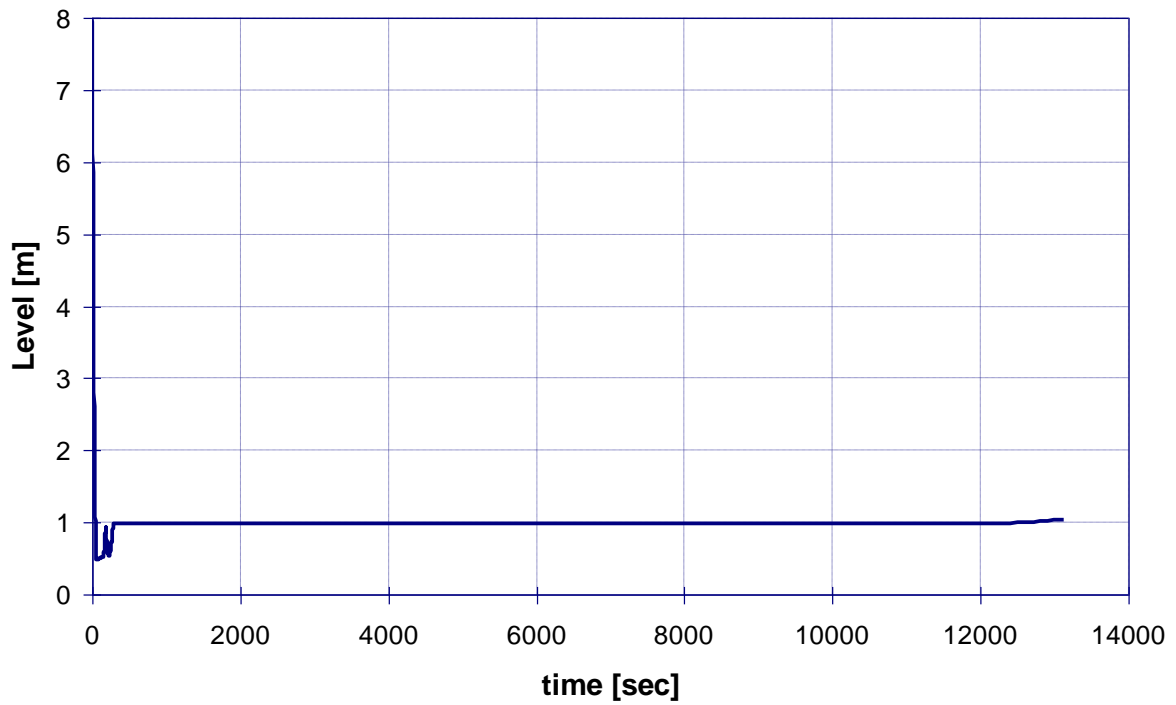


Figure 3.3: Reference case - Steam generator A level

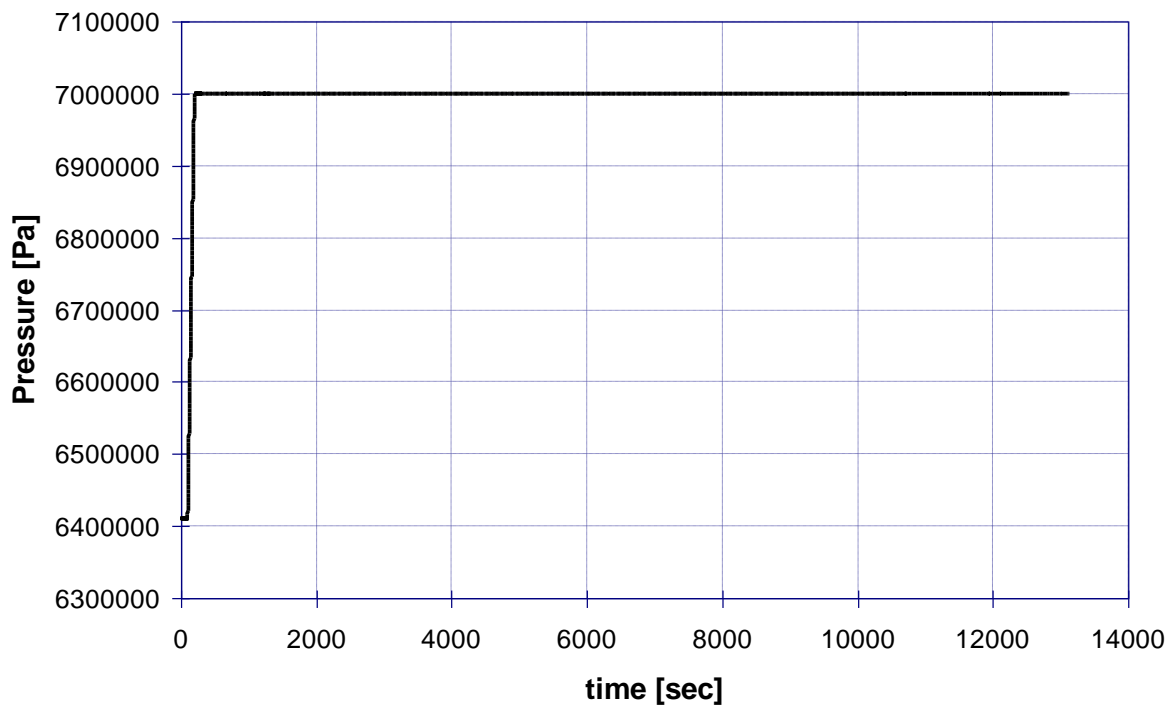


Figure 3.4: Reference case - Steam generator A pressure

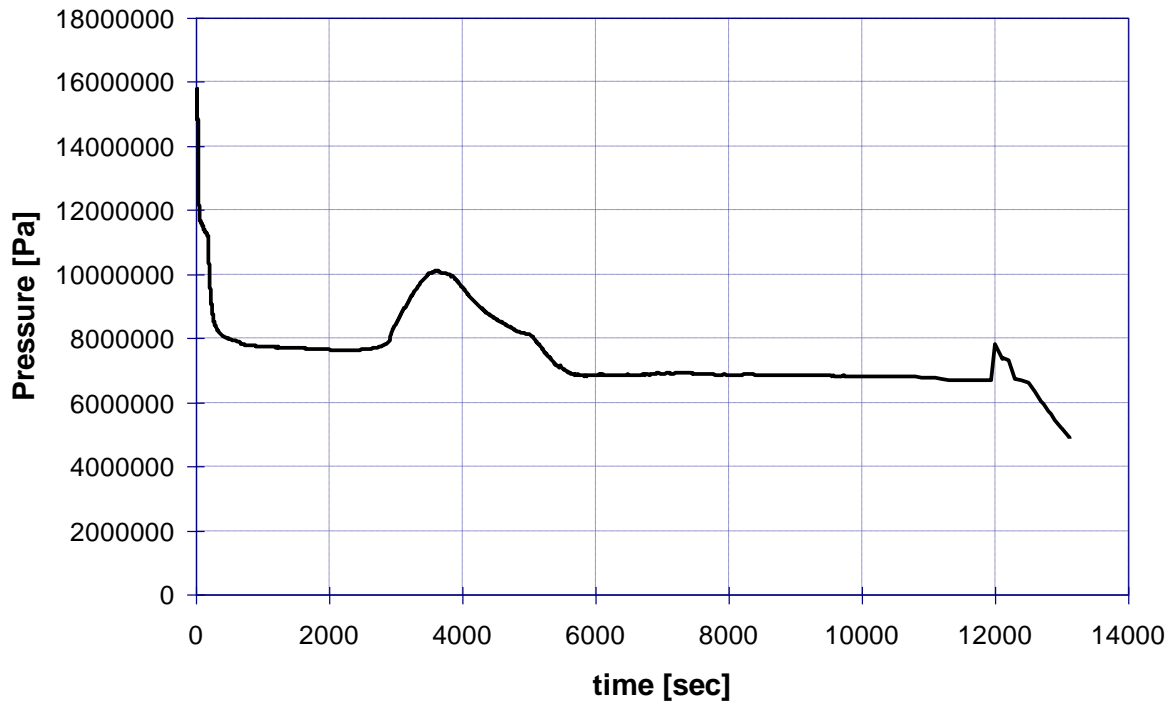


Figure 3.5: Reference case - Pressurizer pressure

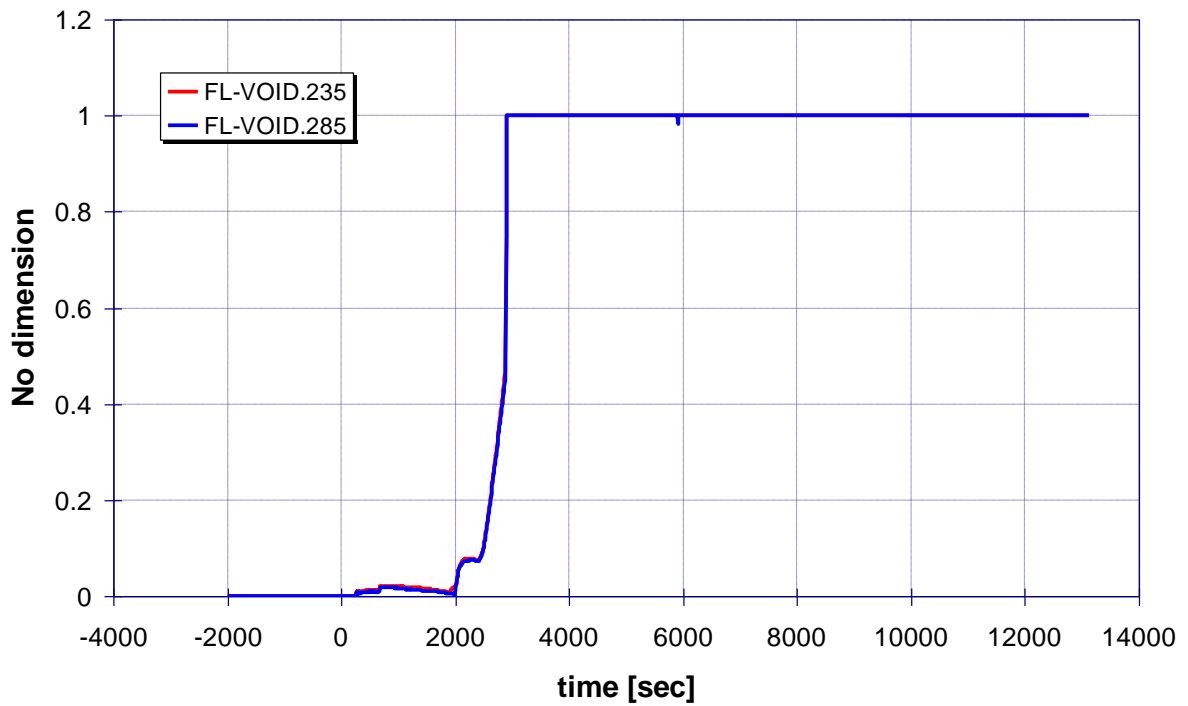


Figure 3.6: Reference case - Main pumps void fraction

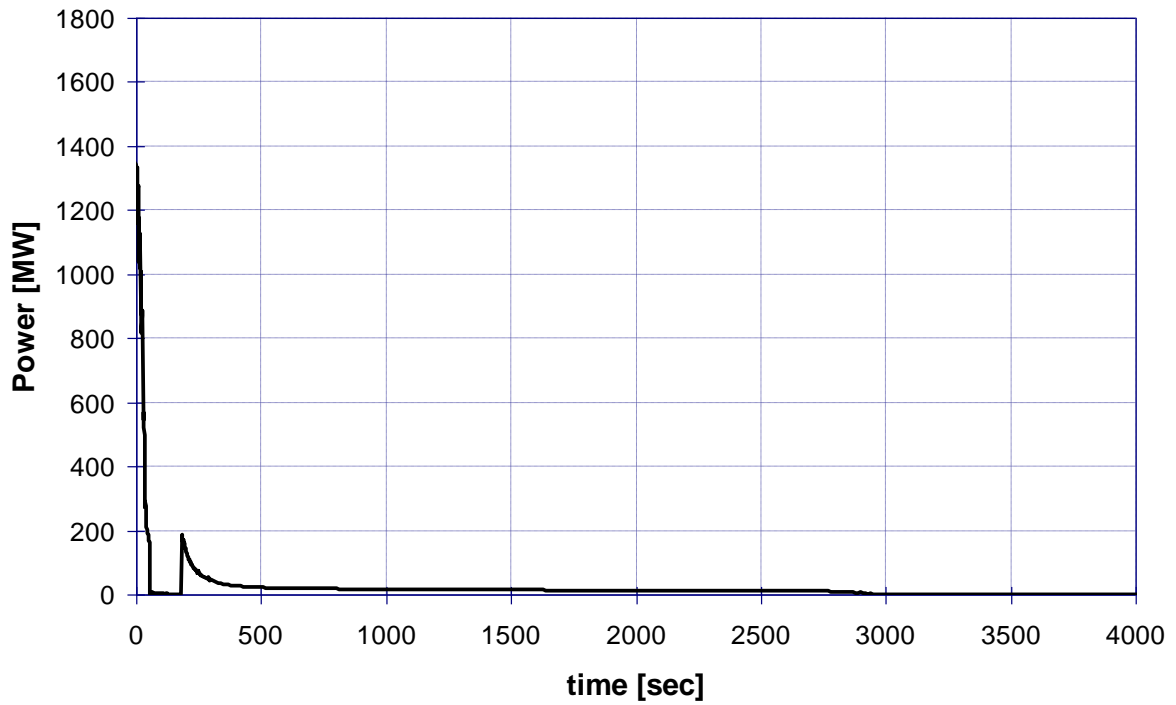


Figure 3.7: Reference case - Steam generator A removed power

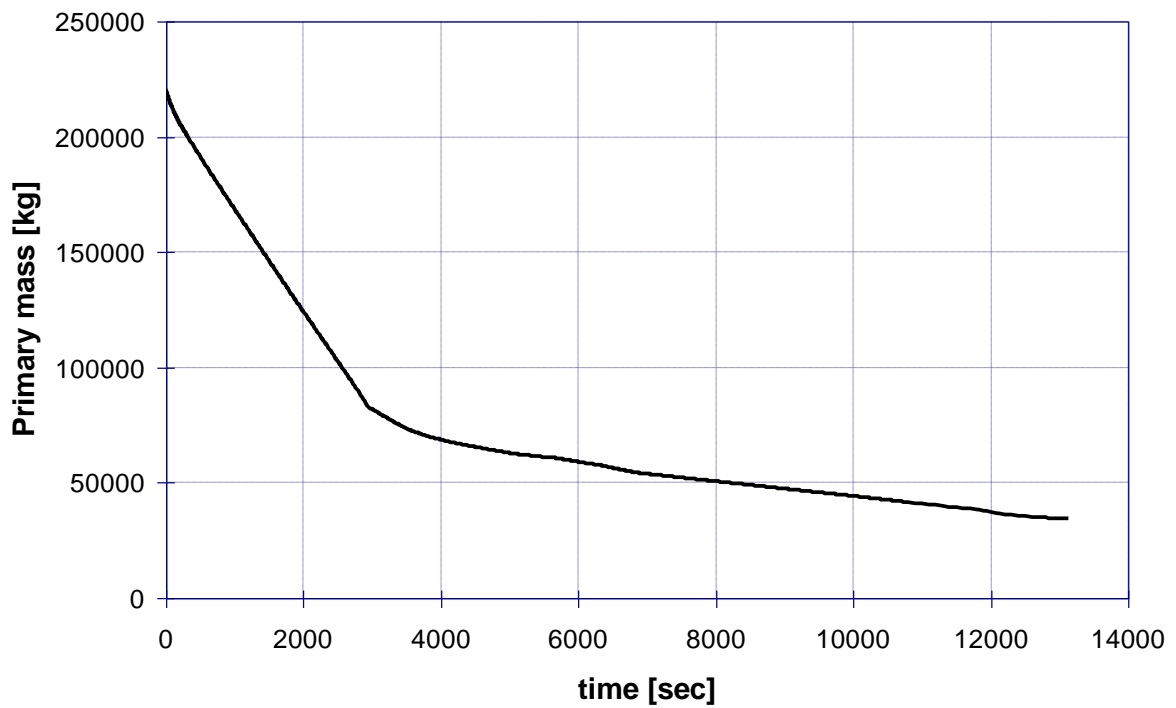


Figure 3.8: Reference case - Total primary water mass



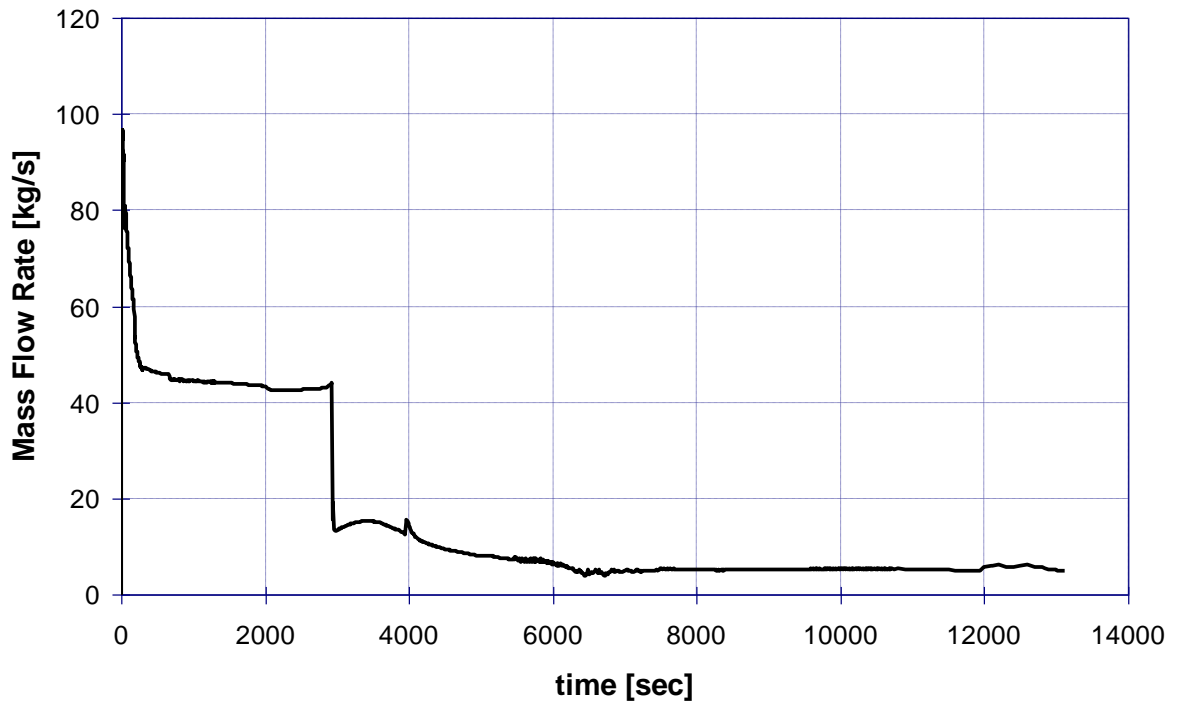


Figure 3.9: Reference case - Break mass flowrate

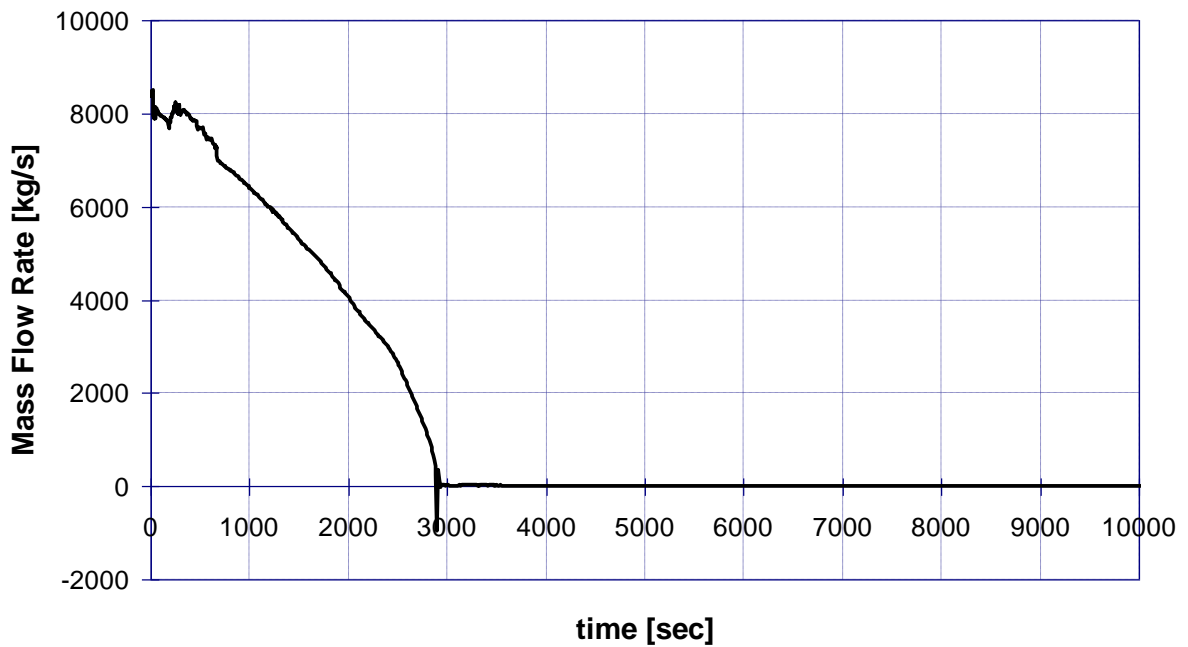


Figure 3.10: Reference case - Loop A mass flowrate

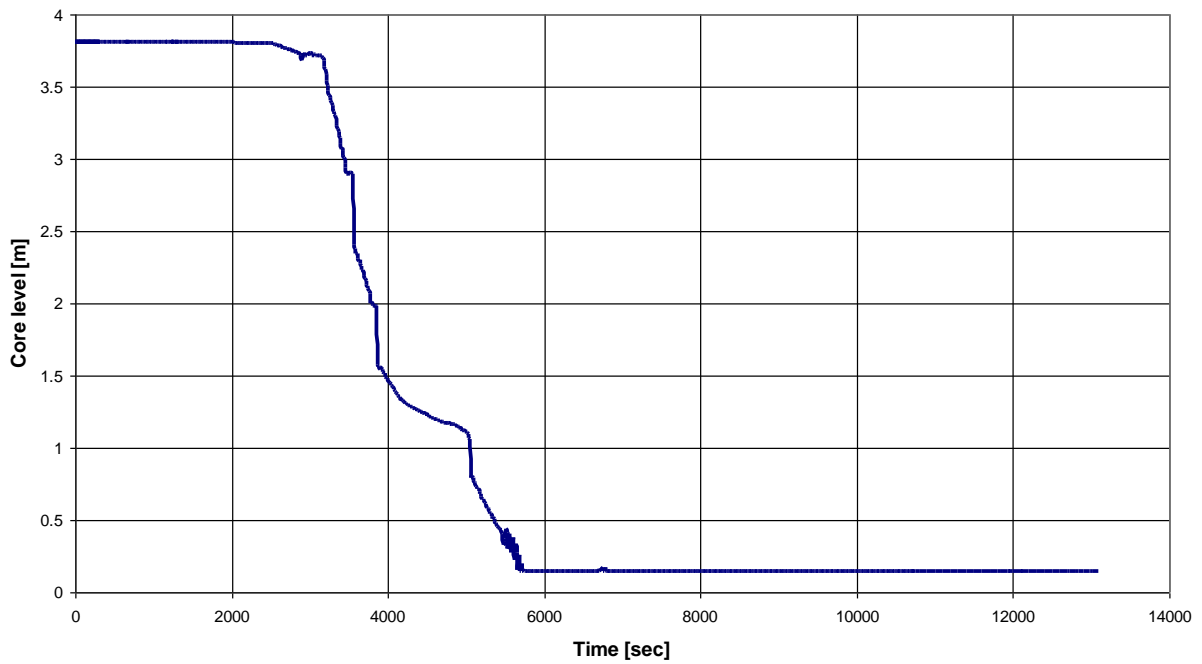


Figure 3.11: Reference case - Core collapsed water level

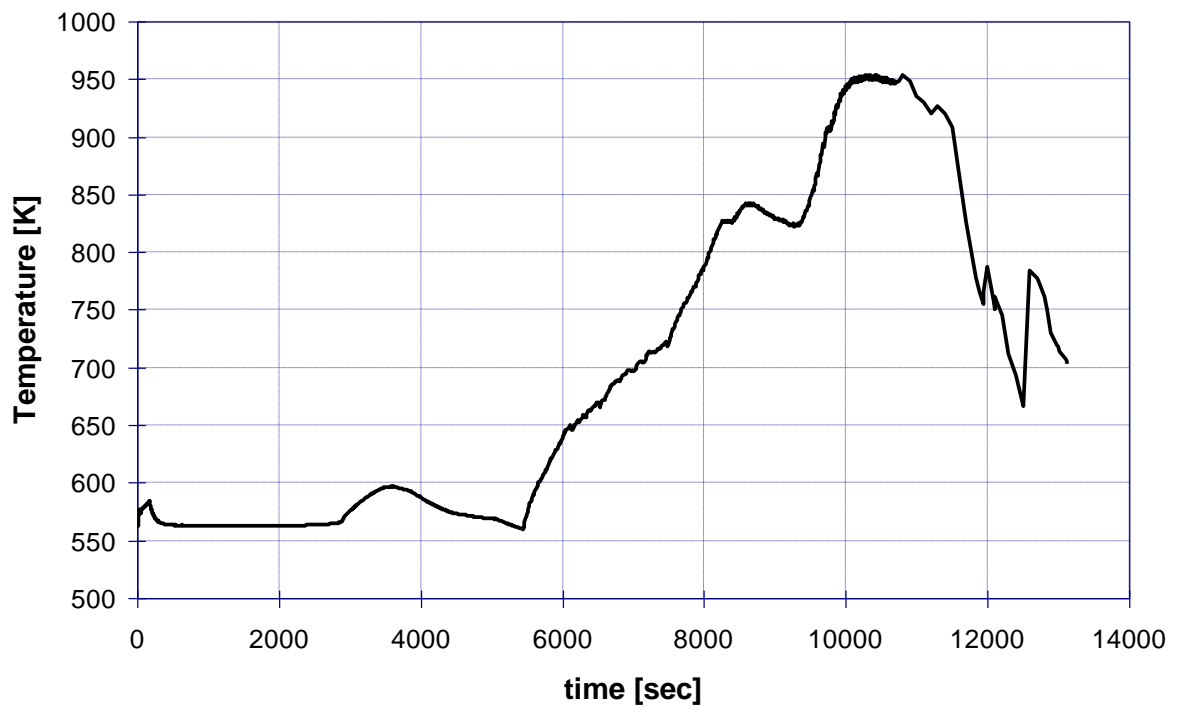


Figure 3.12: Reference case - Cold leg A temperature

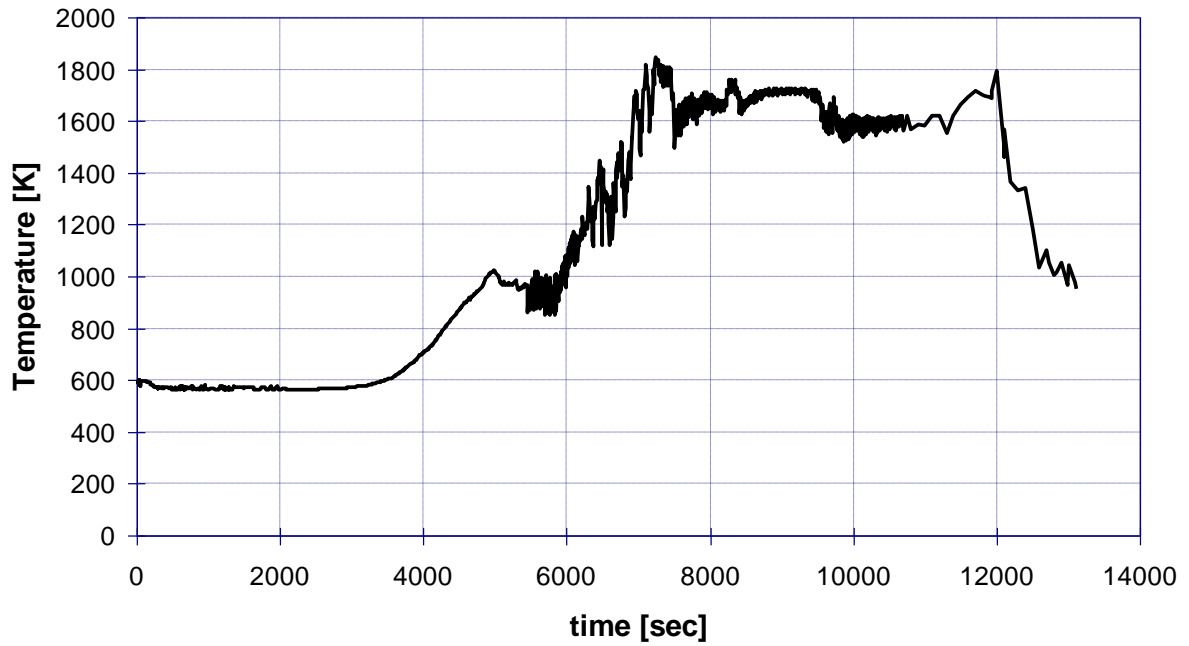


Figure 3.13: Reference case - Hot leg A temperature

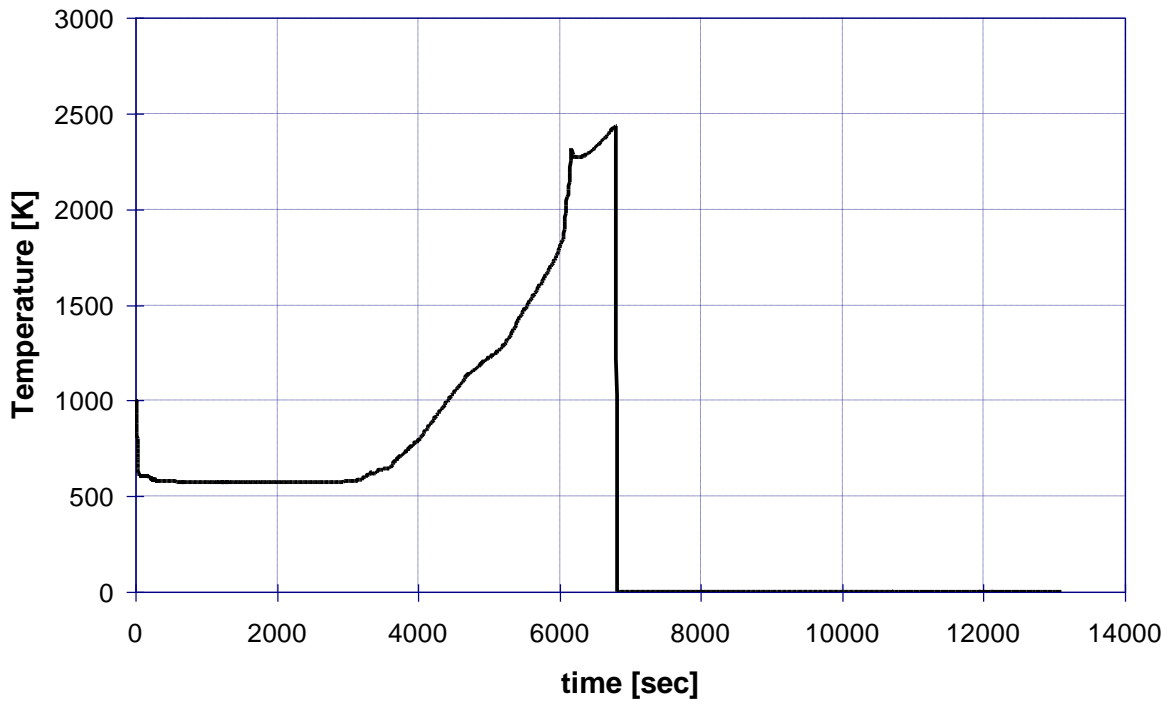


Figure 3.14: Reference case - Fuel rod temperature at the top of the core

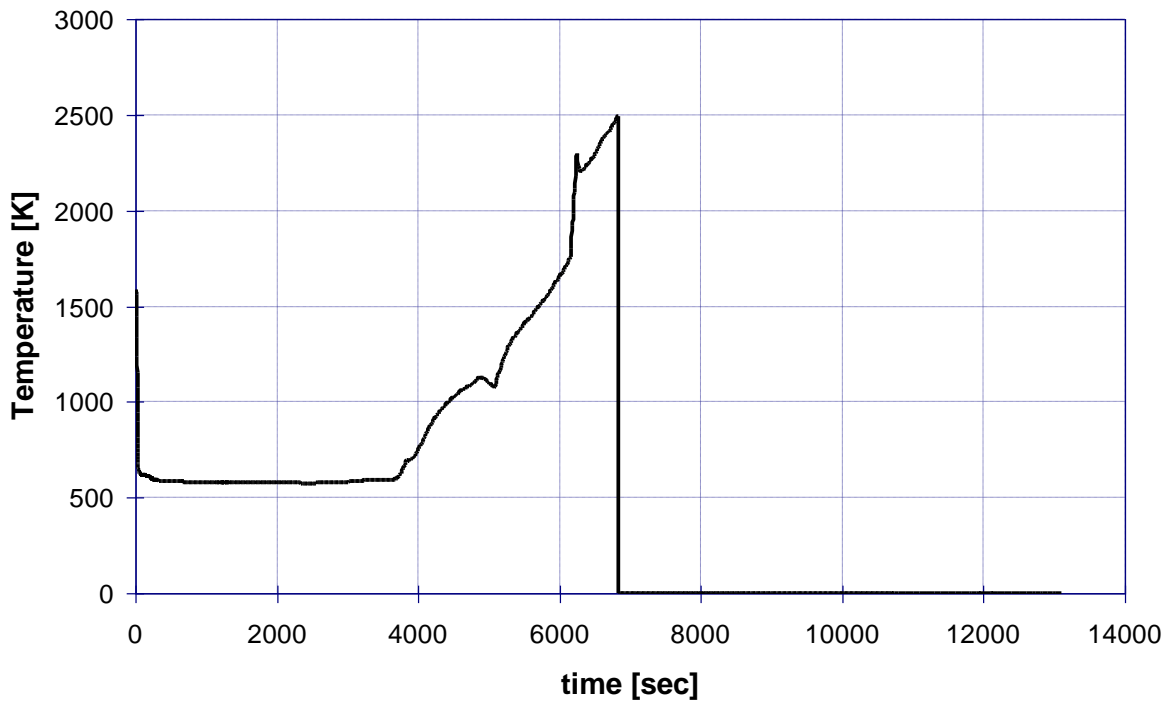


Figure 3.15: Reference case - Fuel rod temperature at the middle of the core

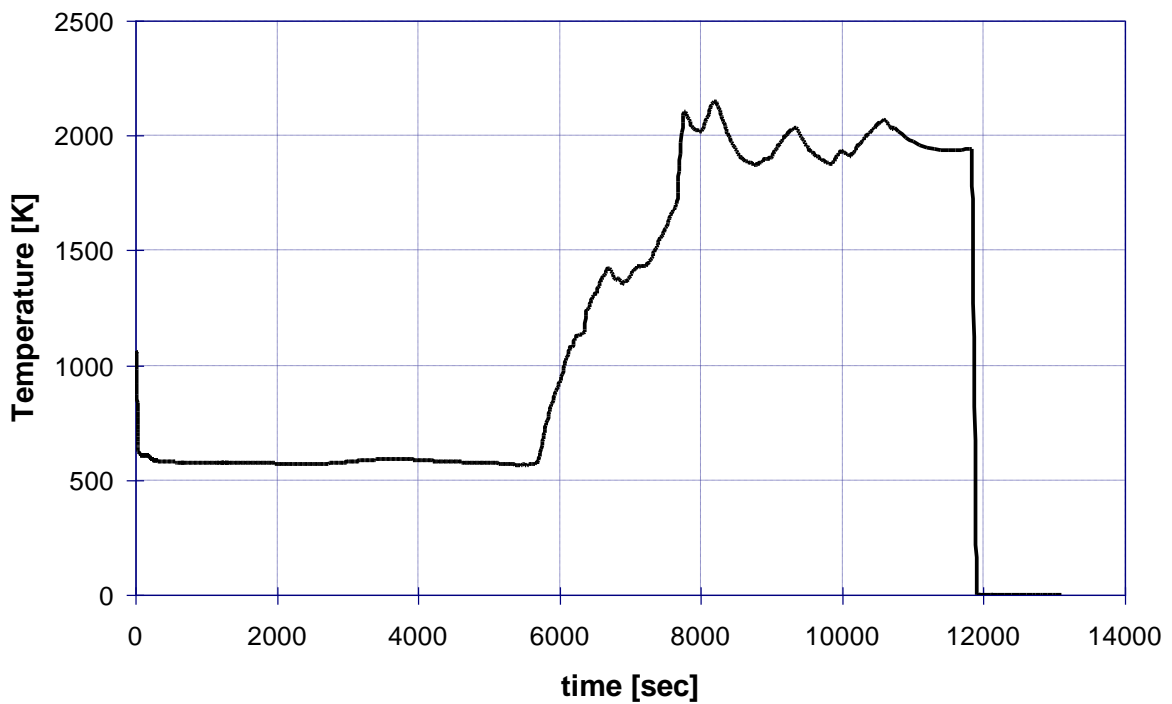


Figure 3.16: Reference case - Fuel rod temperature at the bottom of the core

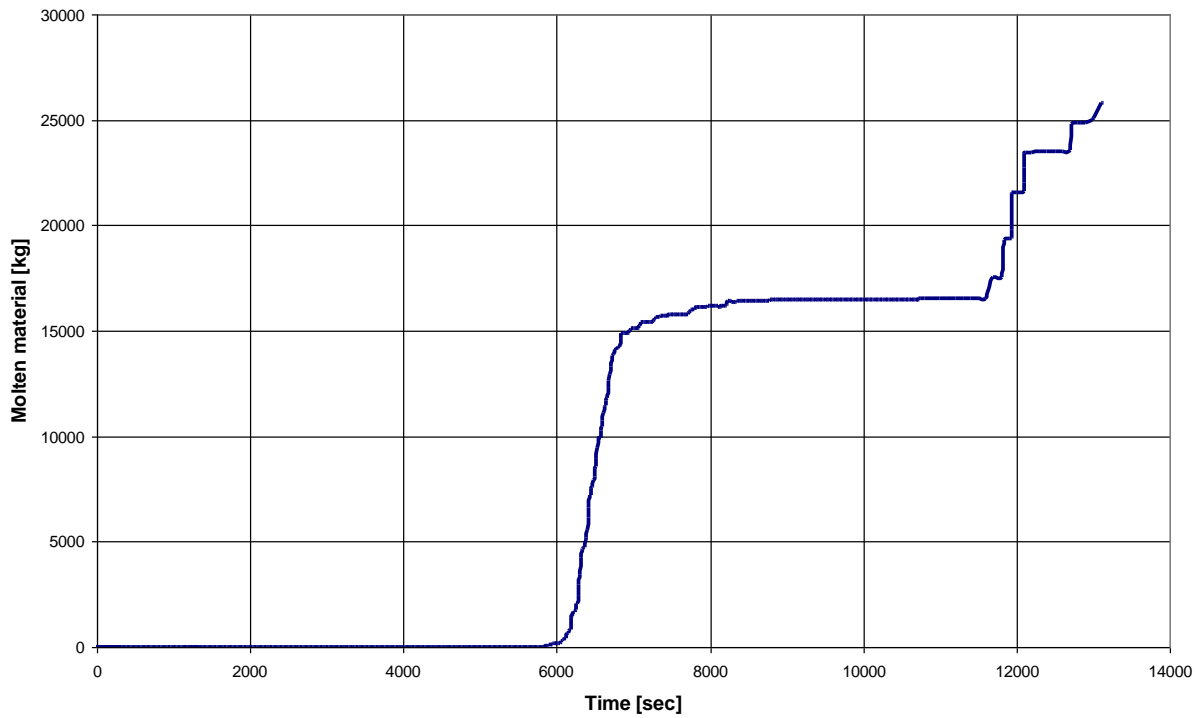


Figure 3.17: Reference case - total mass of molten or relocated metals in the core

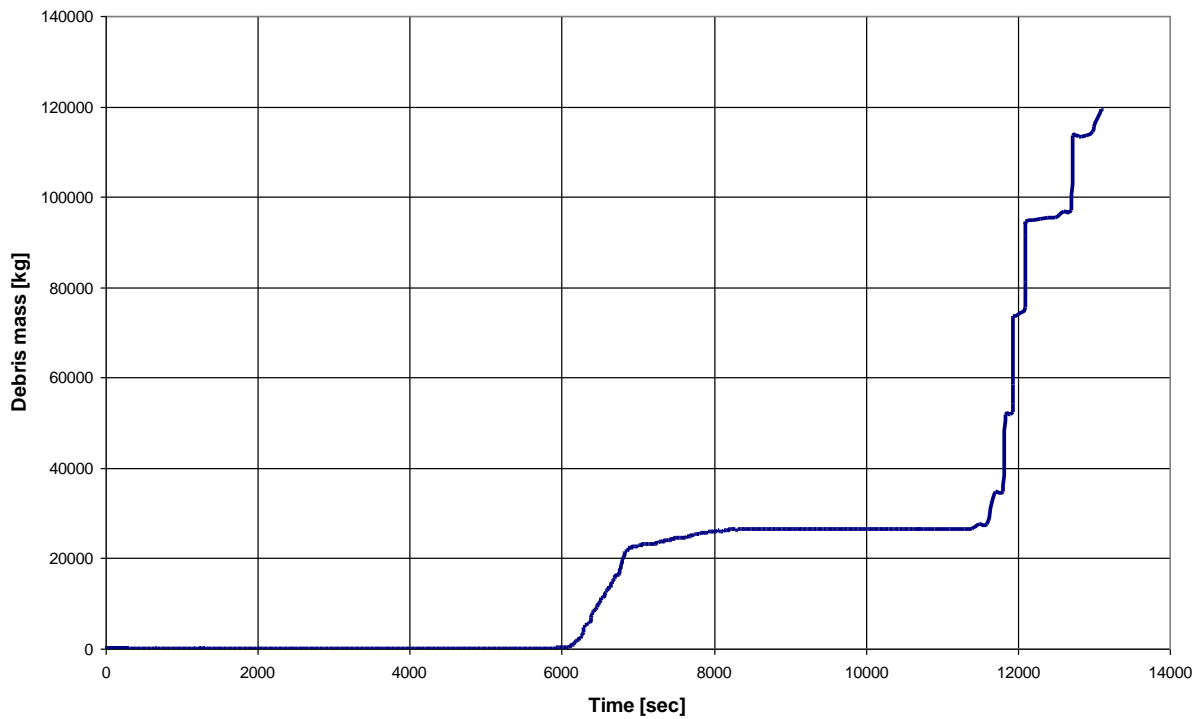


Figure 3.18: Reference case - total mass of debris in the core

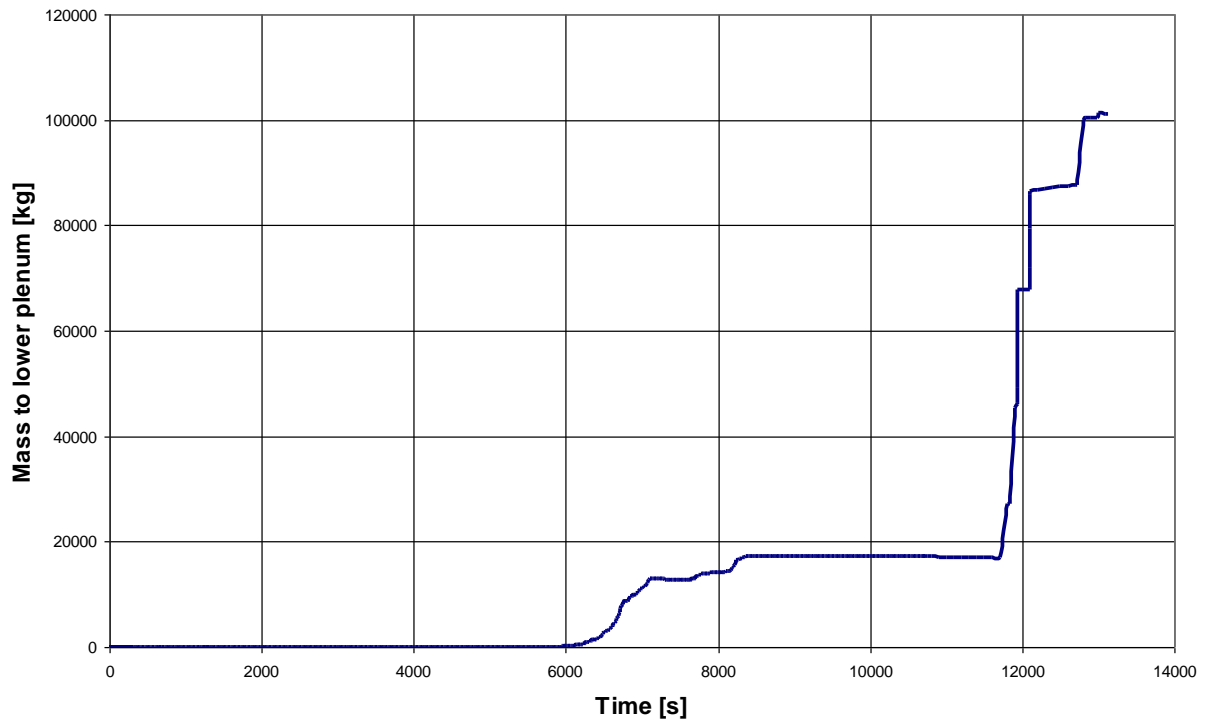


Figure 3.19: Reference case - total mass of core material reaching the lower plenum

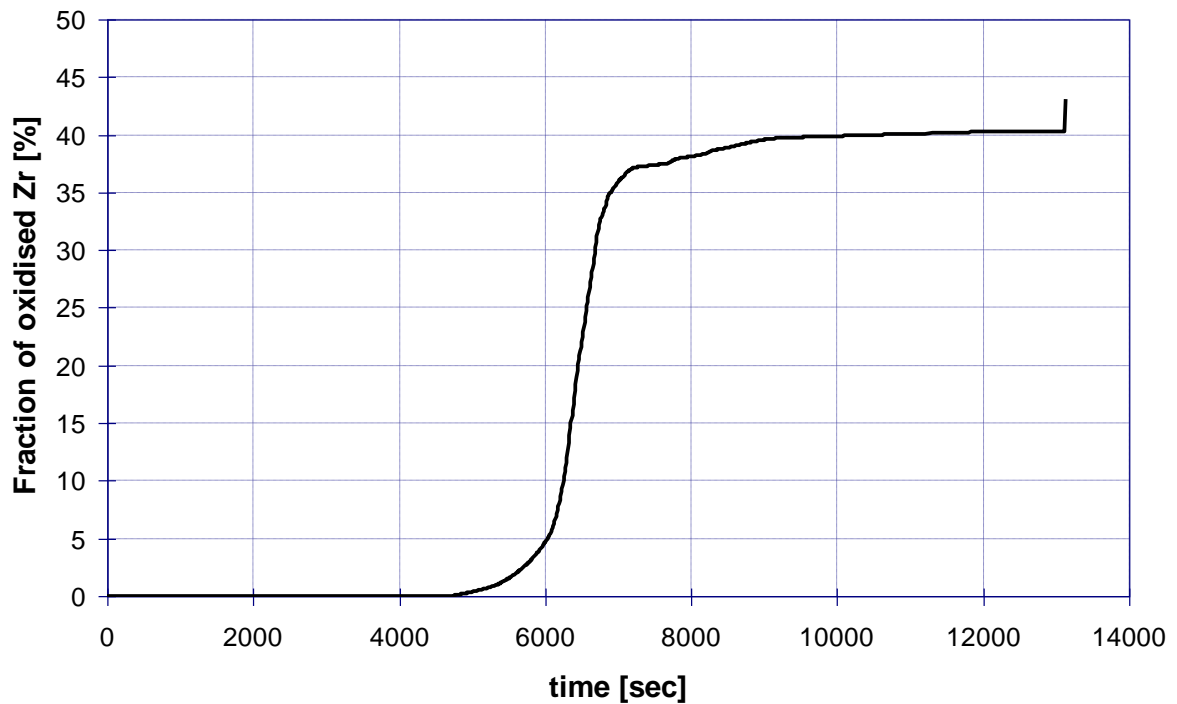


Figure 3.20: Reference case - fraction of oxidised Zr

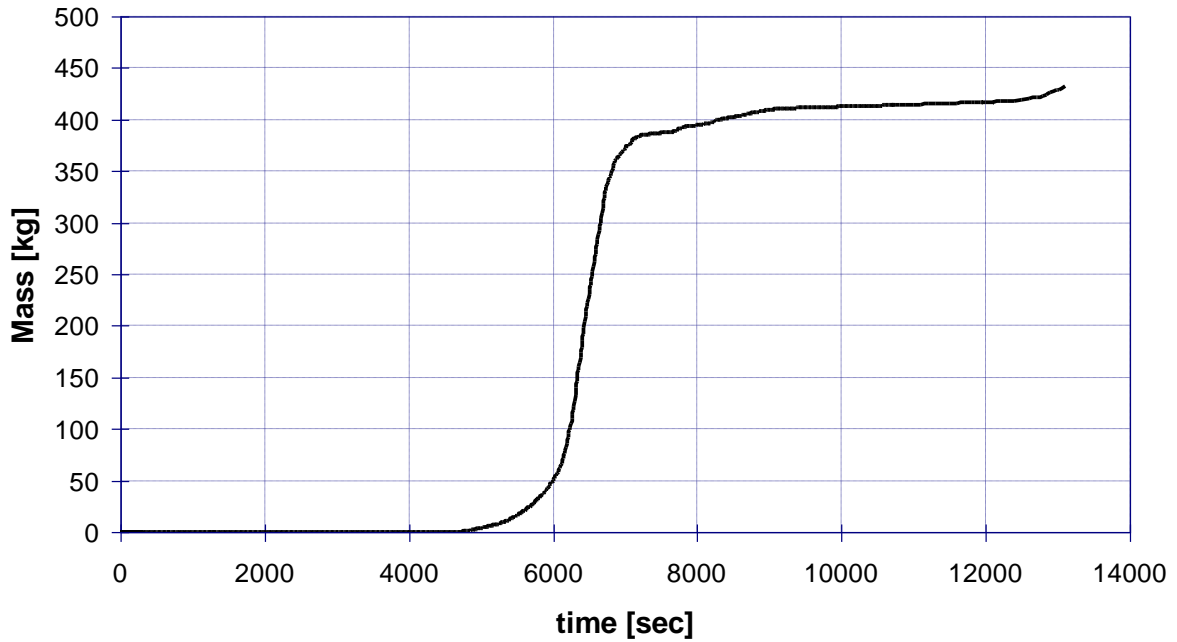


Figure 3.21: Reference case - Cumulated mass of Hydrogen

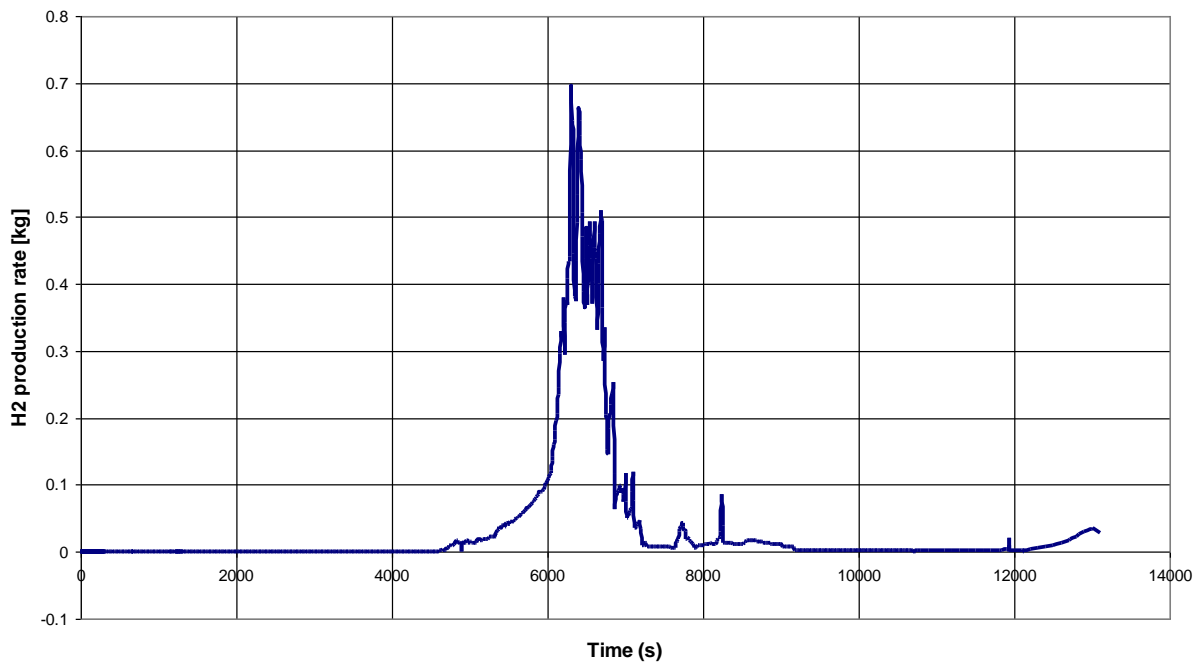



Figure 3.22: Reference case - Hydrogen production rate



 <b>Ricerca Sistema Elettrico</b>	<b>Sigla di identificazione</b>	<b>Rev.</b>	<b>Distrib.</b>	<b>Pag.</b>	<b>di</b>
	ADPFISS-LP1-054	0	L	35	106

### 3.4.2 Sensitivity case A

In this calculation the actuation of the HPI (15 kg/s of water at 413 K in both cold legs of primary loop B) is assumed to take place after 6300 s since the beginning of the transient, when an amount of about 5 tons of debris is evaluated to be formed as a consequence of core damage.

Of course, the primary pressure (Fig. 3.23) is equal to the Reference case up to HPI actuation, when the strong steaming which follows the interaction between the relatively cold injected water with the lower part of the fuel elements causes a second pressure peak from the value of about 6.8 MPa to a maximum of about 10 MPa. Reflooding of the core finally lead the primary pressure to a constant value of about 6.8 MPa, mainly affected by imposed secondary side pressure.

The void fraction is predicted in the primary system (Fig. 3.24) reaching almost the 50% when the main pumps trip, due to the low primary mass. After pumps trip the void fraction in the cold legs jumps to almost 100 %, up to HPI injection which causes a slightly decrease of this variable in the cold legs of primary loop B where HPI injection takes place.

Heat transfer through the two steam generators (Fig. 3.25) is directly correlated to the primary system saturation temperature up to the trip of the main pumps, when heat removal steeply decreases to zero. HPI injection cause a weak inversion of heat transferred through steam generators up to temperature equilibration between primary and secondary systems.

The mass of water in the primary system (Fig. 3.26) decreases with an almost constant rate during liquid flowrate through the break. After HPI the primary system inventory starts increasing again up to the value of about 110 tons after 8000 s, when water level reaches the break (Fig. 3.27), determining a new steady condition in the plant.

Core uncovering clearly takes place in a very similar way as in the reference calculation, starting at 2600 s (Fig. 3.28) as a consequence of the break and pumps trip. Core level is predicted to reach the bottom of the active fuel after 5700 s since the beginning of the transient, but starts to increase again at 6700 s (400 s after HPI actuation) and the core is completely flooded in about 20 minutes.

The temperature in the cold legs (Fig. 3.29) and in the hot legs (Fig. 3.30) of the primary system is also identical to the Reference case up to HPI injection, after which an effective decrease of temperature up to saturation values is detected.

The fuel rod temperature in the central ring, as evaluated by MELCOR at the upper core elevations (Figures from 3.31 to 3.32), shows a steep increase during the oxidation phase as in the Reference case and the failure condition is reached almost at the same time in both cases. At the bottom of the core, the fuel rod heatup is initially stopped as a consequence of core reflood (Fig. 3.33), but the fuel temperature starts to increase again as fast as before, eventually reaching the failure limit. This unexpected behavior is detected also in the other circumferential rings modeling the core: despite of the gradual inlet of water from the lower plenum to the core, a reduction of heat transfer (probably both convective and radiative) is

predicted in some of the lower axial nodes of the fuel rods. This seems to be due to a drastic decrease of natural circulation of vapor still present in those locations as a consequence of the partial blockage of surrounding flow paths. The mismatch between decay heat still produced inside the fuel rod and removed power causes an increase of void fraction (Fig. 3.34) and a consequent additional degradation of heat transfer. Failure of lower zone of fuel rods leads to the complete relocation of the whole fuel element.

A much larger amount of debris is therefore predicted (almost 100 tons) to relocate towards the lower supporting plate (Fig. 3.35), even though the water injected through the HPI and entering the core is able to maintain the coolability of this material. Even though a partial failure of the lower supporting plate with core material relocation in the lower plenum (Fig. 3.36) is still predicted, the reflooding is sufficient to prevent vessel failure.

The main oxidation phase still takes place (Fig. 3.37) between 4600 s and 7300 s since the beginning of the transient. During this phase almost 380 kg of hydrogen are generated (Fig. 3.38). While the maximum H<sub>2</sub> generation rate of about 0.7 kg/s at 6300 s (Fig. 3.39) is similar to the Reference case, the total amount of produced hydrogen is slightly lower due to reflooding which inhibited the steam-metal reaction during the very last phase of this phenomenon.

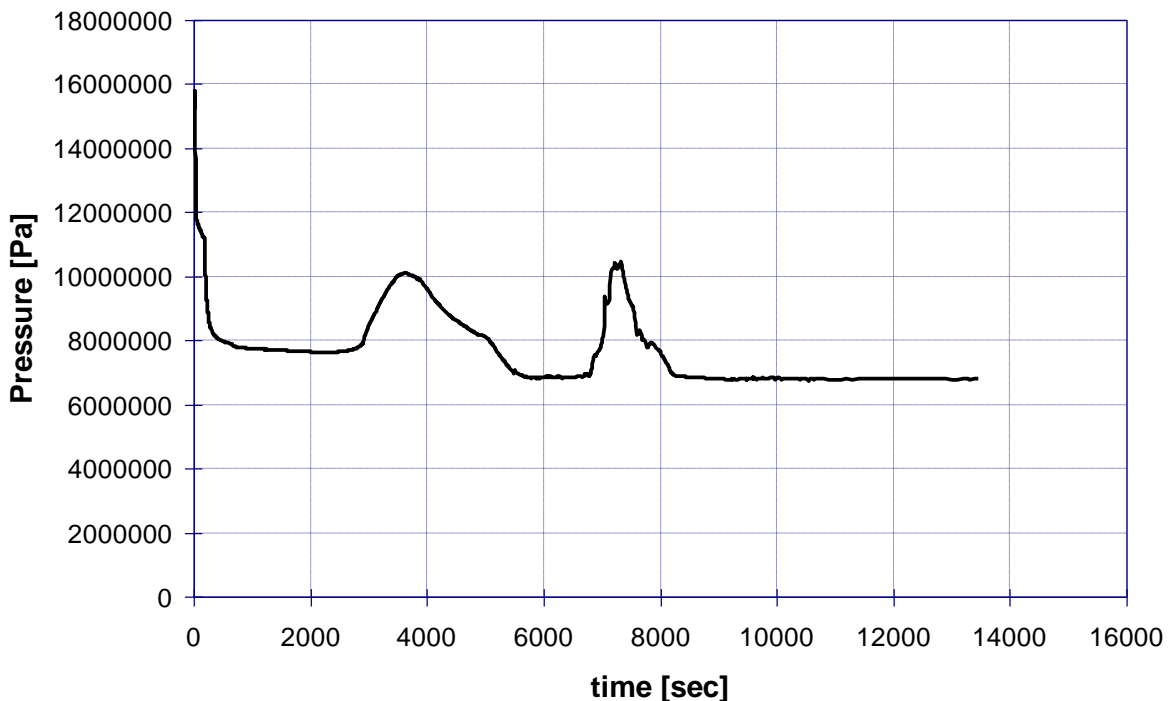


Figure 3.23: Sensitivity case A - Pressurizer pressure

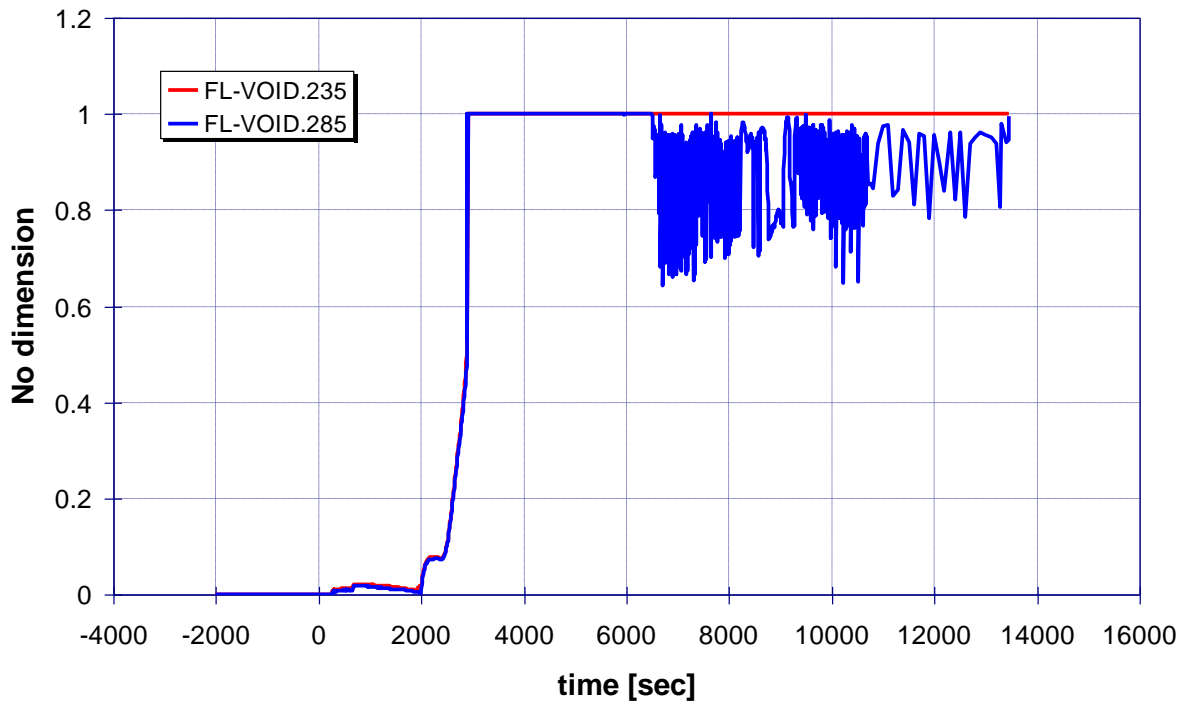


Figure 3.24: Sensitivity case A - Main pumps void fraction

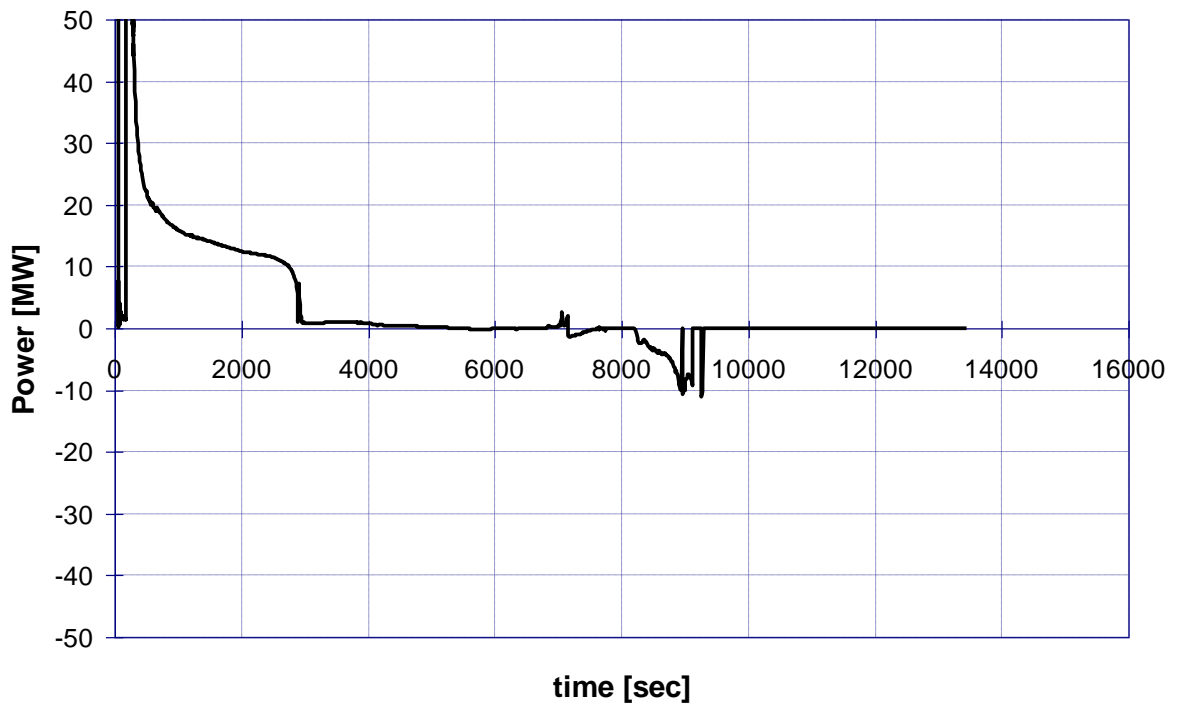


Figure 3.25: Sensitivity case A - Steam generator A removed power

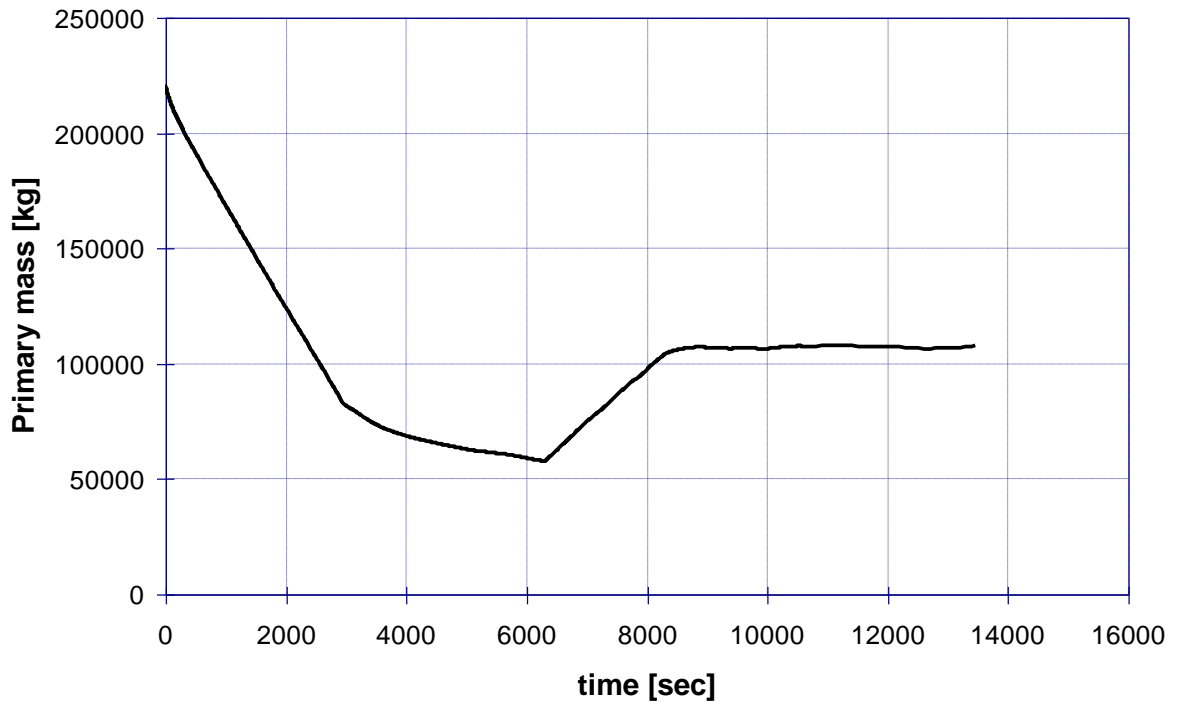


Figure 3.26: Sensitivity case A - Total primary water mass

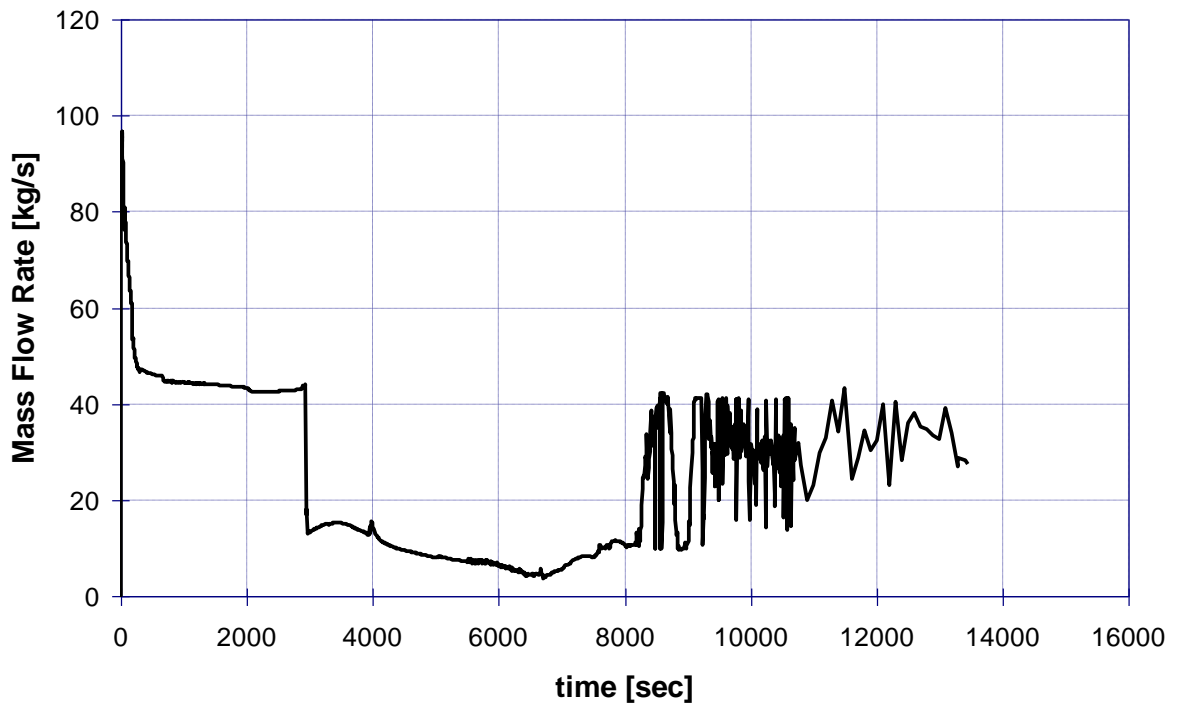


Figure 3.27: Sensitivity case A - Break mass flowrate

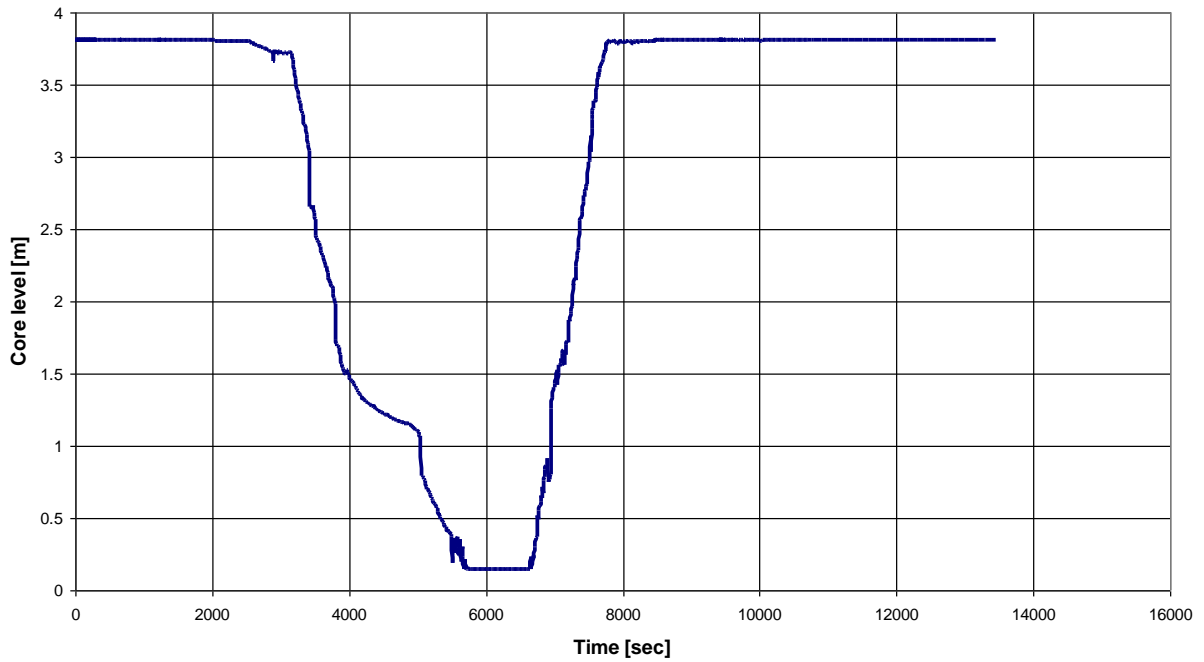


Figure 3.28: Sensitivity case A - Core collapsed water level

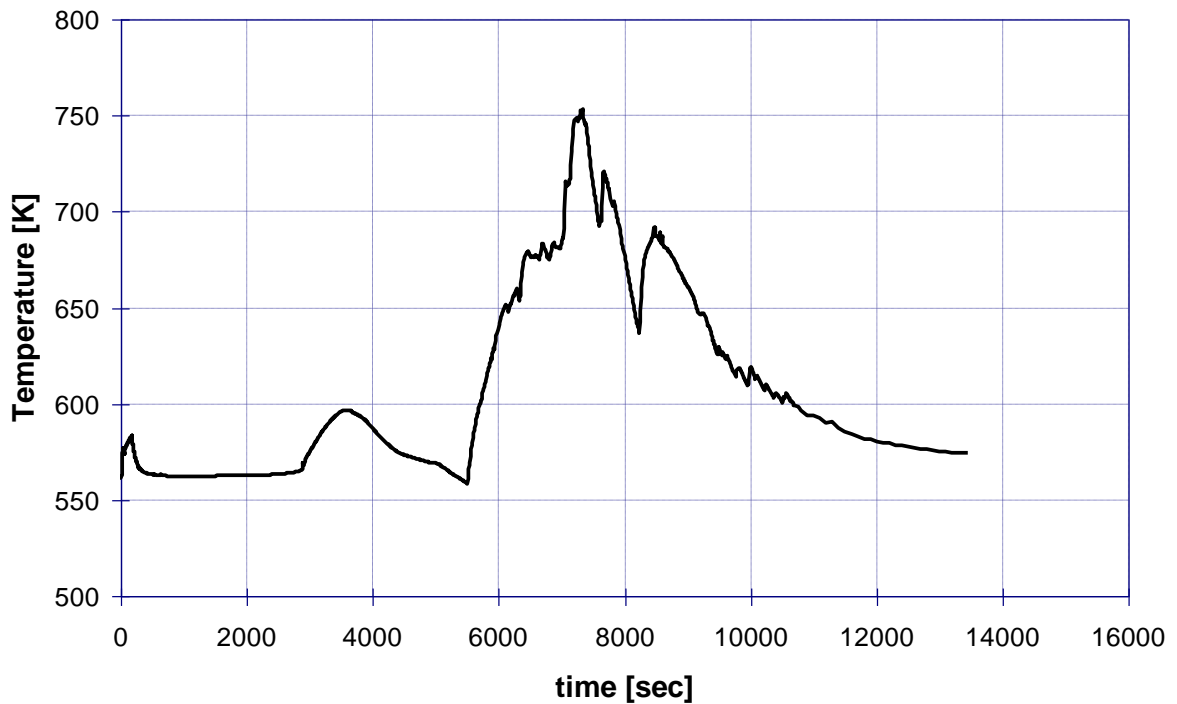


Figure 3.29: Sensitivity case A - Cold leg A temperature

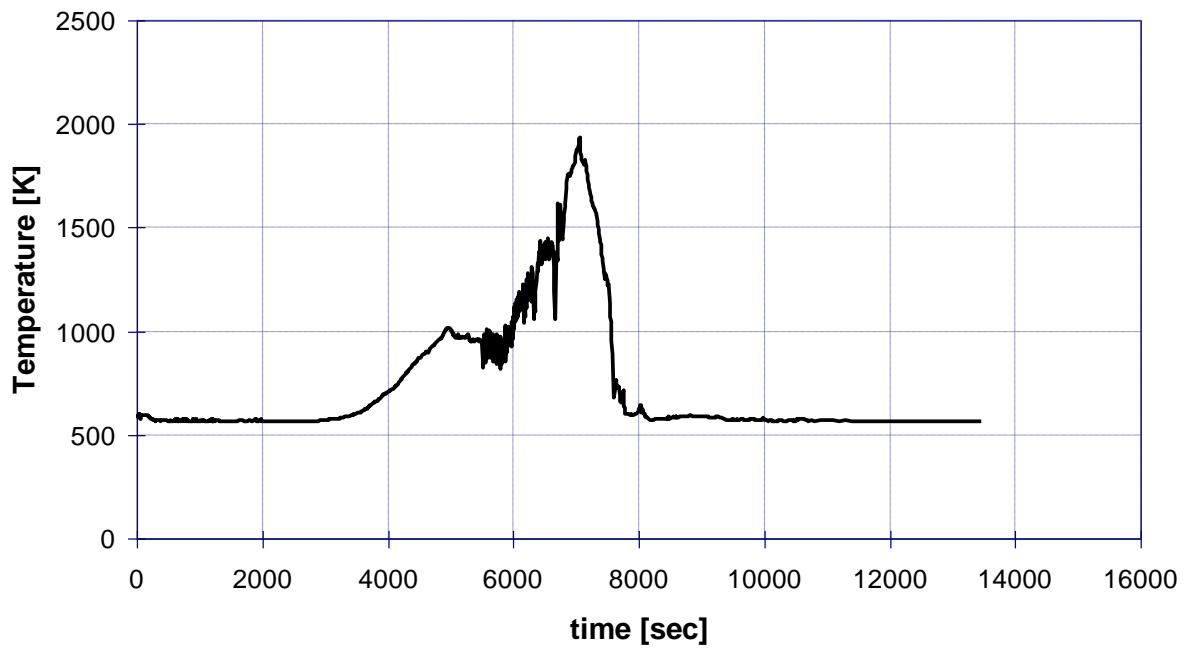


Figure 3.30: Sensitivity case A - Hot leg A temperature

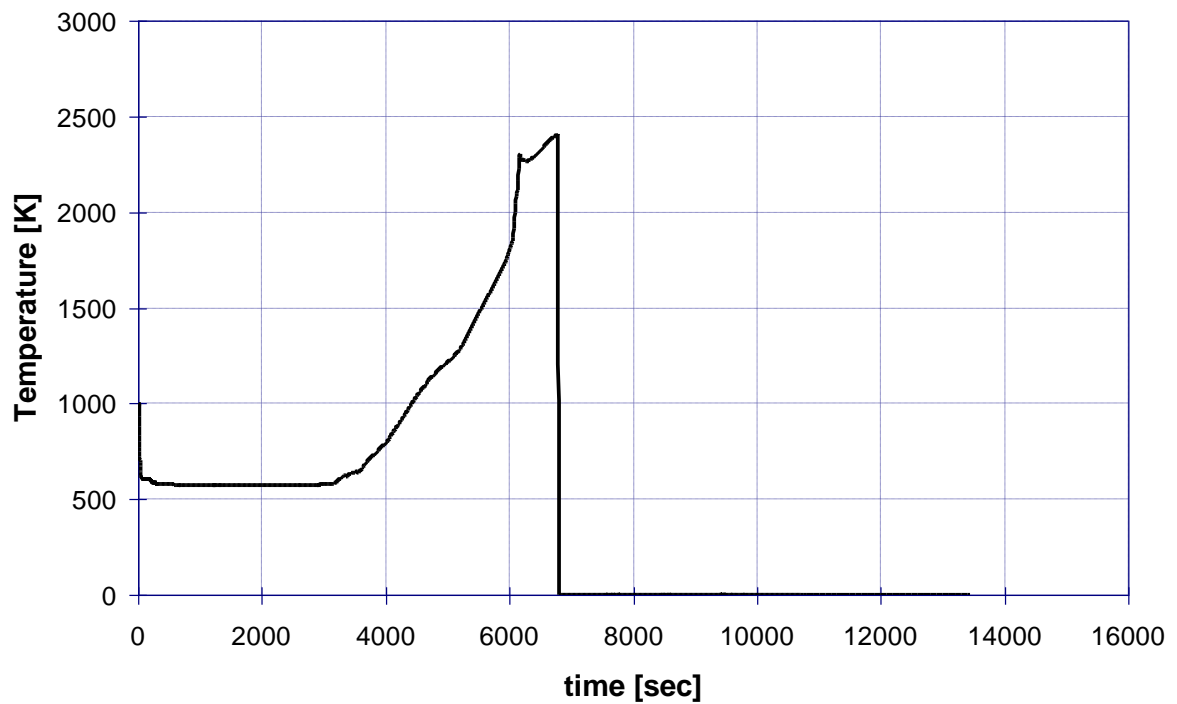


Figure 3.31: Sensitivity case A - Fuel rod temperature at the top of the core

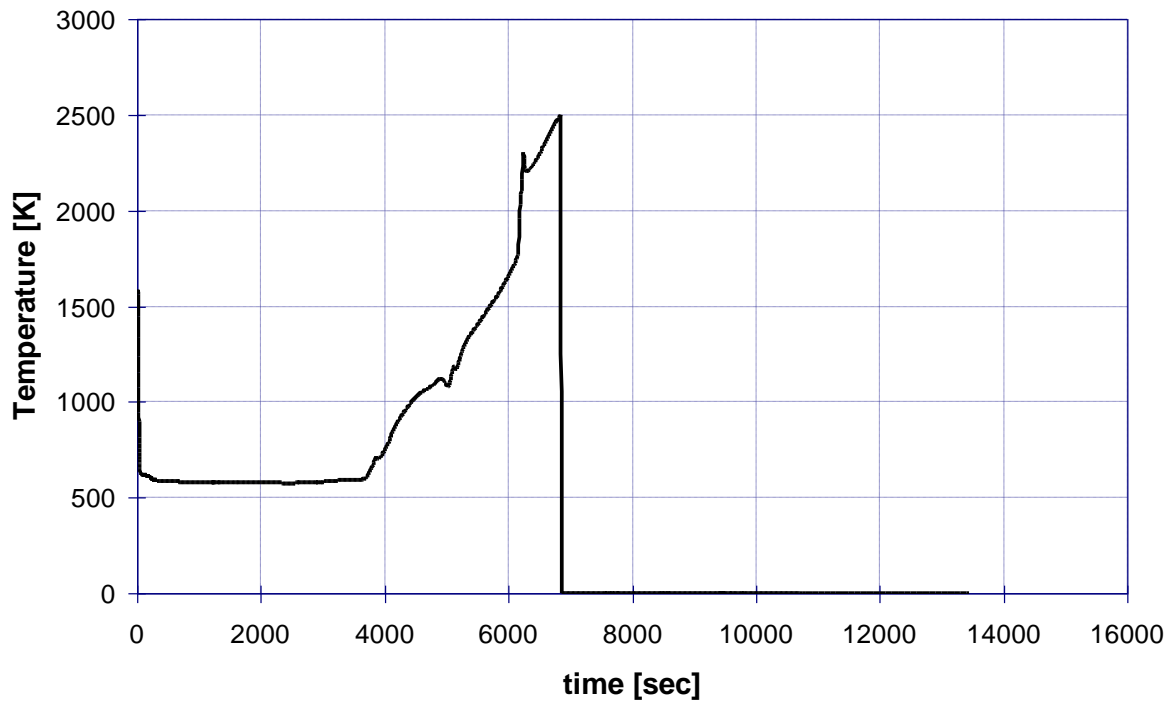


Figure 3.32: Sensitivity case A - Fuel rod temperature at the middle of the core

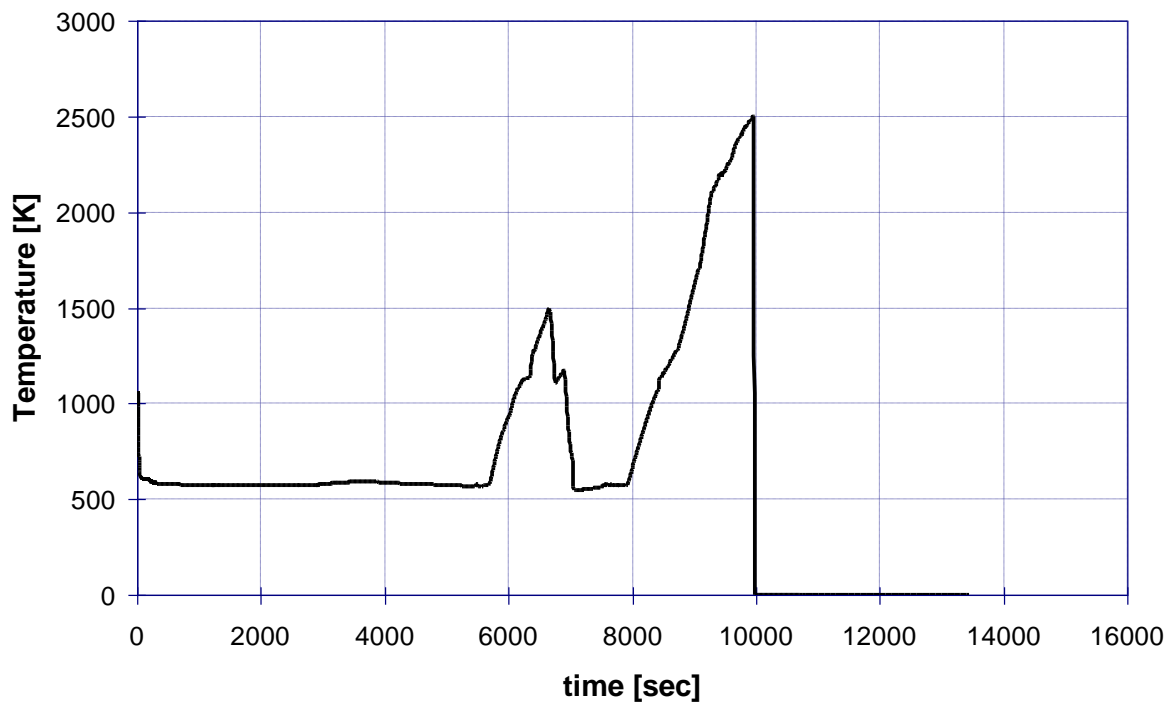


Figure 3.33: Sensitivity case A - Fuel rod temperature at the bottom of the core

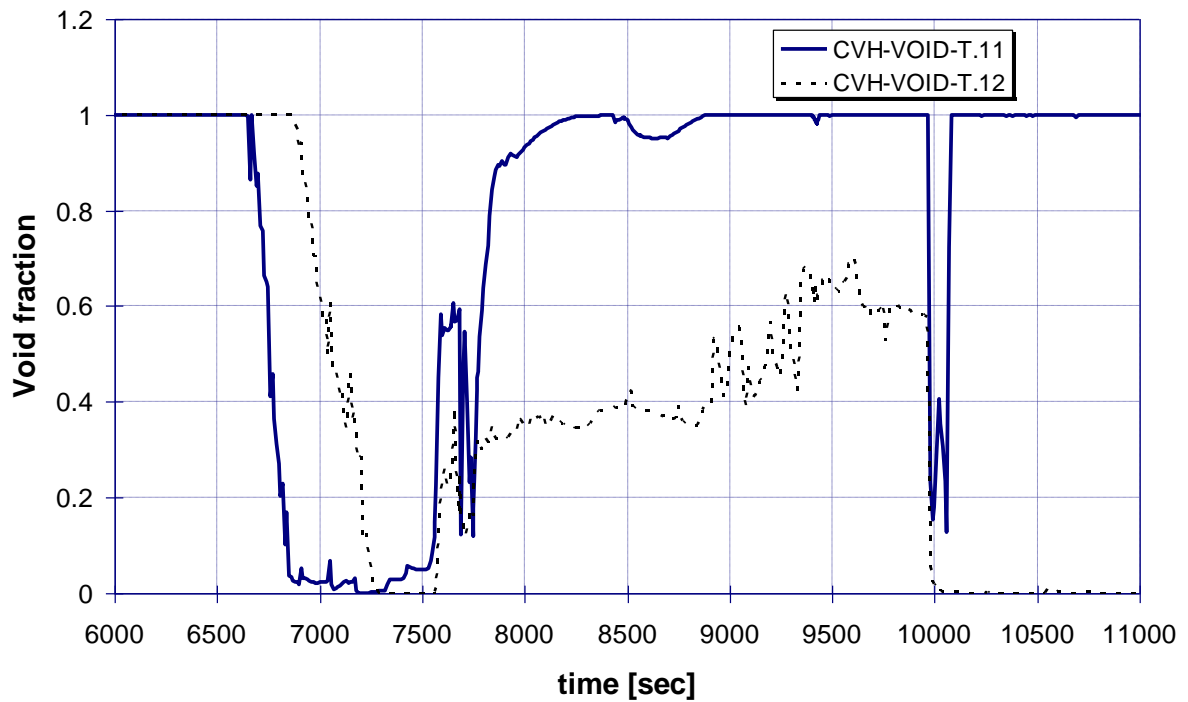


Figure 3.34: Sensitivity case A – void fraction in the central-lower part of the core

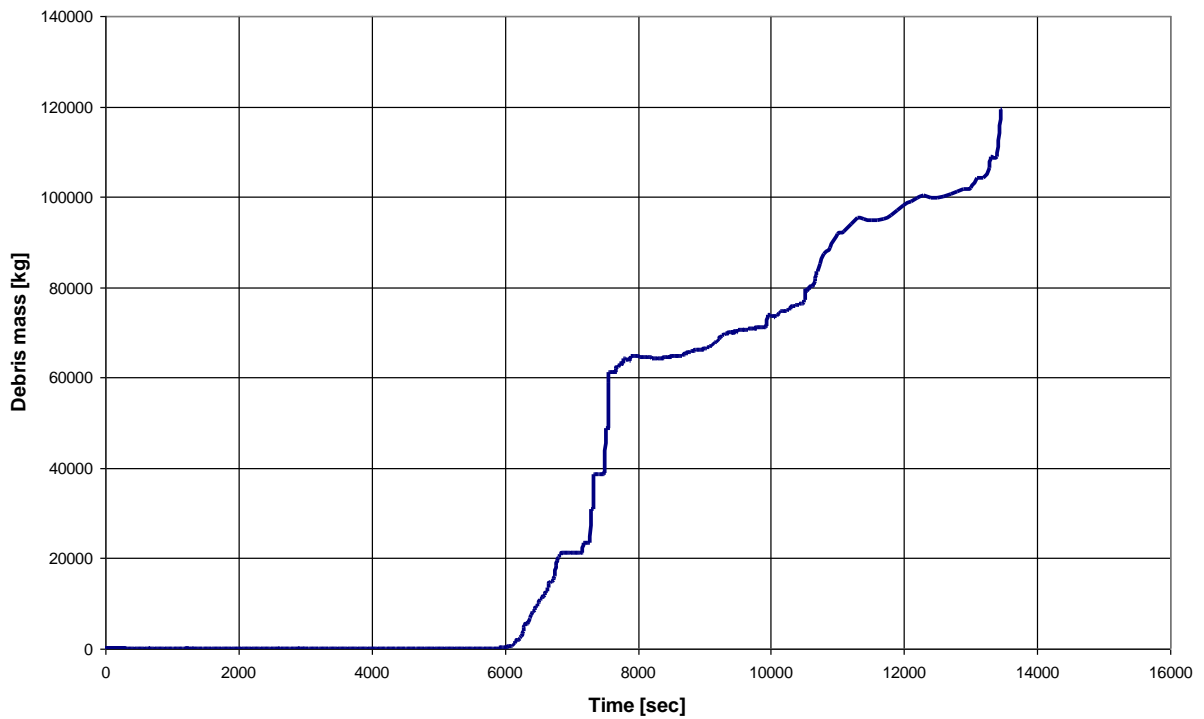


Figure 3.35: Sensitivity case A - total mass of debris in the core



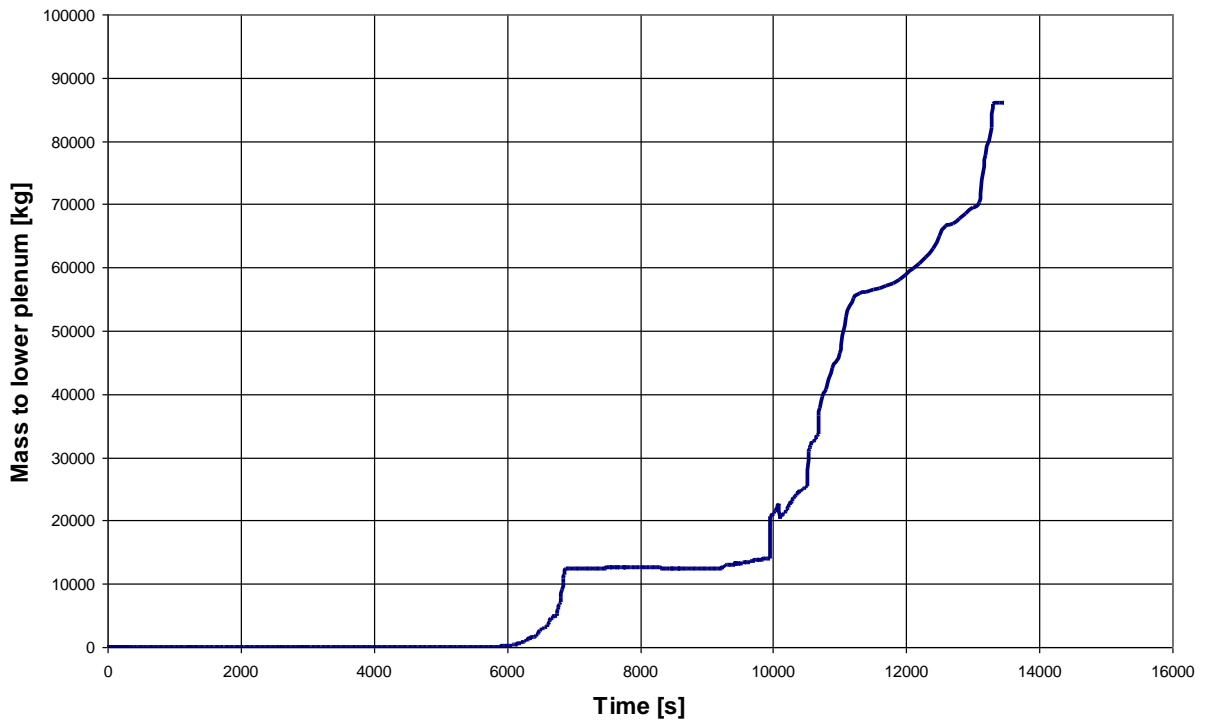


Figure 36: Sensitivity case A - total mass of core material reaching the lower plenum

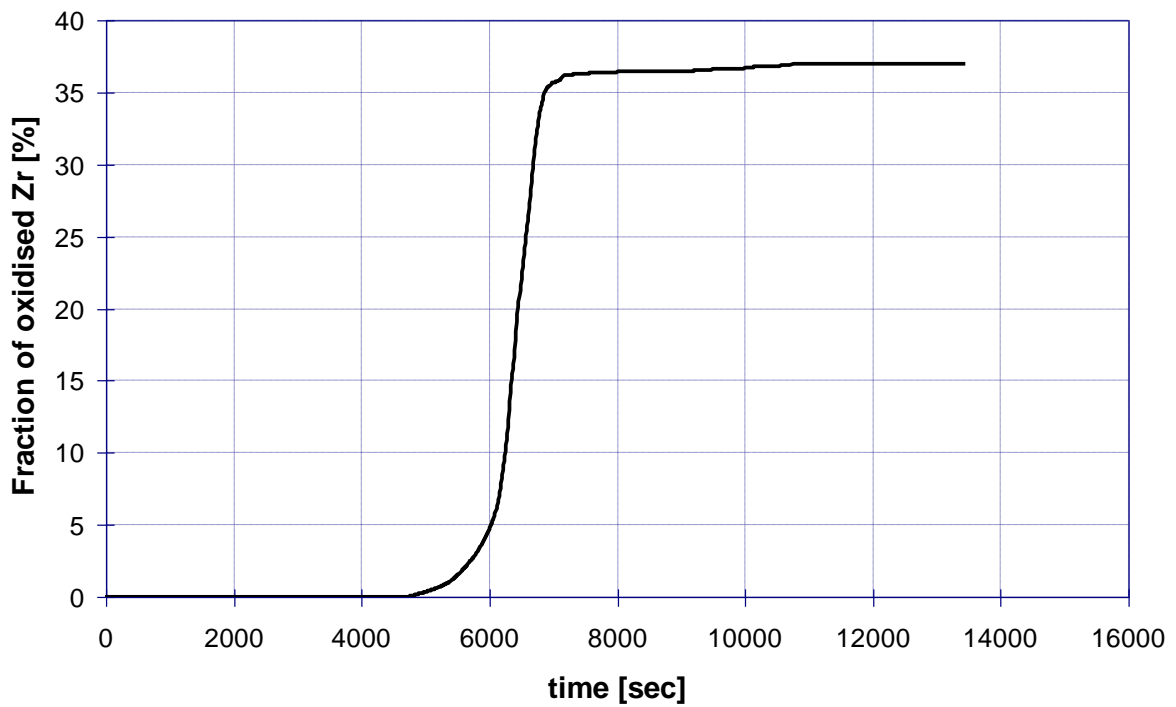


Figure 3.37: Sensitivity case A - fraction of oxidized Zr

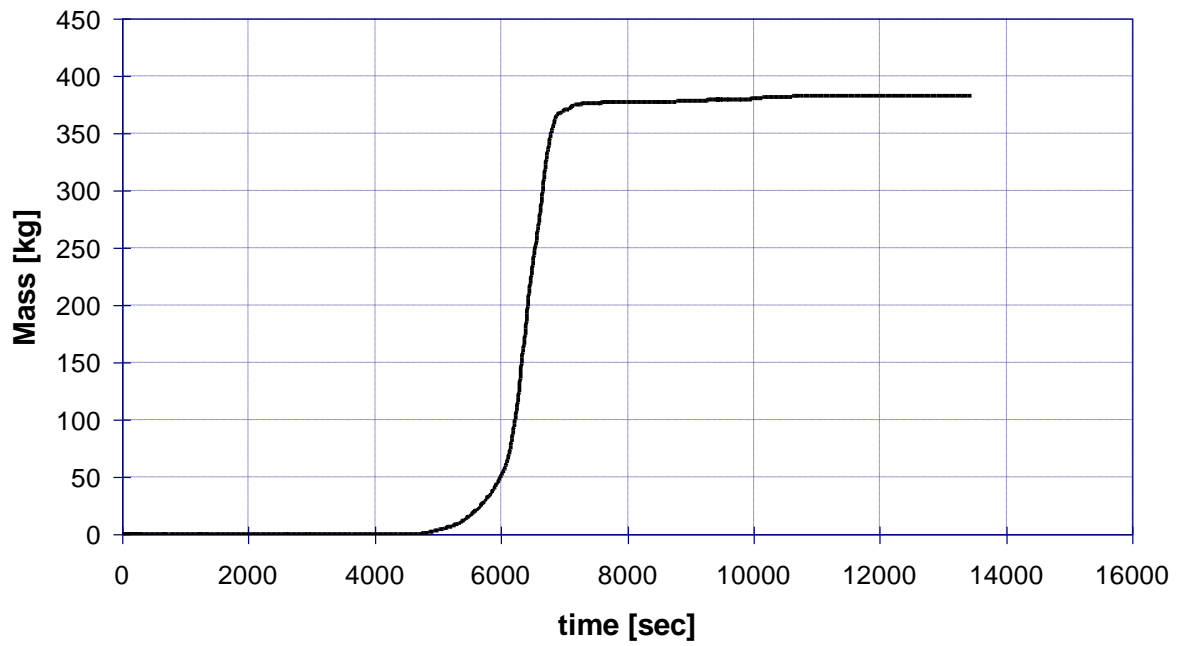


Figure 3.38: Sensitivity case A - Cumulated mass of Hydrogen

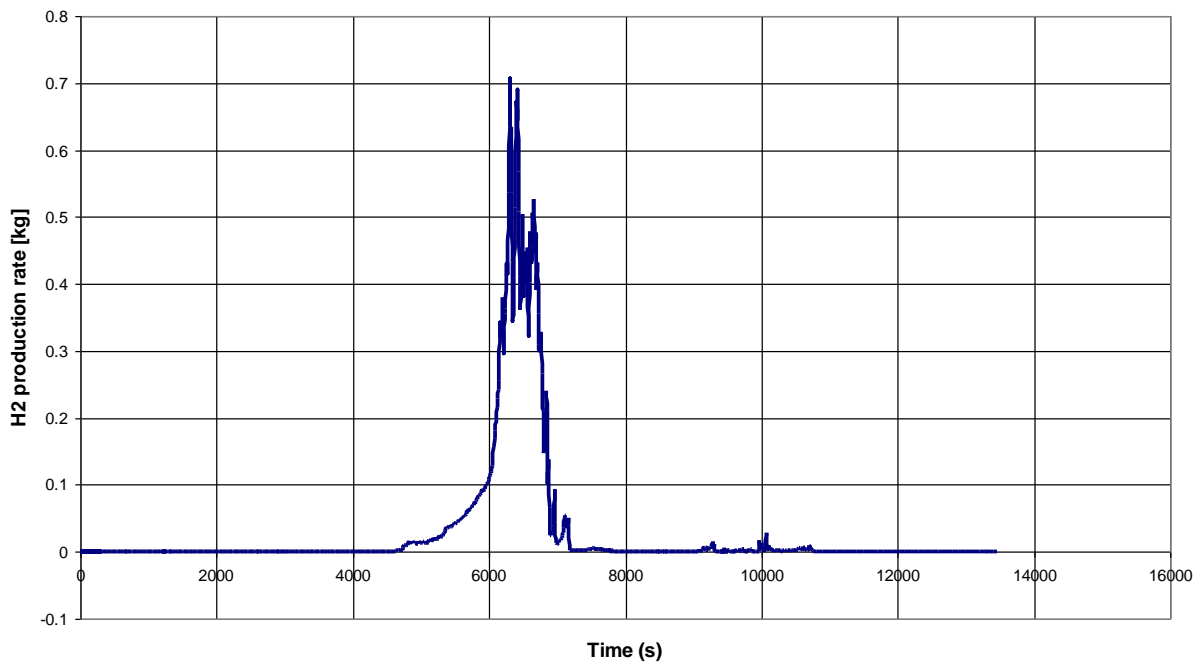



Figure 3.39: Sensitivity case A - Hydrogen production rate

 <b>Ricerca Sistema Elettrico</b>	<b>Sigla di identificazione</b>	<b>Rev.</b>	<b>Distrib.</b>	<b>Pag.</b>	<b>di</b>
	ADPFISS-LP1-054	0	L	45	106

### 3.4.3 Sensitivity case B

In the last sensitivity case the actuation of the HPI (15 kg/s of water at 413 K in both primary cold legs) is assumed to take place after 7300 s since the beginning of the transient, when a larger amount of about 20 tons of debris is evaluated to be formed as a consequence of core damage. The results are quite similar to previous sensitivity calculation and therefore in the following only the main differences will be discussed.

The primary pressure (Fig. 3.40) still shows a second pressurization peak following the HPI actuation. The maximum value of the pressure is now slightly higher (11.1 MPa) and also a larger timing is predicted for this peak. Reflooding of the core finally lead the primary pressure to a constant value of about 6.8 MPa, mainly affected by imposed secondary side pressure.

The actuation of the HPI causes a reduction of void fraction in both the cold legs of the primary system (Fig. 3.41) pointing out that, after core reflooding water is able to enter also the cold leg of primary loop A.

Heat transfer through the two steam generators (Fig. 3.42) still shows a weak inversion of heat transferred through steam generators up to temperature equilibration between primary and secondary systems, as a consequence of HPI actuation.

The mass of water in the primary system (Fig. 3.43) decreases with an almost constant rate during liquid flowrate through the break. After HPI the primary system inventory starts increasing again up to the value of about 120 tons after 9700 s, when water level reaches the break (Fig. 3.44), determining a new steady condition in the plant.

Core uncovering takes place in a very similar way as in the previous calculations (Fig. 3.45). Core level is still predicted to reach the bottom of the active fuel after 5700 s since the beginning of the transient, starts to increase again at about 7800 s and the core is completely reflooded in about 20 minutes.

The temperature trends in the cold legs (Fig. 3.46) and in the hot legs (Fig. 3.47) of the primary system is also similar to the previous cases up to HPI injection, after which an effective decrease of temperature up to saturation values is detected.

Relating to the fuel rod temperature in the central ring (Figures from 3.48 to 3.50), a similar behavior with respect to Sensitivity case A is predicted by MELCOR. The explanation of unexpected temperature increase in the lower zone of the fuel elements can be still found in the mismatch between decay heat still produced inside the fuel rod and removed power causes an increase of void fraction (Fig. 3.51) and a consequent additional degradation of heat transfer. Failure of lower zone of fuel rods leads to the complete relocation of the whole fuel element.

The amount of debris predicted to relocate towards the lower supporting plate (Fig. 3.52) and reaching the lower plenum (Fig. 3.53) is comparable with the quantity predicted

during the Sensitivity case A, even though with a slightly different timing. The HPI is anyway able to maintain the coolability of the degraded core.

The main oxidation phase still takes place (Fig. 3.54) between 4600 s and 7300 s since the beginning of the transient. The delay in the HPI actuation causes the generation of 418 kg of hydrogen (Fig. 3.55) as in the Sensitivity case A, while the maximum H<sub>2</sub> generation rate is still of about 0.7 kg/s at 6300 s (Fig. 3.56).

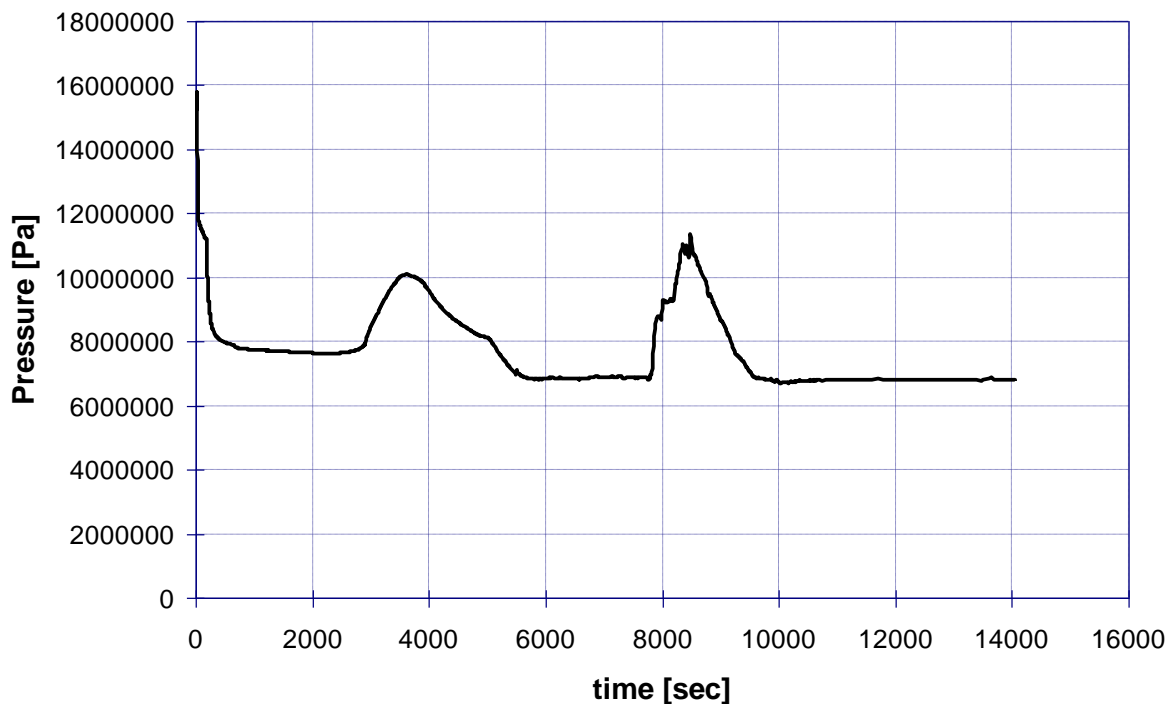


Figure 3.40: Sensitivity case B - Pressurizer pressure

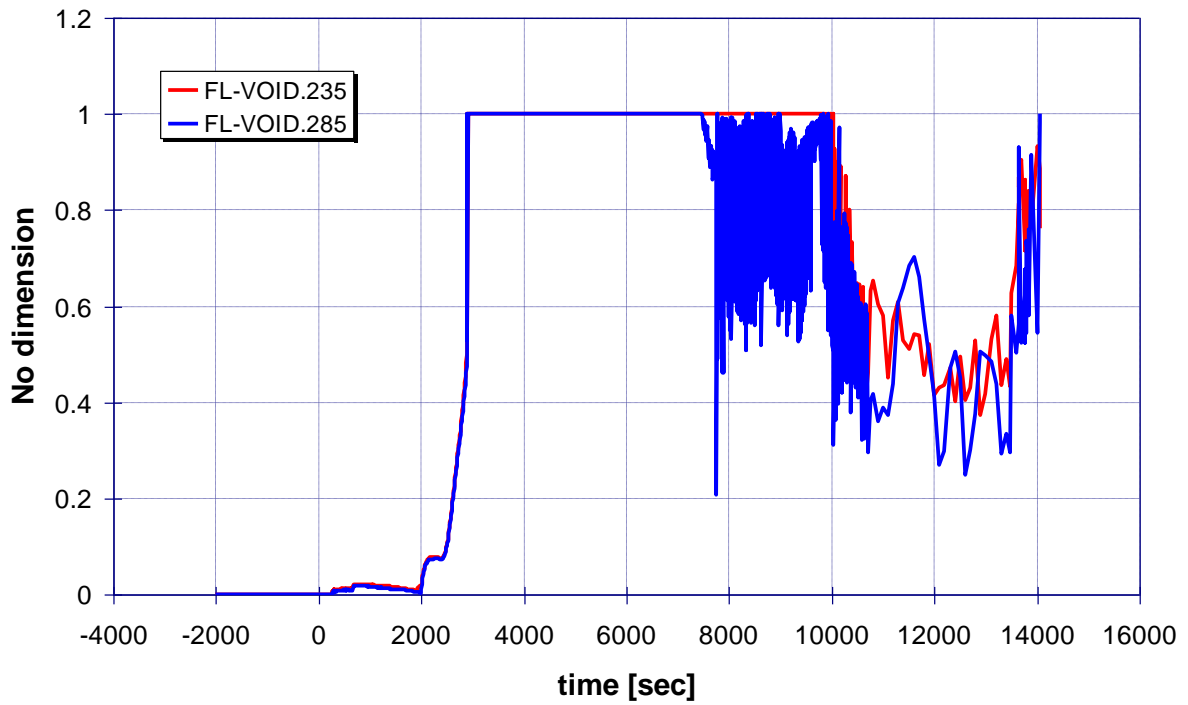


Figure 3.41: Sensitivity case B - Main pumps void fraction

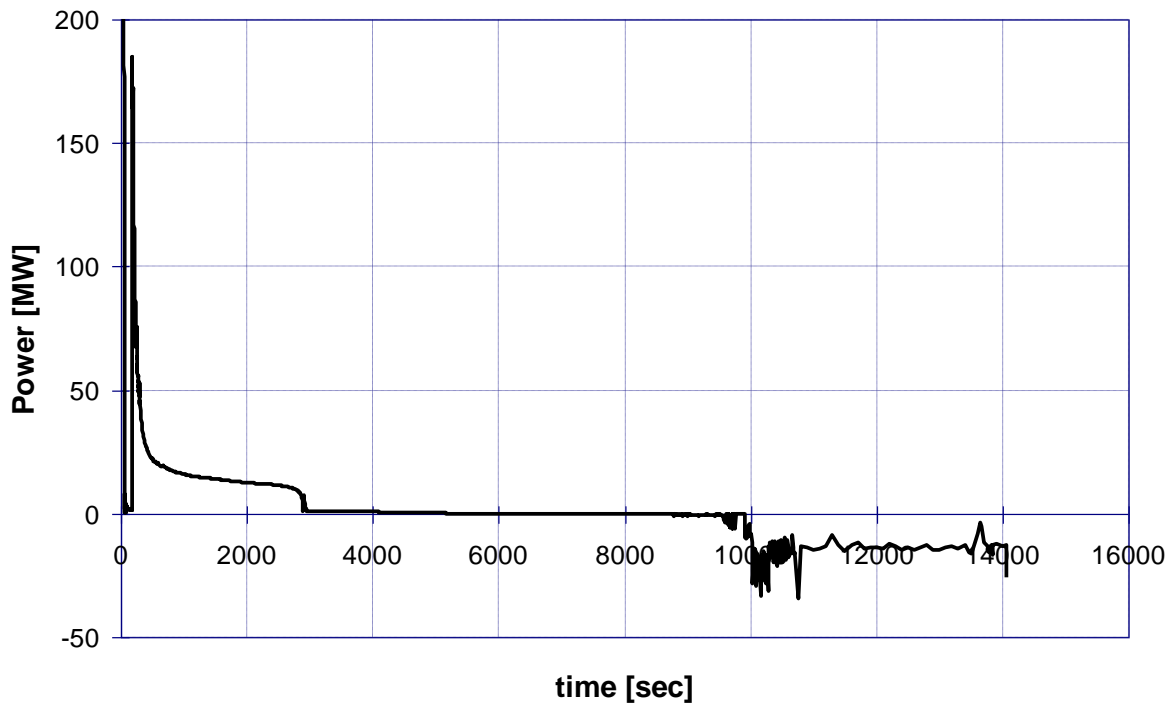


Figure 3.42: Sensitivity case B - Steam generator A removed power

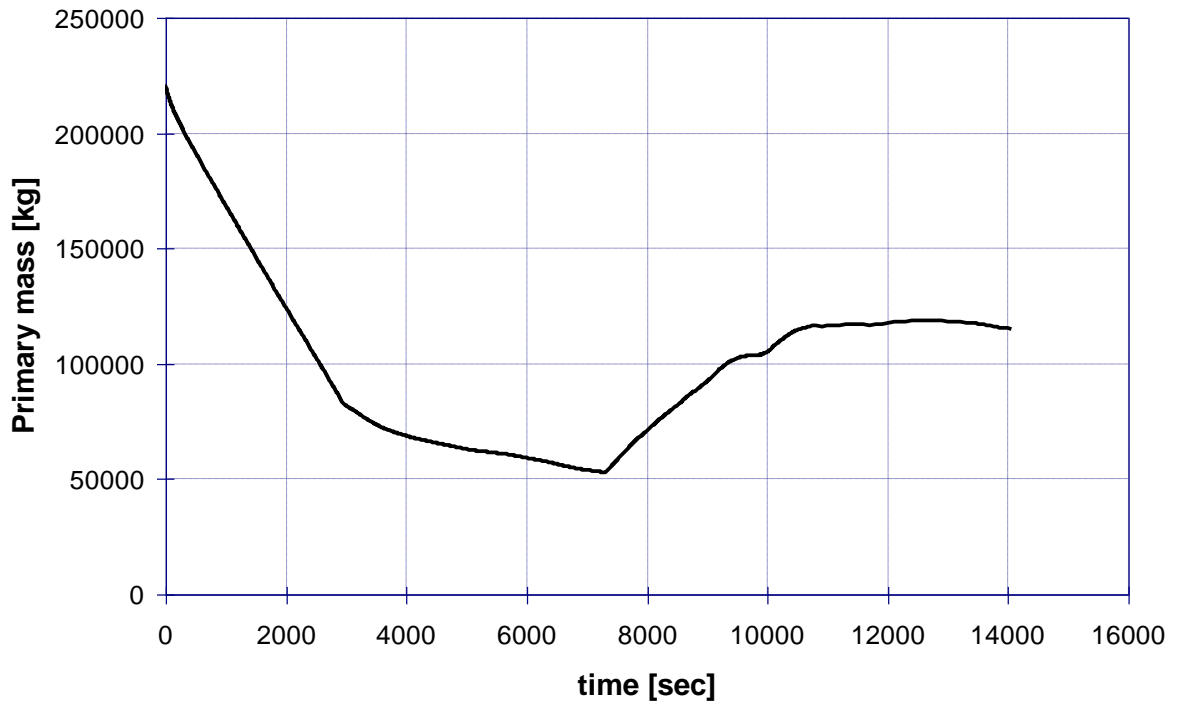


Figure 3.43: Sensitivity case B - Total primary water mass

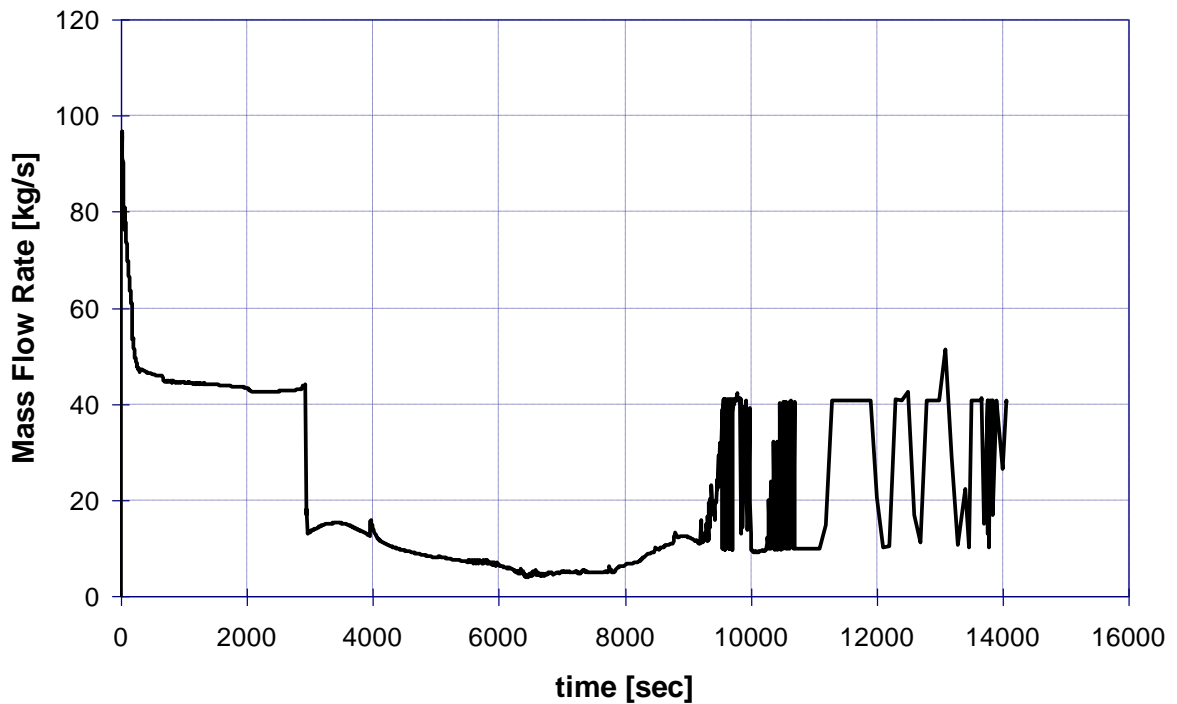


Figure 3.44: Sensitivity case B - Break mass flowrate

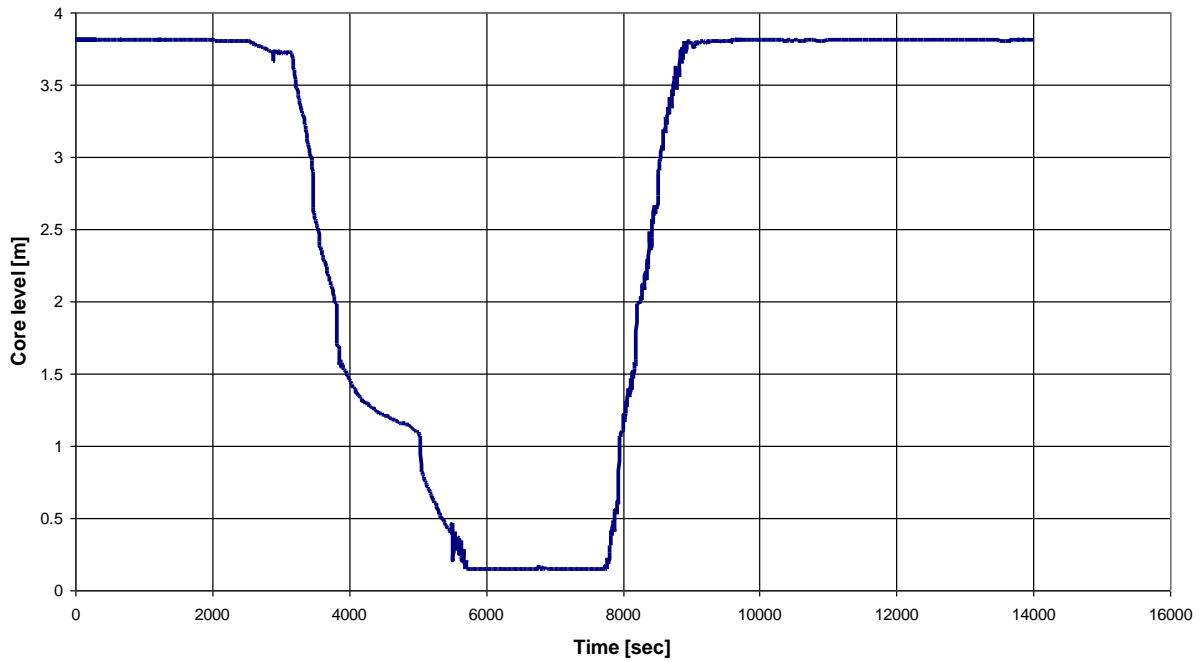


Figure 3.45: Sensitivity case B - Core collapsed water level

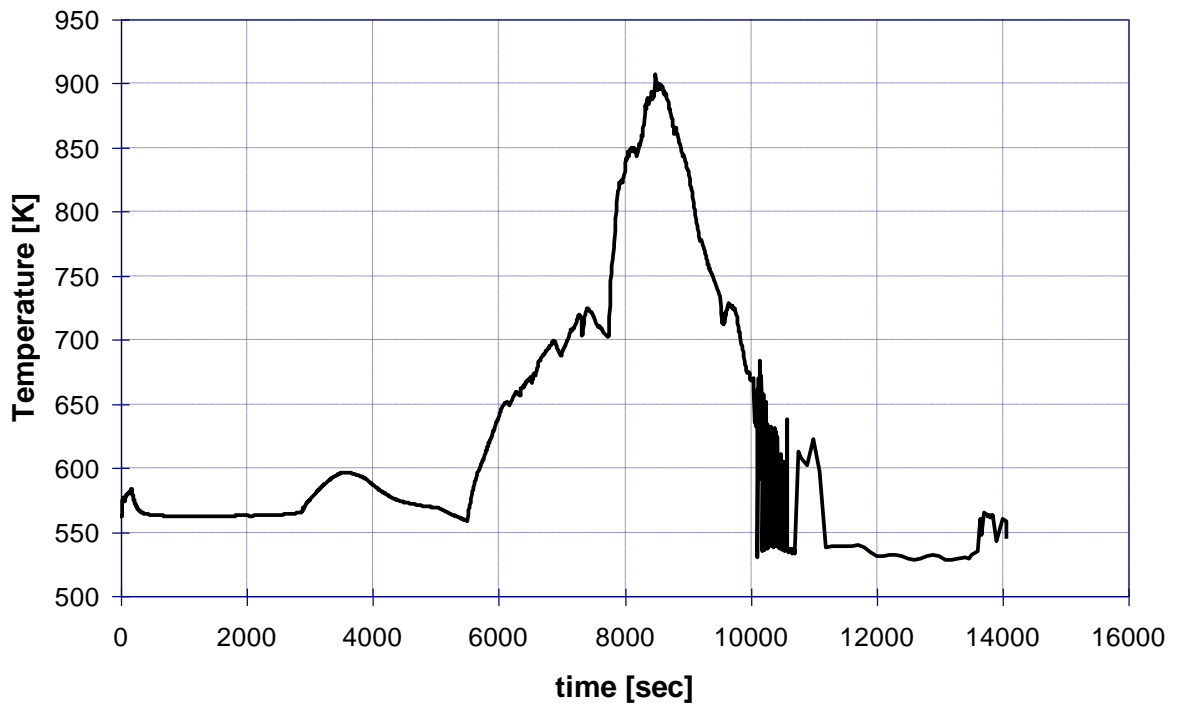


Figure 3.46: Sensitivity case B - Cold leg A temperature

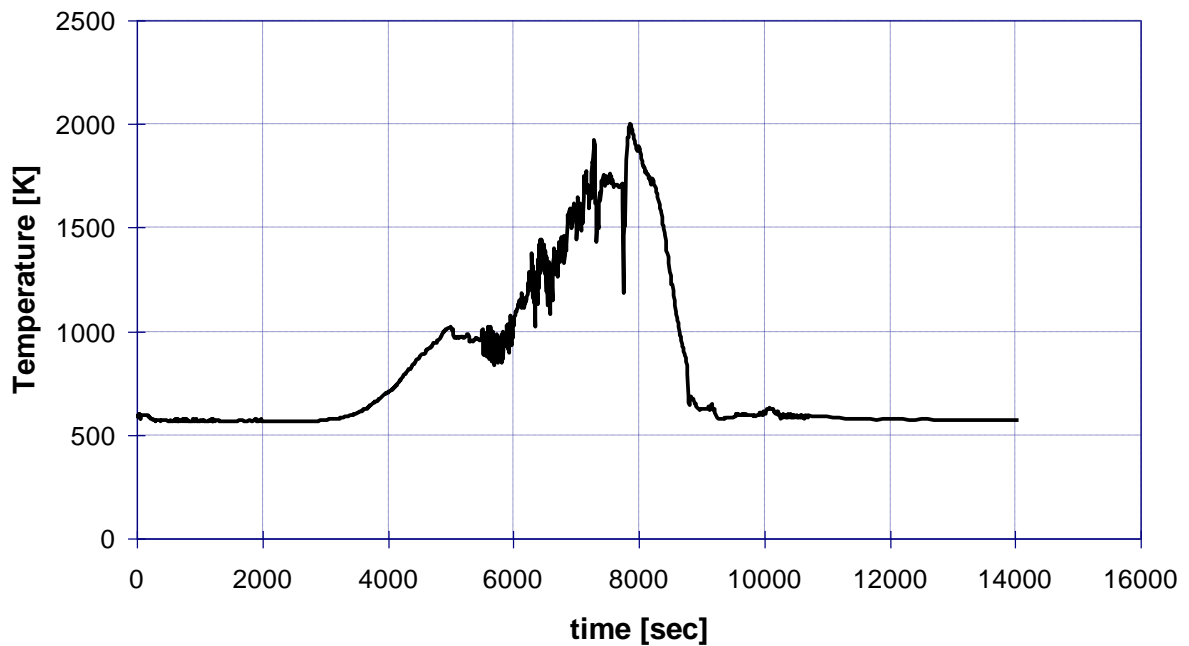


Figure 3.47: Sensitivity case B - Hot leg A temperature

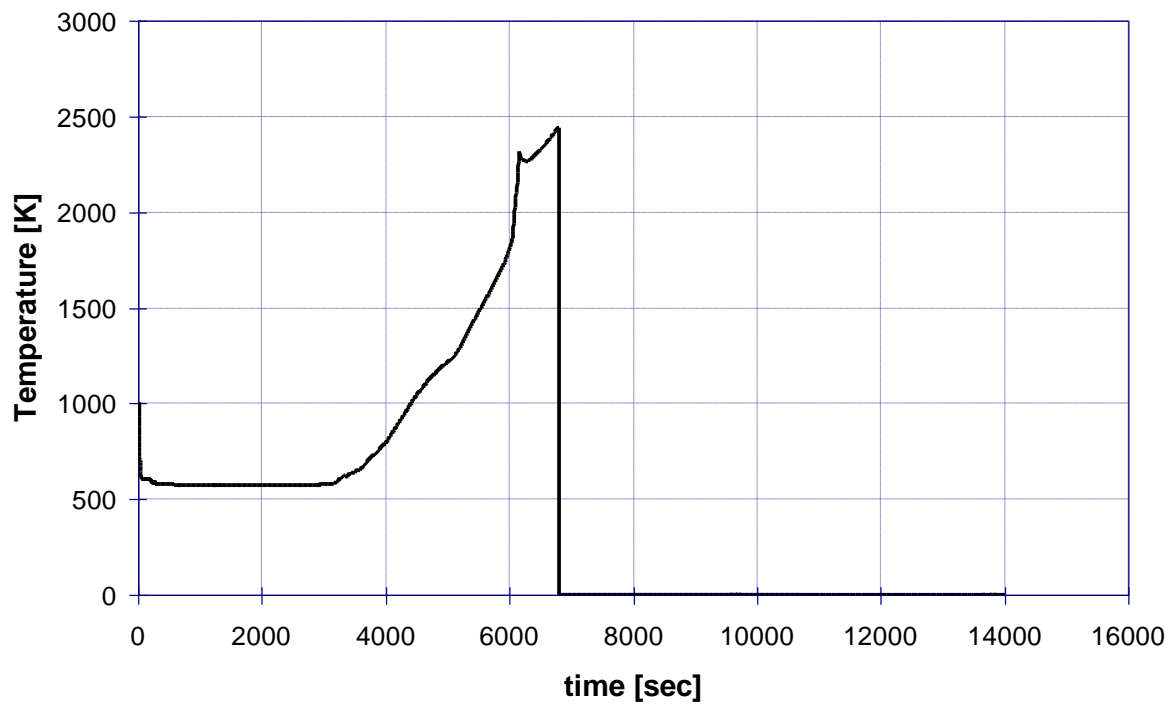


Figure 3.48: Sensitivity case B - Fuel rod temperature at the top of the core



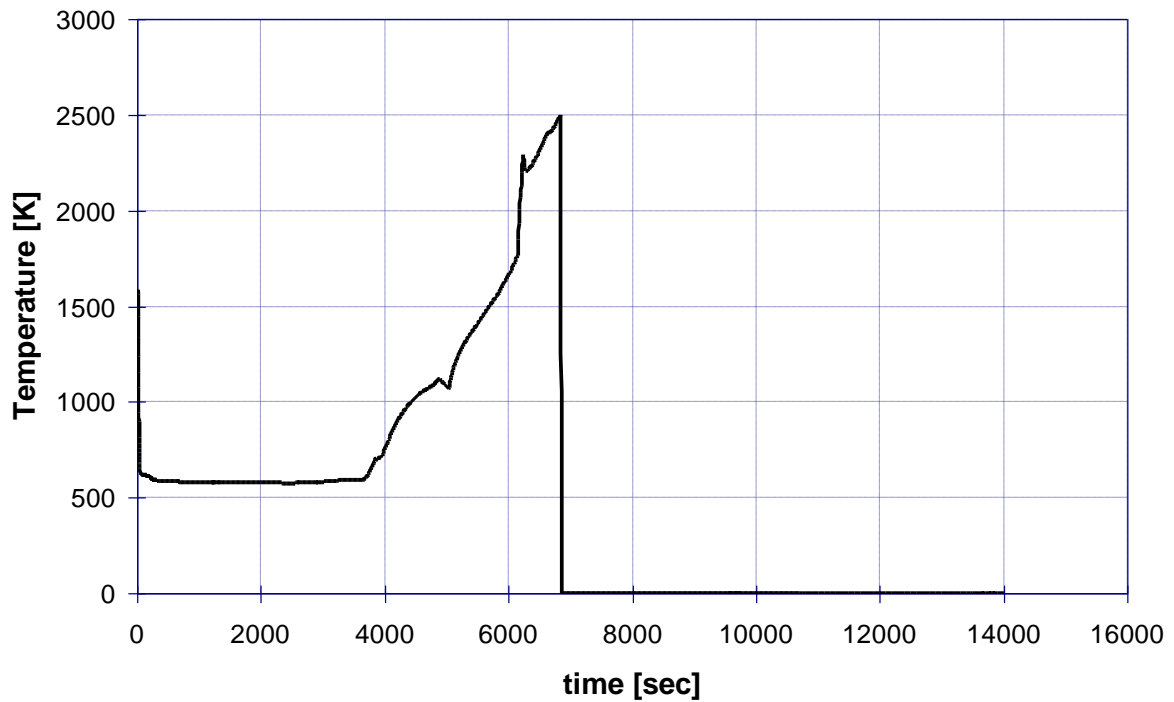


Figure 3.49: Sensitivity case B - Fuel rod temperature at the middle of the core

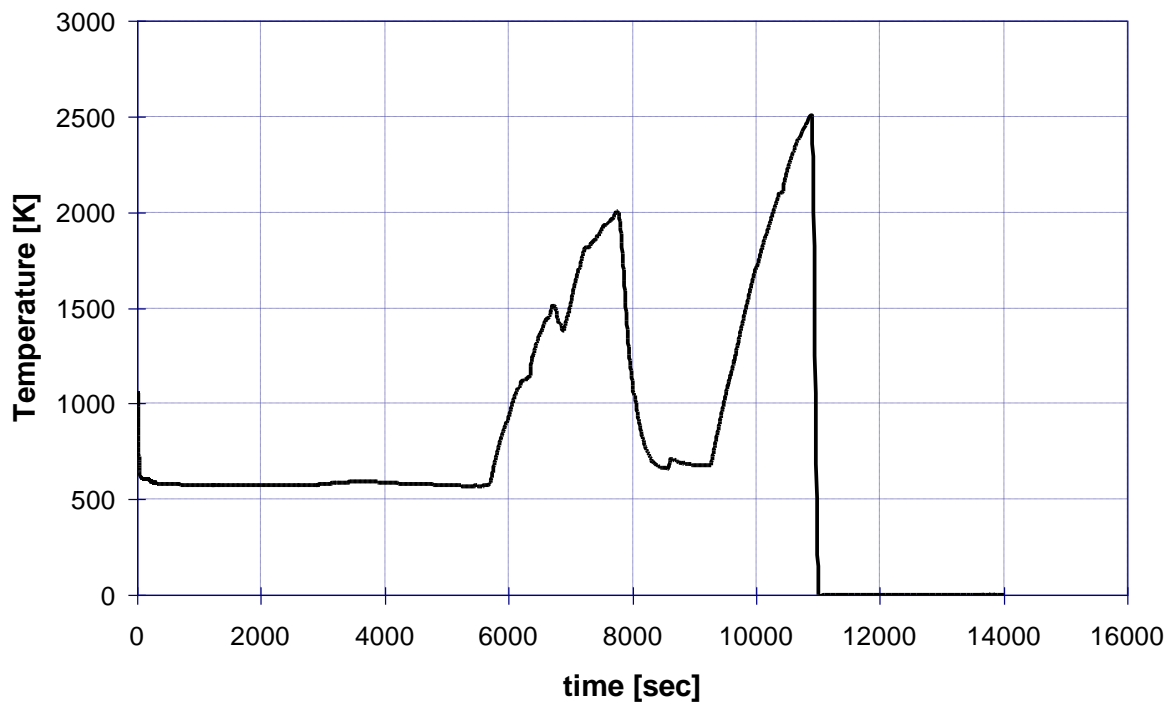


Figure 3.50: Sensitivity case B - Fuel rod temperature at the bottom of the core

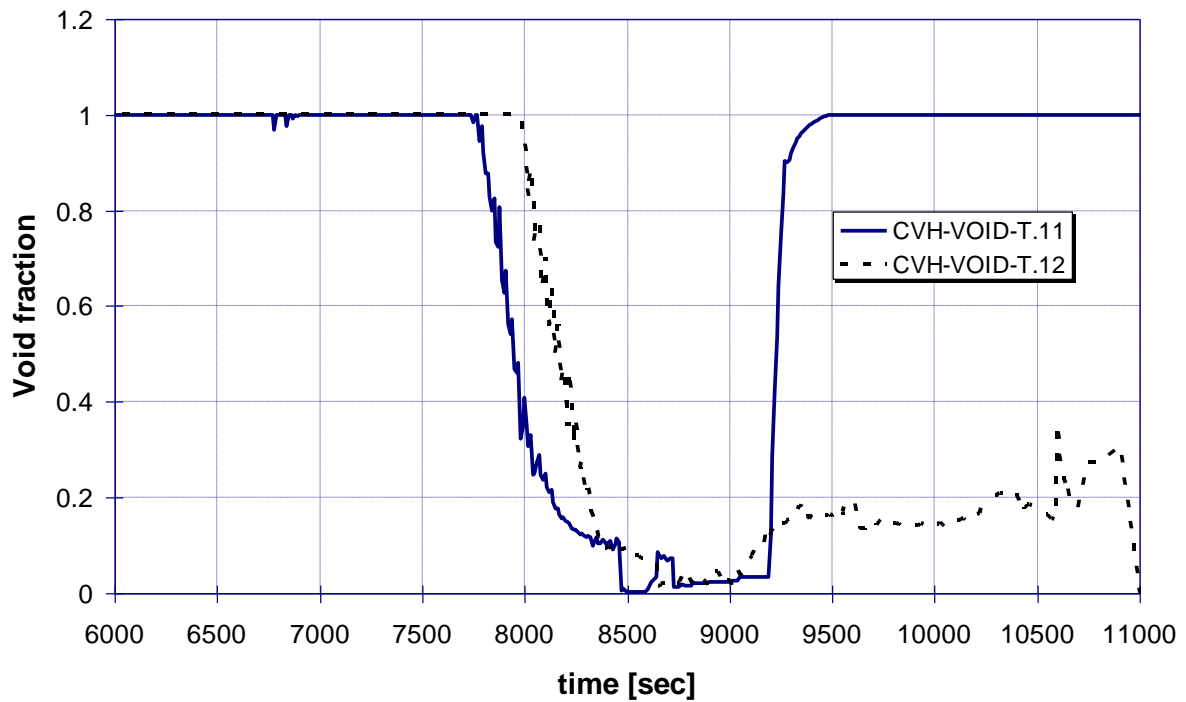


Figure 3.51: Sensitivity case B – void fraction in the central-lower part of the core

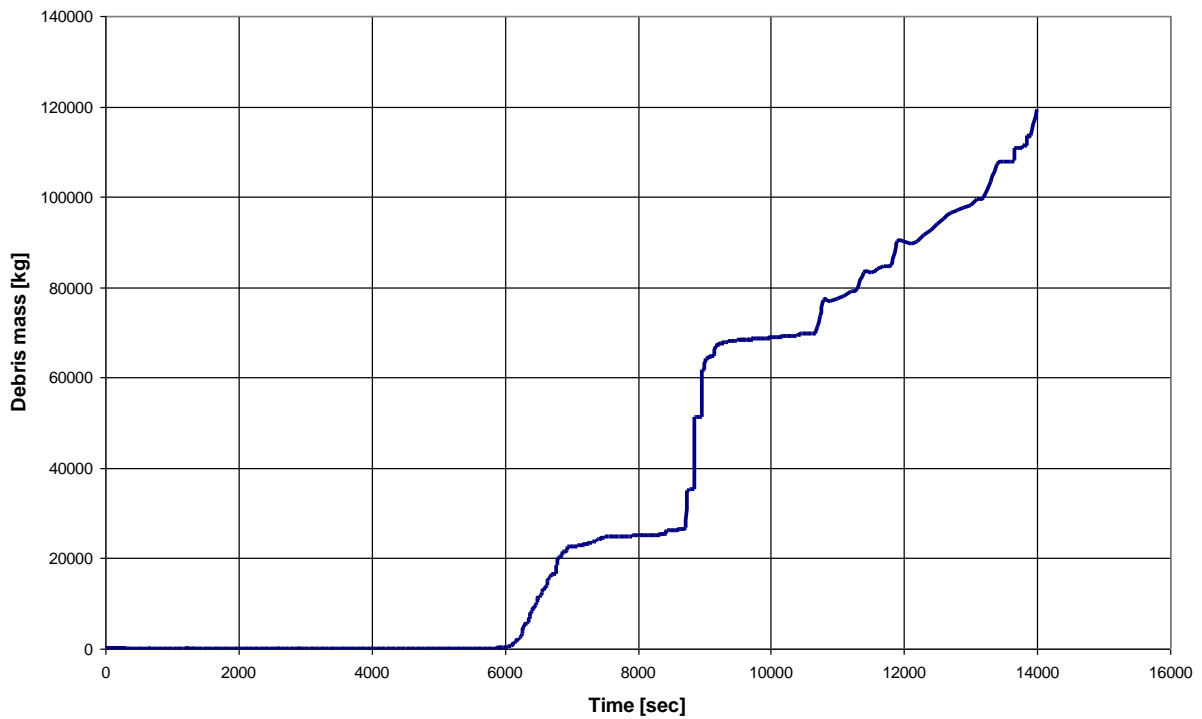


Figure 3.52: Sensitivity case B - total mass of debris in the core

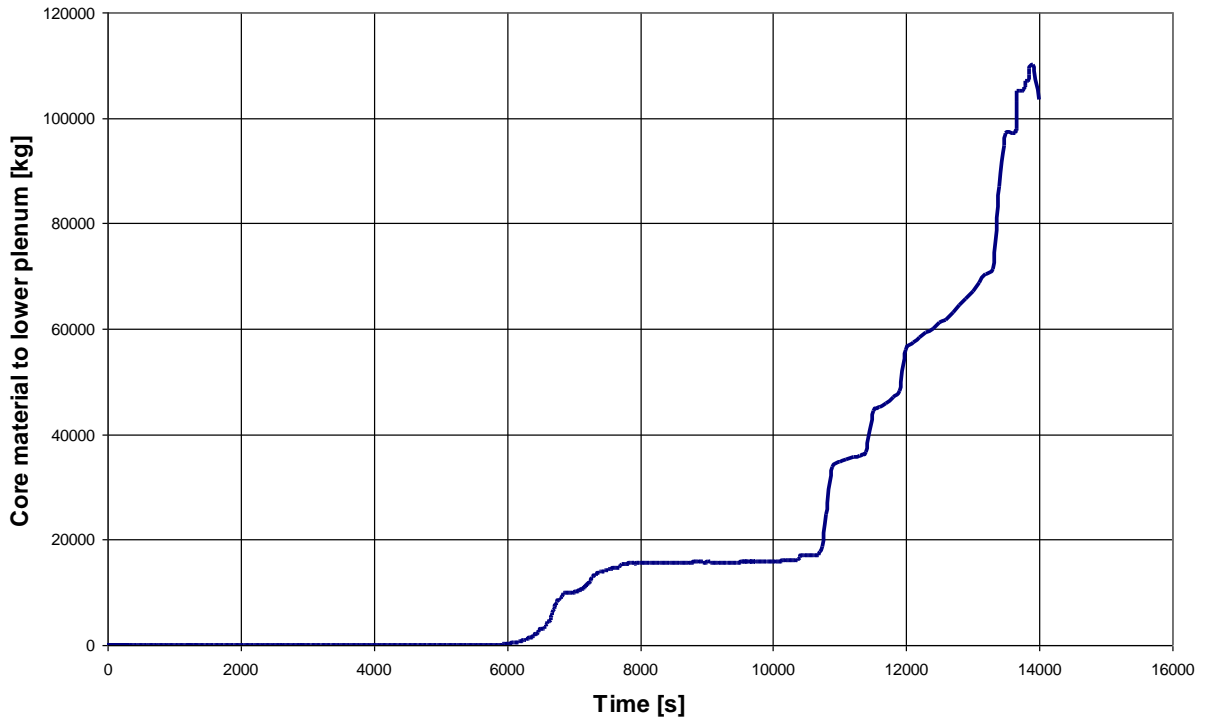


Figure 3.53: Sensitivity case B - total mass of core material reaching the lower plenum

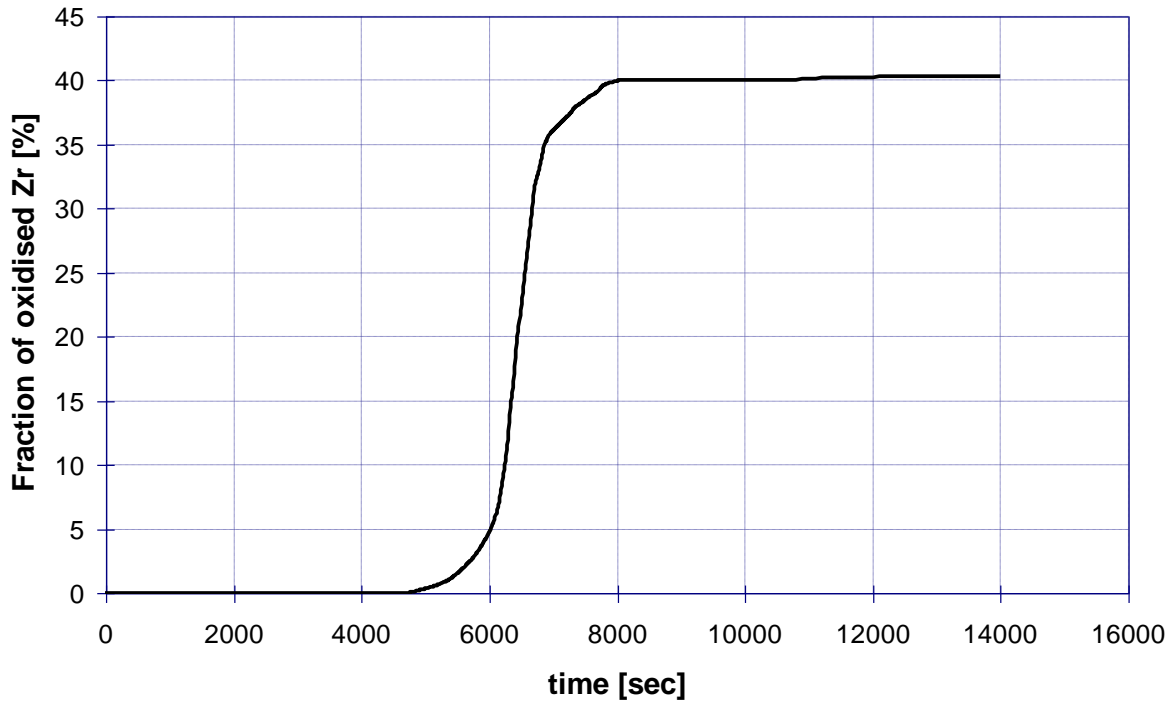


Figure 3.54: Sensitivity case B - fraction of oxidised Zr

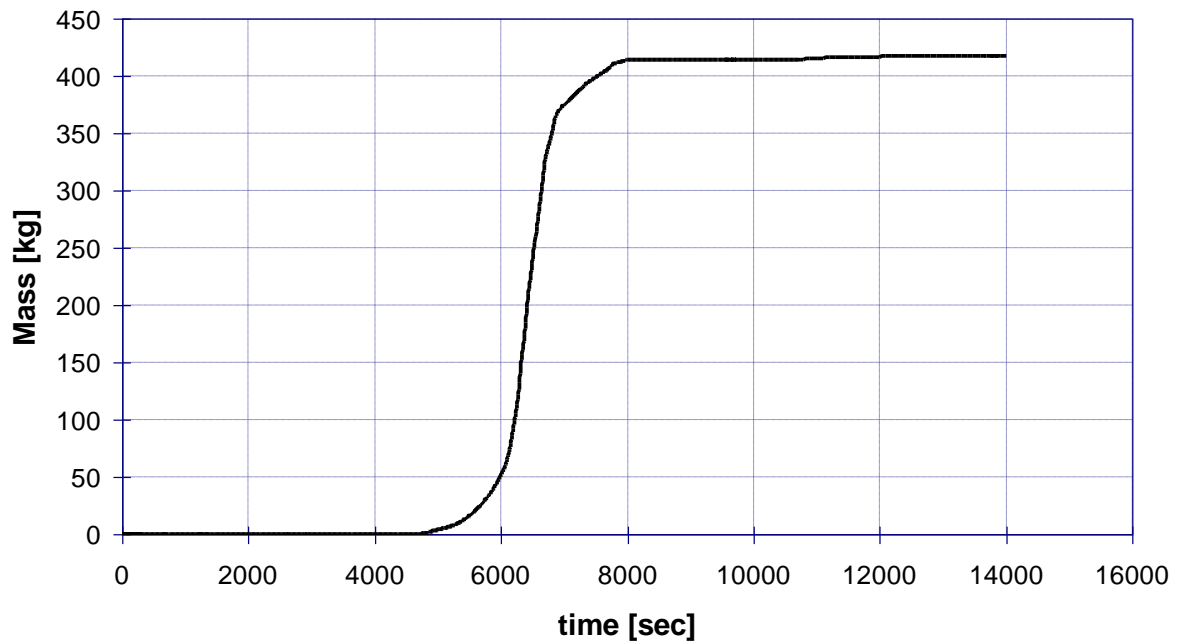


Figure 3.55: Sensitivity case B - Cumulated mass of Hydrogen

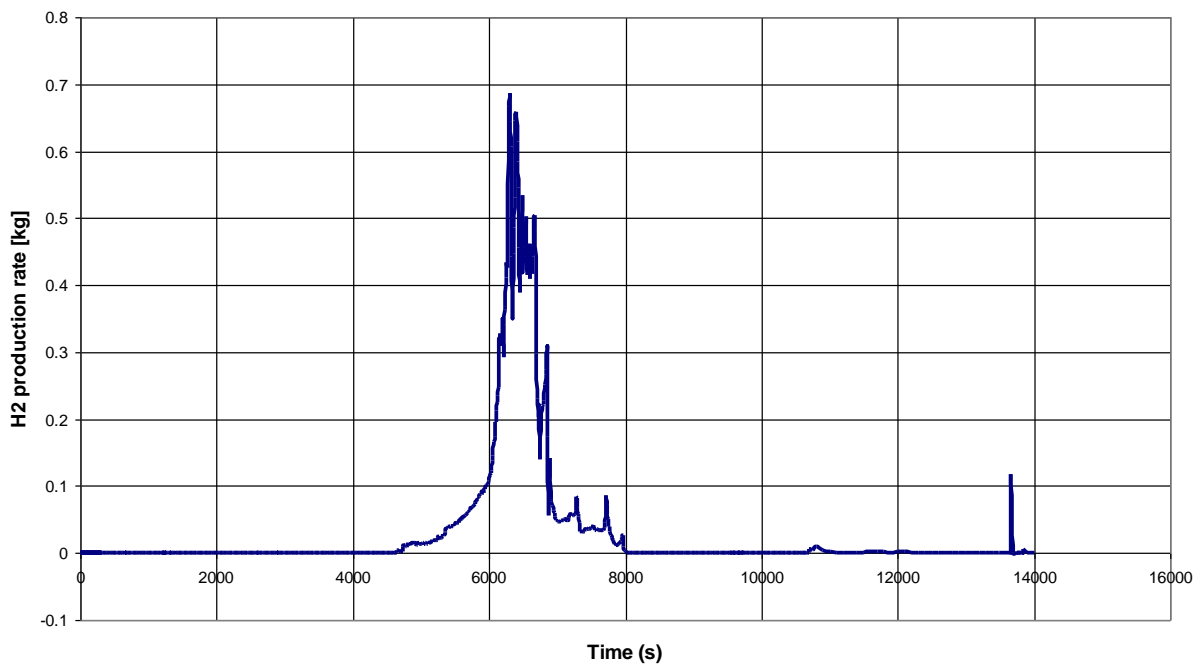



Figure 3.56: Sensitivity case B - Hydrogen production rate

 <b>Ricerca Sistema Elettrico</b>	<b>Sigla di identificazione</b>	<b>Rev.</b>	<b>Distrib.</b>	<b>Pag.</b>	<b>di</b>
	ADPFISS-LP1-054	0	L	55	106

### 3.5 Final remarks


The results obtained using the MELCOR 1.8.6 code in the simulation of a reference severe accident scenario with prescribed boundary conditions have been presented and analyzed. This exercise follows a similar activity promoted by NEA 30 years ago to assess the capacity of current codes to predict severe accidents. In order to allow for a comparison with other codes results, a reference severe accident scenario, starting with a small break LOCA with prescribed boundary conditions was defined. The transient is supposed to take place in a plant similar to the TMI-2 reactor and a model of the primary system of this plant was set up for MELCOR. Moreover some parameters allowing for judging the quality of the predicted results were proposed, in order to assess the quality of the code results and the effect of the code user.

The same nodalization used to simulate the first two phases of the TMI-2 accident has been used for this benchmark, with proper boundary conditions. Moreover, minor changes were performed with respect to this benchmark, in order to reduce stratification in the primary side and improve heat transfer through steam generators. Particular attention was devoted to the modelling of the primary vessel, in order to allow natural circulation flows, which TMI-2 evidence showed as extremely important in the correct simulation of core degradation. A refinement of the primary system model has been set up in order to obtain a better agreement with the results showed in a previous comparison with the ASTEC code. The goal was to investigate the severe phase of the transient, starting from similar physical conditions and time histories. Also, for the degradation phase particular care was devoted to choose similar conditions and models for the two codes.

A sensitivity analysis has also been performed aimed to investigate the effect of a delayed actuation of HPI (something similar to actual TMI accident) on the core damage progress and vessel integrity.


Some weaknesses of the MELCOR code have been identified in this context. During the initial phase of core reflooding an unexpected increase of the temperature of the lower zone of the fuel rods is predicted and the failure limit is reached with a subsequent relocation of the fuel rod towards the core supporting plate. The COR package of MELCOR contains several simple models that consider the structural integrity and support of intact components, and convert them to particulate debris when either is lost. Most are logical models rather than structural models; no stress calculations are performed for any component other than supporting structure. Complex debris formation mechanisms, such as quench-induced shattering, have not been implemented into the COR package at this time.

The reason of the predicted degradation is due to an insufficient rewetting of the fuel rods, along with a contemporary degradation of natural circulation flows due to partial blockage of core flow paths. In spite of this larger core damage, the actuation (even with a larger delay) of the HPI assures the safe removal of decay heat from the debris, preventing any damage to the primary vessel.

 <b>Ricerca Sistema Elettrico</b>	<b>Sigla di identificazione</b>	<b>Rev.</b>	<b>Distrib.</b>	<b>Pag.</b>	<b>di</b>
	ADPFISS-LP1-054	0	L	56	106

## References

- 3.1. MELCOR Computer Code Manuals – Vol. 1 Primer and Users’ Guide Version 1.8.6 September 2005 - R. O. Gauntt, J.E. Cash, R. K. Cole et al. - NUREG/CR-6119, Vol. 1, Rev. 3 - SAND 2005-5713.
- 3.2. G. Bandini, M. Di Giuli, M. Sumini, A. Manfredini, W. Ambrosini – Lessons Learned from the Result Comparison of a Reference Severe Accident Sequence on a TMI2-like Reactor of 900 MWe Power with the Integral Codes ASTEC and MELCOR – ENEA - ADPFISS - LP1 – 032 – Settembre 2014.
- 3.3. K. N. Ivanov, T. M. Beam, A. J. Baratta, “Pressurized Water Reactor Main Steam Line Break (MSLB) Benchmark”, Volume 1: Final Specifications, NEA/NSC/DOC(99)8, April 1999.

 <b>Ricerca Sistema Elettrico</b>	<b>Sigla di identificazione</b>	<b>Rev.</b>	<b>Distrib.</b>	<b>Pag.</b>	<b>di</b>
	ADPFISS-LP1-054	0	L	57	106

## 4. ASTEC calculations

In this section, three different severe accident sequences are investigated using the ASTEC integral code. The input deck adopted is the same reactor model realized to simulate the real TMI-2 accident. All severe accident scenarios selected starting with a Small Break Loss-Of-Coolant Accident (SBLOCA) on the hot leg and loss of main feedwater to the steam generators, but the recovery phases are different. In the first calculation, no operator intervention was taken into account. In the other two simulations, different timings of operator actions to start HPIS injection were assumed. Among the topics of interest in this work, there are:


- understanding how the adoption of different ‘tunable’ parameters or models can affect the simulation results;
- verifying the capability of the ASTEC code, to simulate the accident management actions and associated plant response in case of core reflooding;

In order to enhance the first topic, the no reflooding scenario has been supported by sensitivity studies, to estimate the overall uncertainties of the results. Starting from a reference case, six different physical parameters were modify separately, and their effect on the results has been examined. To assess the ASTEC code capability on simulating reflooding transients, two distinct calculations, with different core degradation states, have been performed and the results discussed.

### 4.1 Brief description of the ASTEC code

The Accident Source Term Evaluation Code (ASTEC) is a severe accident code developed in common by IRSN and GRS [4.1]. The code calculates the transient sequences from the initiator events until the eventual radioactive fission product releases to the atmosphere, named source term. The ASTEC code is mainly used for safety analyses on nuclear installations and development/specification of severe accidents management guidelines. The code includes several coupled modules that can deal with the different severe accident phenomena: thermal-hydraulics in the reactor system, core degradation and melt release, fission product release and transport, ex-vessel corium interaction, aerosols behavior and iodine chemistry in the containment, etc. Among them, the CESAR module is used to compute the thermal-hydraulics in the primary and secondary systems of the reactor [4.2]. Such module is coupled to the ICARE2 module that computes core degradation, melt relocation and behavior in the lower head up to vessel failure. The CESAR module allows a detailed representation of all components of primary and secondary circuits including auxiliary, emergency and control systems [4.3].

CESAR is a two-phase flow thermal-hydraulic code. The gas phase can be a mixture of steam and hydrogen. The solution of the problem is based on two mass equations, two energy equations, one equation for steam velocity, and a drift flux correlation for water velocity. The state variables computed by CESAR are: total pressure, void fraction, steam and

 <b>Ricerca Sistema Elettrico</b>	<b>Sigla di identificazione</b>	<b>Rev.</b>	<b>Distrib.</b>	<b>Pag.</b>	<b>di</b>
	ADPFISS–LP1-054	0	L	58	106

water temperature, steam and water velocity, and partial pressure of hydrogen. All hydraulics components can be discretized by volumes (one mesh) or axial meshed volumes and connected by junctions. The volumes can be homogeneous or with a swollen level. Thermal structures are used to model the walls of the components, and compute thermal heat exchange between primary and secondary systems and heat losses to the environment.

The ICARE2 module can simulate the thermal-hydraulics in the part of the vessel below the top of the core: downcomer, lower plenum and the core itself including the core bypass. The model of the lower head of ICARE2 has one single mesh for fluids, three layers for corium (pool, metal and debris), and a 2D meshing for the vessel. The ICARE2 [4.4] module is activated to compute core heatup and degradation, in coupled mode with CESAR, at the onset of core uncovering. Before ICARE2 activation, the thermal-hydraulics in the vessel and the core is computed by CESAR through an automatic vessel model creation based on ICARE2 input deck. The convective and radiative heat exchanges between core components and structures are computed by ICARE2.

Most important core degradation phenomena are dealt with in ICARE2 [4.5] including: core material oxidation and hydrogen generation, control rod material interaction, melting and relocation, zircaloy clad melting and fuel dissolution, fuel rod clad failure and metallic melt relocation, debris bed and molten pool formation and spreading in the late degradation phase. When corium accumulates in the lower plenum, three 0-D layers are represented: oxide, metals, and debris. The heat transfers between neighboring layers, between layers and vessel walls or residual water, use recent literature correlations, depending on layer mean temperature and power. Then, the corium layers heat up the lower head until its possible melt-through or mechanical failure (by plasticity, creep, etc.).


## 4.2 TMI-2 reactor ASTEC model

The input data for ASTEC V2r2p2 code was prepared to simulate only in-vessel phenomena. In order to perform this kind of simulation, two ASTEC modules were activated:

- CESAR to simulate the thermal-hydraulics in the RCS, secondary circuit and vessel (with simplified core modelling) up to the beginning of core degradation phase;
- ICARE to simulate in-vessel core degradation phenomena, and thermal-hydraulics in the reactor vessel during this phase;

The drawing of the Babcock and Wilcox lowered loop plant and the graphical representation of the ASTEC primary and secondary circuits are given in Fig. 4.1 and Fig. 4.2 respectively. In the spirit of the way in which ASTEC is typically used in plant applications, a comparatively simple hydraulic model is used, with standard or default code model options and parameter values to represent the RCS. Indeed, the primary part of the RCS input model is a coarse node representation of the hydraulic system and structures comprising about 39 hydraulic control volumes, of which 22 cells are used for the shell side



 <b>Ricerca Sistema Elettrico</b>	<b>Sigla di identificazione</b>	<b>Rev.</b>	<b>Distrib.</b>	<b>Pag.</b>	<b>di</b>
	ADPFISS-LP1-054	0	L	59	106

of the steam generators. The secondary circuits is nodalized in 30 fluid meshes. The plant simulation includes a detailed modelling of the primary coolant system with:

- reactor pressure vessel volumes and structures, including the VENT valve between the cold collector and the hot collector,
- two primary coolant loops (1 hot leg and 2 cold legs in each loop) with once-through steam generators and main coolant pumps,
- pressurizer with surge-line, PORV, heaters, spray-line and valve,
- main emergency and control systems.

The modelling of the secondary systems is limited to the pipe side of the steam generators, the steam lines with isolation valves, and main feedwater and auxiliary feedwater injections. The simplified reactor vessel adopted by CESAR, to compute the steady state conditions, consists of four volumes: the core, bypass, downcomer and lower plenum, each of these volumes is divided into 20 axial row. The ICARE core model shares the same volumes and axial nodalization with the CESAR simplified model, but in this case, the core is further subdivided by 6 radial rings for a total of 161 mesh. In each ring, only one representative component of the fuel and control rods is considered, weighted by the number of rods. The baffle, the barrel and the thermal shield at the core periphery are also represented. The control rod component simulates all the full and part-length control rods, all the guide tubes (including those containing burnable poison rods) and all the instrument tubes. Mass and energy rates of change for core materials are calculated for each core node. The radial peaking factor are fixed for each ring, and an axial peaking factor is assigned for each row.

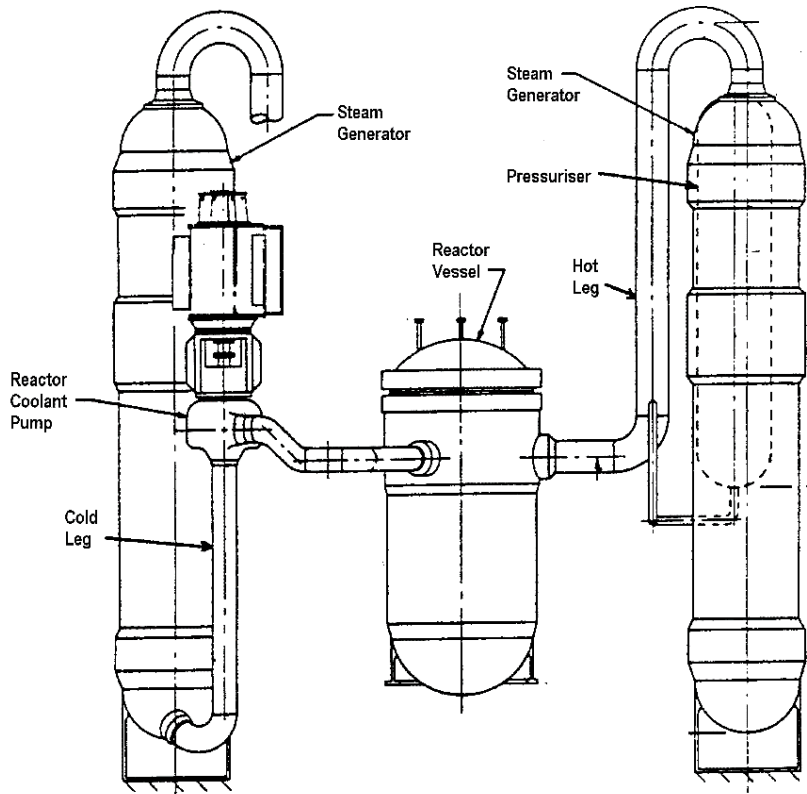


Figure 4.1: Babcock & Wilcox Lowered loop

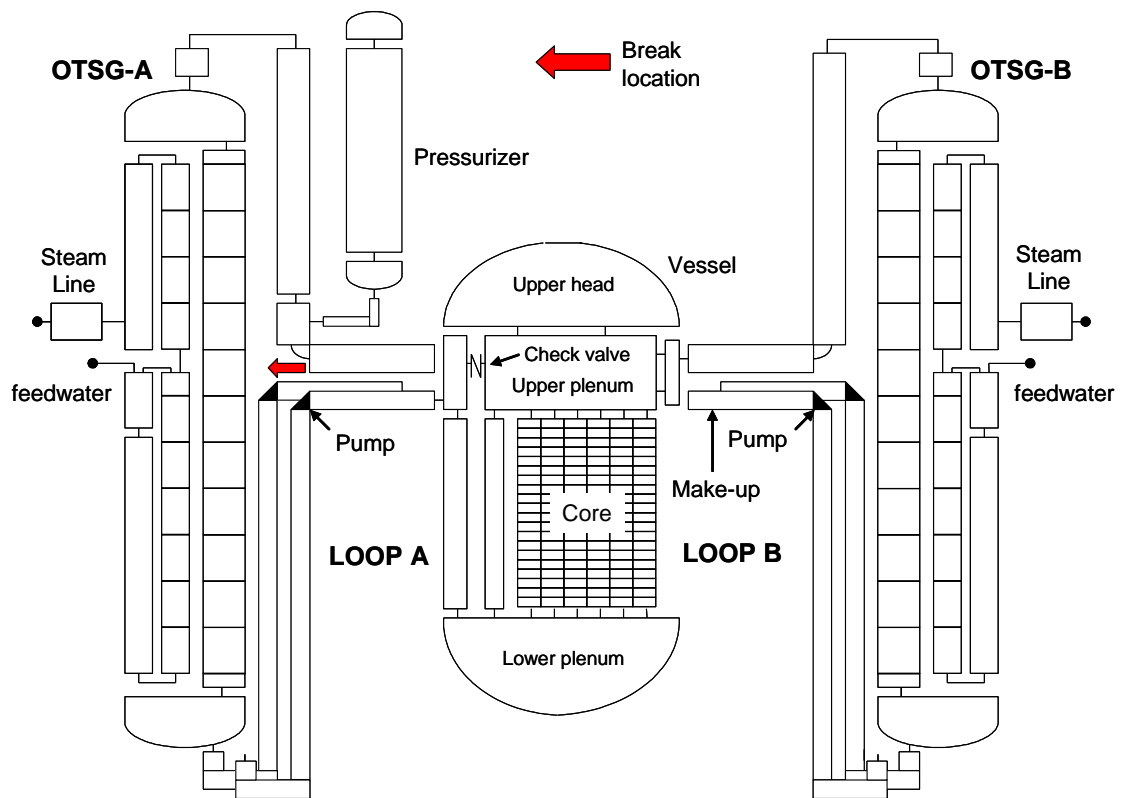


Figure 4.2: Babcock & Wilcox ASTEC nodalization

### 4.3 Reference scenario and sensitivity analysis

Depending on the level of accuracy that is needed, the modelling options may be crucial for each one of the physical processes occurring during a severe accident. However, despite the diversity and complexity of the phenomena, a few models will have a much stronger impact than others will on the relevance and accuracy of the calculation. Therefore, to summarize the importance of the choice of models, it is necessary pay very careful attention to:

- Thermo-hydraulics: The ASTEC code usually assumes a simplified thermo-hydraulic model for the primary circuit while inside the vessel, does not compute the flow pattern according to the changes of geometry and porosity in the core and to the flow regime. This assumption may lead to inconsistent results. In this sensitivity analysis, the only thermo-hydraulic parameter studied is the COLLAPSE model. In the reference case (COLLAPSE =0) the void fraction at the break is the same of the control volume while if the specific model is activated (COLLAPSE =2) , it takes into account the position of the collapsed water level in the control volume compared to the position of the break.
- Zircaloy oxidation model: The reference case adopts the BEST-FIT correlation, which consist of the use of the Cathcart-Pawel model in the low temperature range and of the Prater-Courtright model in the high temperature range. For the sensitivity analysis the applied model will be the Urbanick-Heidrick on all the temperature range.
- Melt progression: The ICARE module of ASTEC consider several modes of material relocation (rod candling, fuel melting and collapse and 2D relocation of the corium material). The ICARE module uses lump model for zircaloy and fuel melting phases together. The modelling of cladding failure, which determines the start of relocation, is also very important, it can depend on two parameters the temperature and the thickness of zirconium dioxide. In the sensitivity analysis the Zr-UO<sub>2</sub> temperature was increased to 2800 K versus 2550 K of the reference case, and the cladding failure criteria were modified,  $T_{clad} > 2350$  K and ZrO<sub>2</sub> thickness  $< 100$   $\mu\text{m}$  versus  $T_{clad} > 2300$  K for ZrO<sub>2</sub> thickness  $< 300$   $\mu\text{m}$  or  $T > 2500$  K for ZrO<sub>2</sub> thickness  $> 300$   $\mu\text{m}$
- Debris formation: The reference case uses the magma macro-component and takes into account the formation of a debris bed by mean of the DEBRIS model the activation. In this case, the user can define the threshold values of some variables, which, once achieved, will lead to the debris bed collapse. The temperature chosen for the reference case was  $T_{\text{DEBRIS-FORMATION}} > 2500$  K versus the  $T_{\text{DEBRIS-FORMATION}} > 3100$  K for the sensitivity study.

- Failure model of the lower plenum: In the reference case the failure criterion adopted is the total fusion of the lower head wall, while in the sensitivity case studied it was used a creep criterion for the failure of the vessel lower head

Table 4.1 summarizes the models used in the reference case and the parameters and criteria utilized for the sensitivity analysis.

Table 4.1: In-vessel core degradation parameters/criteria

	<b>ASTEC Reference case</b>	<b>ASTEC Parameters for sensitivity analysis</b>
Zircaloy oxidation kinetics	BEST-FIT correlation: Cathcart-Pawel in the low temperature range and Prater-Courtright in the high temperature range	Urbanick Heidrick
Cladding failure criteria	$T_{clad} > 2300 \text{ K}$ and $ZrO_2$ thickness $< 300 \mu\text{m}$ ; or $T > 2500 \text{ K}$	$T_{clad} > 2350 \text{ K}$ and $ZrO_2$ thickness $< 100 \mu\text{m}$
Melting point of $UO_2$ - $ZrO_2$ ceramic material	$UO_2$ $T_m = 2550 \text{ K}$ and $ZrO_2$ $T_m = 2550 \text{ K}$ (Phébus test)	$UO_2$ $T_m = 2800 \text{ K}$ and $ZrO_2$ $T_m = 2800 \text{ K}$
Debris formation criteria	Fuel rod temperature $> 2500 \text{ K}$	Fuel rod temperature $> 3100 \text{ K}$ $UO_2$ $T_m = 3100 \text{ K}$
Molten core relocation into the lower plenum	Baffle melting (relocation through core by-pass) or melting at core bottom (relocation through core support plate)	Baffle melting (relocation through core by-pass) or melting at core bottom (relocation through core support plate)
Reactor pressure vessel failure	Vessel wall melting (100%)	Creep-rupture failure criterion

#### 4.3.1 Calculation results

The Table 4.2 illustrates the different cases studied, in the sensitivity analysis. Five out of six ‘tunable’ parameters concern the degradation process, the last one the thermo-hydraulic one.

Table 4.2: Cases analyzed

CALCULATIONS	ASTEC
Old reference case	PAR-2013 input deck
Sensitivity case 1 (oxidation correlation criteria)	Yes
Sensitivity case 2 (clad failure criteria)	Yes
Sensitivity case 3 (UO <sub>2</sub> -ZrO <sub>2</sub> melting point criteria)	Yes
Sensitivity case 4 (debris formation criteria)	Yes
Sensitivity case 5 (vessel failure criteria)	Yes
Sensitivity case 6 (COLLAPSE = 2 criteria)	Yes

As it is possible to see in Fig. 4.3 and Fig. 4.4, the selected parameters do not affect the thermal-hydraulic of the coolant in the primary circuit but one, the case, 6, which predicts a steam release only after about 2700 s, versus 500 s of the other cases. This difference is entirely due to the distinct collapse model at the break. However, observing the RCS water inventory evolution in Fig. 4.5, and in particular in the first 3000 s, the time range of interest, it seems that the collapse model does not strongly affect, the emptying time of the RCS. Concerning the pressurizer pressure the only observable difference, is an earlier RCS depressurization around 3800 s, see Fig. 4.6.

Nevertheless, the effects on the lower head failure time of the collapse model chosen are undeniable; indeed the failure time of the reference case is at 13370 s whilst that one of the case 6 is at 11674 s. This discrepancy is due to the different ICARE- CESAR switching time predicted by the two cases. The switch time is an important parameter for the ASTEC code because it indicates the starting of the core degradation computations and depends on the switch conditions imposed by the user. In these simulations the switch condition is cladding temperature greater than 773 K, when it is fulfilled, the ICARE module is activated.

The earlier switch time computed by the case 6 could be partially explained observing the Fig. 4.7, which illustrates the core-collapsed water level calculated during the transient. The case 6 predicts a slightly faster water level decrease and once the level decrease below 2m, the cladding temperature increases over 773 K, in a about 100 s. The cumulative hydrogen produced does not only determine by the model selected for the zirconium oxidation (see Fig. 4.8), indeed the results of the case 2 and the reference case show a very good agreement in quantity and quality.

The main parameters, which affect the H<sub>2</sub> production are the amount of Zircaloy present in the core, it is limited by the liquefaction and relocation of Zircaloy and by the availability of steam in the core. Therefore, increasing the cladding failure temperature as in

the case 2 means that the steam will have more time to react with intact cladding surfaces, an increase of 50 K leads to an increase of about 80 kg more of H<sub>2</sub> produced.

A more evident effect on the H<sub>2</sub> comes from the case 4, where the UO<sub>2</sub> failure and melting temperatures are increased up to 3100 K, which means very low debris formation. This assumption leads to a very slow core degradation (Fig. 4.9), a higher core temperature throughout the transient (Fig. 4.10) and a total H<sub>2</sub> production greater than 50% in comparison with the reference case. This higher hydrogen production is strictly connected to the slow loss of the original core geometry calculated during the transient. It is interesting to note (see Fig. 4.10) that, all the studied cases predict the same maximum fuel temperature but one, the case 4. This is because in the ASTEC code the maximum fuel temperature calculation depends on the values used for the failure fuel temperature and not from that one for the melting fuel temperature.

Table 4.3: Summary of the main results

CALCULATIONS	Lower-head failure time [s]	Total H <sub>2</sub> produced [kg]	Total material degraded mass [kg]	Corium mass in the lower head [kg]
Reference case	13370	433.7	140006	117096
Sensitivity case 1 (oxidation correlation criteria)	13339	424.7	123000	105360
Sensitivity case 2 (clad failure criteria)	11776	497.6	124106	102761
Sensitivity case 3 (UO <sub>2</sub> -ZrO <sub>2</sub> melting point criteria)	15015	446.4	172000	155616
Sensitivity case 4 (debris formation criteria)	No failure at 25000 s	660 at 25000 s	84200 at 25000 s	2000 at 25000 s
Sensitivity case 5 (vessel failure criteria)	10673	445	134317	106045
Sensitivity case 6 (COLLAPSE = 2 criteria)	11674	474.84	134901	115898

Concerning the total degraded material produced in the core, it is interesting to observe, that increasing the UO<sub>2</sub>-ZrO<sub>2</sub> eutectic temperature up to 2800 K, the mass of the degraded material increases of about 30 t. Another remarkable point is the core final state calculated in the case 4 and compared with the reference case shown in Fig. 4.11. The case 4 predicts that the core degradation starts from the outer ring 4 and 5 instead of the inner ring 1-2, as calculated and expected by the reference case. These results are not clear, and the reason why the fuel inner rings in the case 4 remain almost intact, is still under investigation.

The last parameter that shows an important impact on the transient result is the lower head failure model. The lower head failure marks the final stage of the in-vessel accident progression. In these study two different lower head failure criteria were analyzed, one based on the total fusion, the other on creep deformation. Comparing the reference case (total fusion rupture criteria) to the case 5 (creep rupture criteria) results, it is clear the impact on the final

results: the failure time for the case 5 is 10673 s against 13370 s. However, it is important to remark that the ASTEC code simulates the corium material behavior in the lower head as different layers up to 3 (heavy metals layer, oxide layer, light metals layer) with homogeneous composition and with a single temperature for each layer. These simplifications could lead to larger uncertainties, given that the temperature profile in the layer could be sharper or in case of rapid transient leading to strong temperature variations.

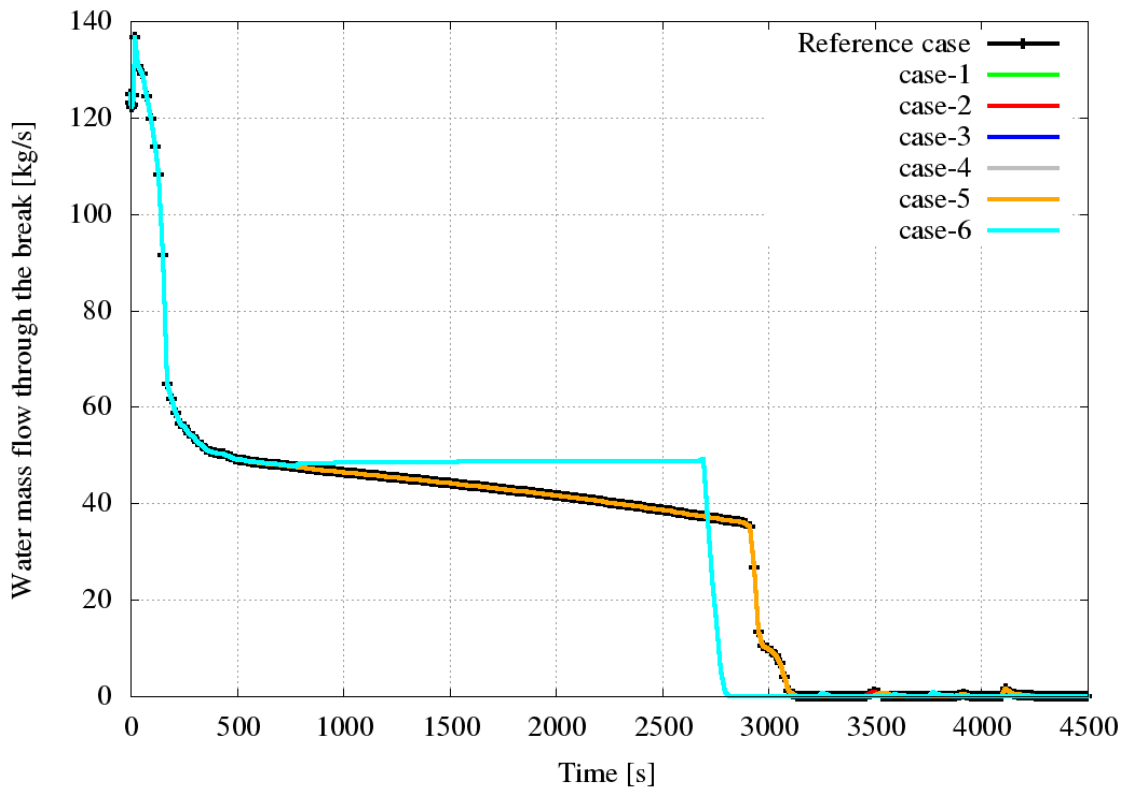


Figure 4.3: Water mass flow through the break

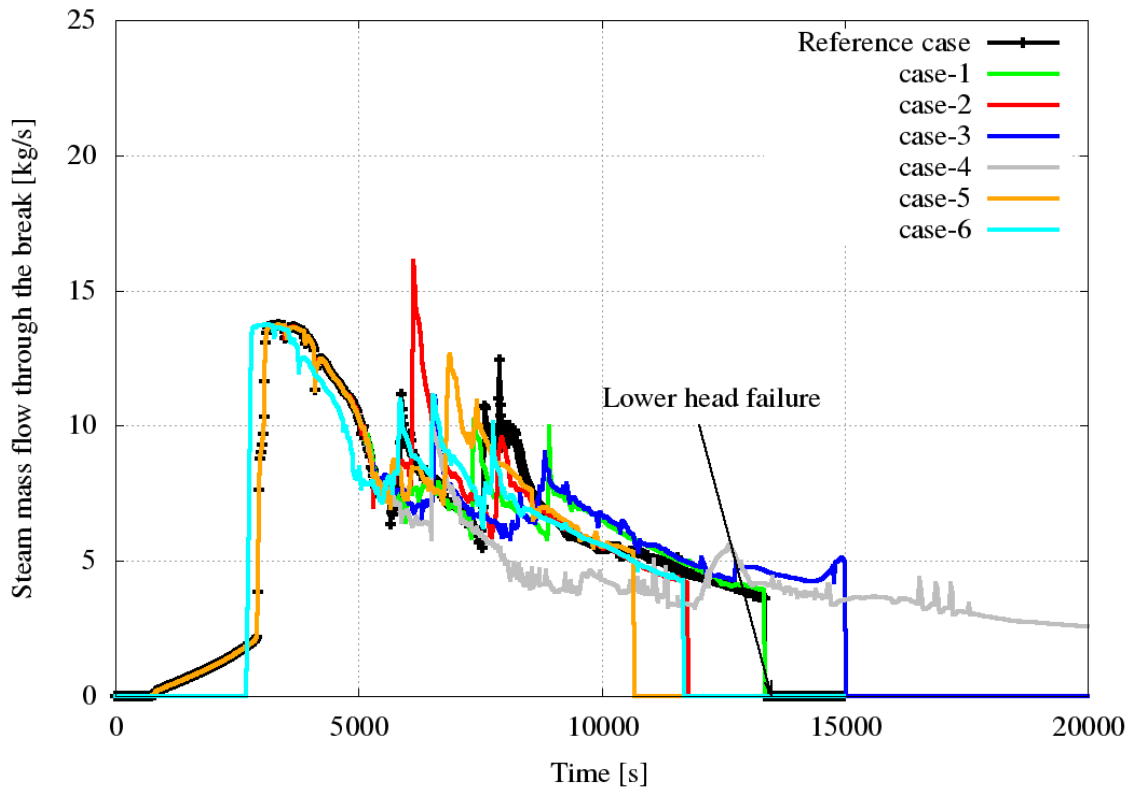


Figure 4.4: Steam mass flow through the break

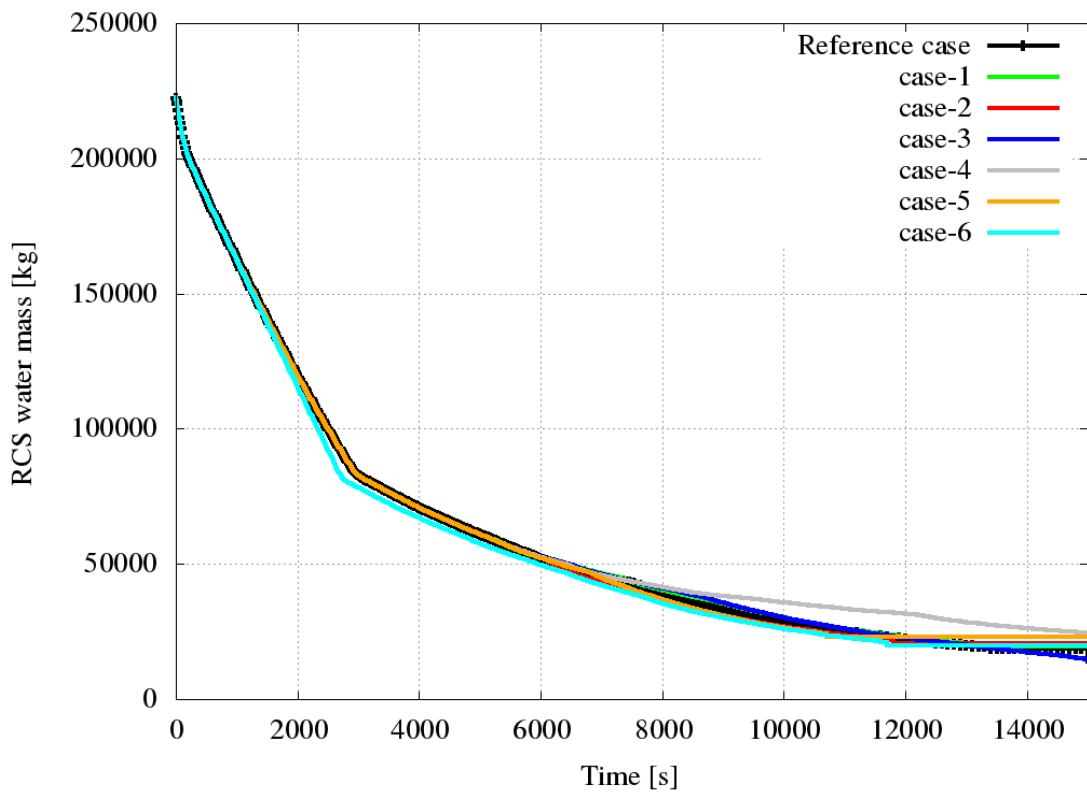


Figure 4.5: RCS water mass



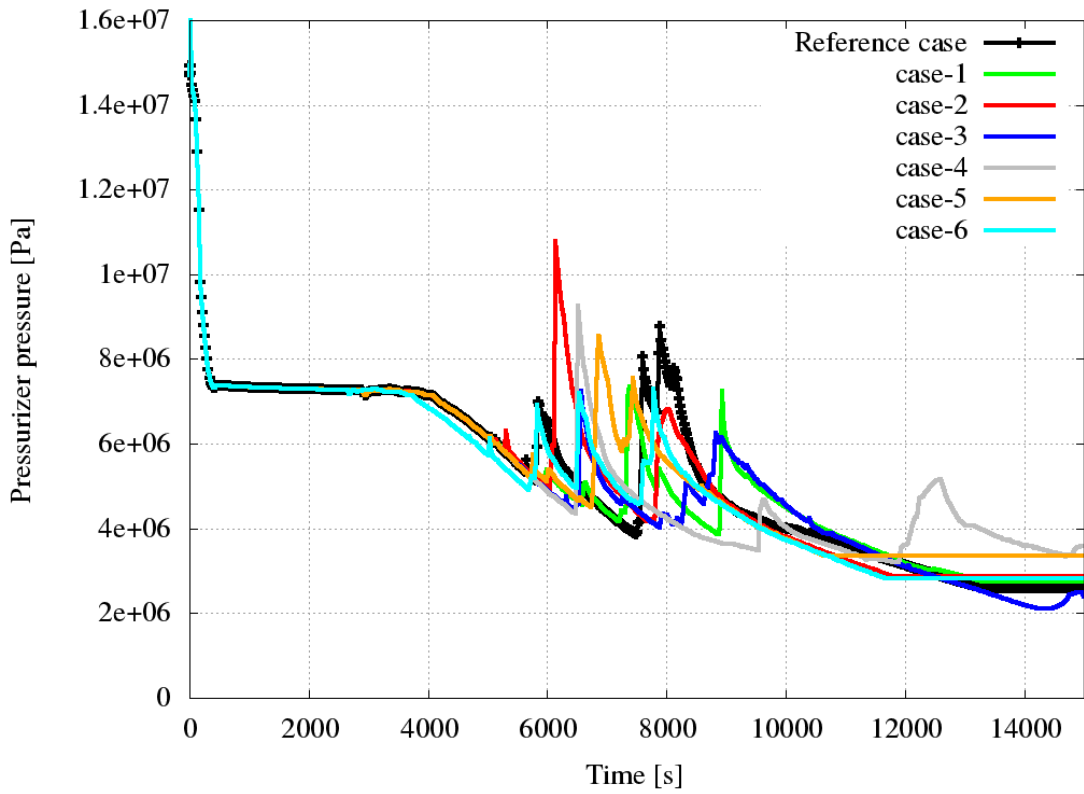


Figure 4.6: Pressurizer pressure

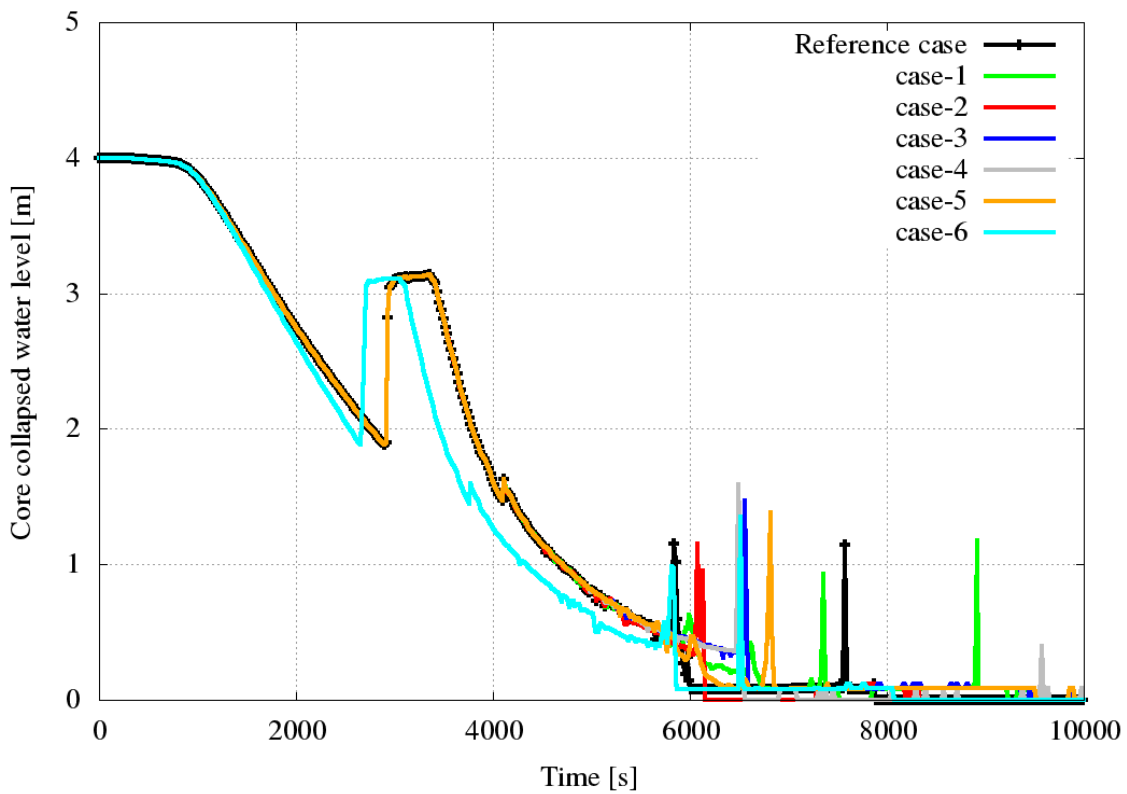


Figure 4.7: Core collapsed water level

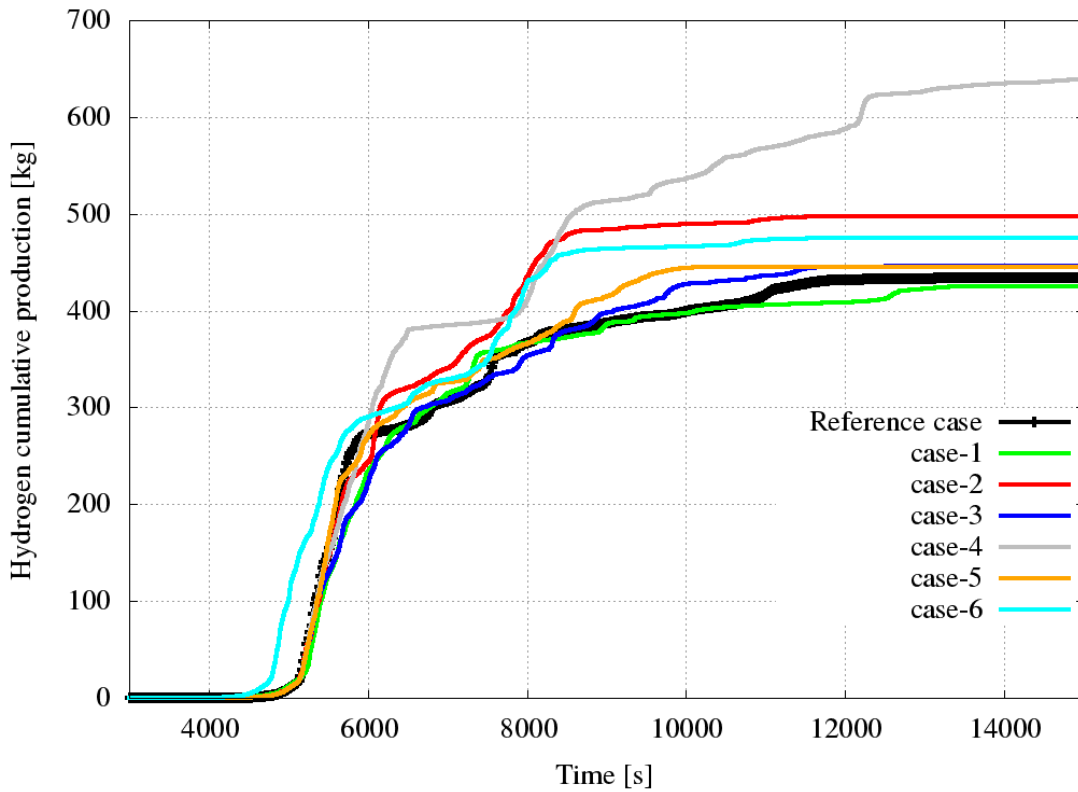


Figure 4.8: Hydrogen cumulative production

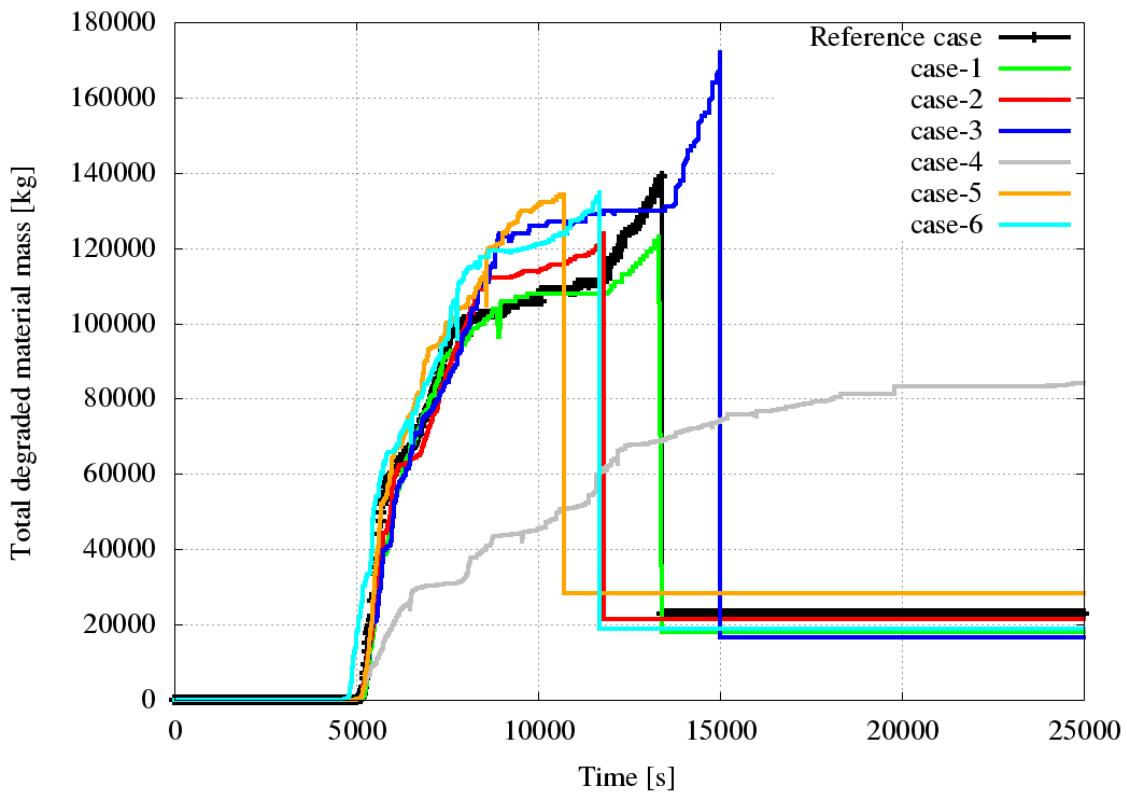


Figure 4.9: Total degraded material mass

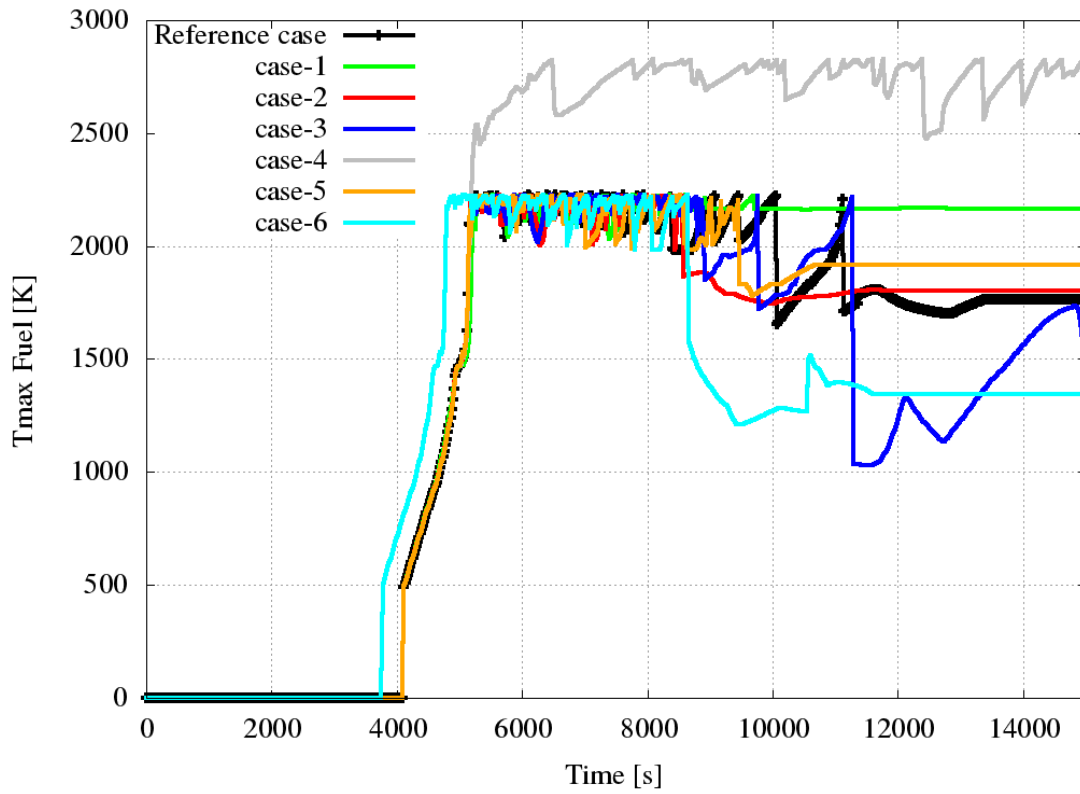


Figure 4.10: Maximum fuel temperature inside the vessel

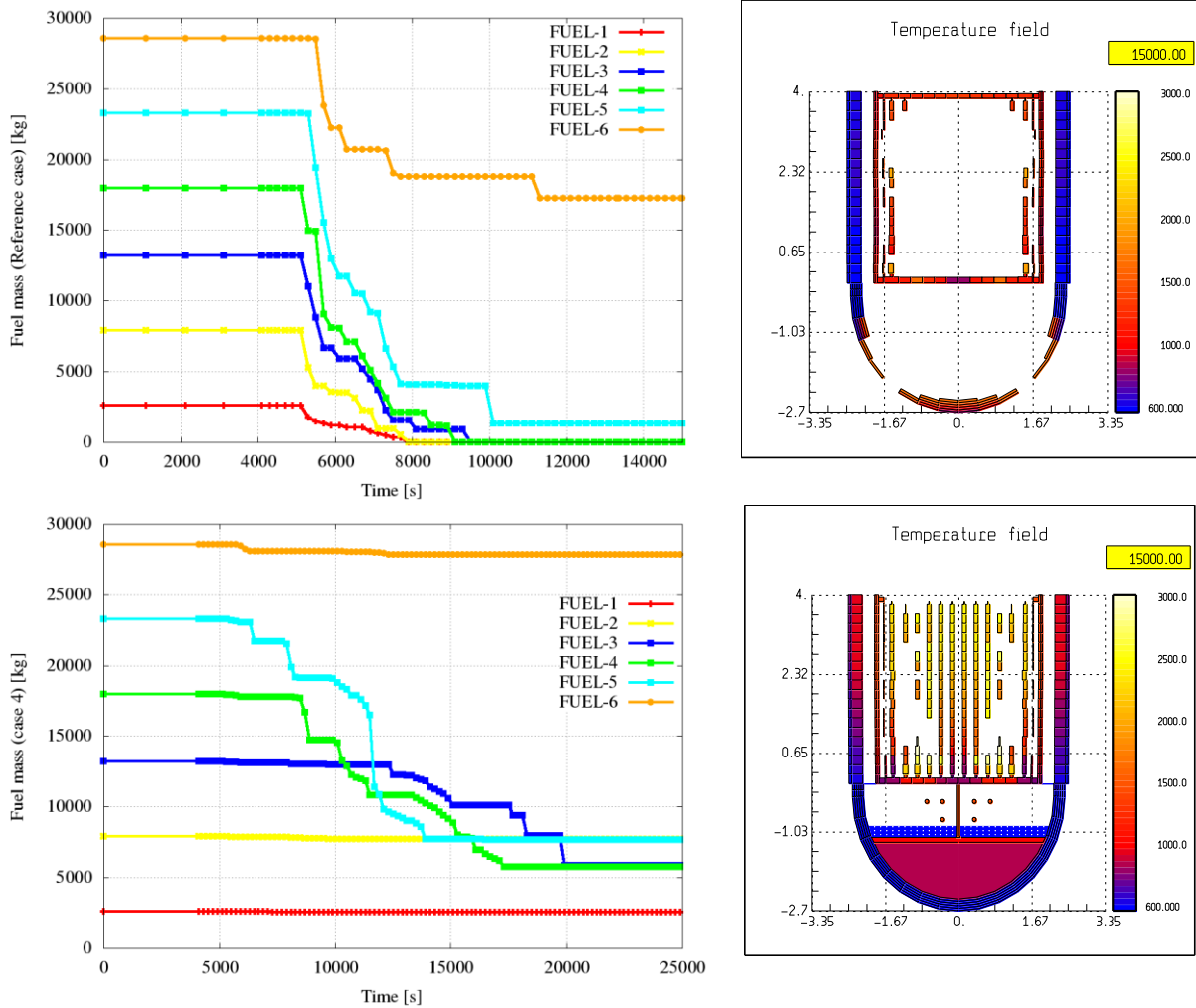


Figure 4.11: Reference case (upper) and case 4 (lower) core final state

#### 4.4 Reflooding cases

The reflooding of a hot core is well understood with respect to thermo-hydraulic behavior. In contrast to it, there are still open questions with respect to the hydrogen production (e.g. loss of protective oxide shell). The more the core is degraded, the less reliable data are available with respect to the thermo-hydraulics. Of course, if the thermo-hydraulics during reflood of a degraded core is not sufficiently known, one cannot expect a reliable simulation of the related hydrogen production. The user is forced to assess the uncertainties based on engineering judgement.

The new version of ASTEC code 2.1 contains a devoted model for reflooding of a rod-like geometry core, this modelling approaches and correlations were developed for design basis accident conditions and are applicable with several limits. The ASTEC version adopted in this work does not fit for this kind of calculations. In any case, the models and correlations developed for the original geometry of the core under accident conditions are not generally applicable to the flow in debris beds or melt pool, particularly during reflooding conditions.

The accident scenarios studied consist of the SBLOCA sequence previously analyzed, but with different recovery phases. The core reflooding occurs by means of the two HPI systems on the two cold leg of the primary loop B, with a flow rate of 15 kg/s each one. The timing of the HPI systems intervention are 5398 s (case R1) and 6398 s (case R2), this means that two different core degradation states.


The ASTEC reactor input deck of the new reference case employed in the reflooding simulations adopts 5 out of 6 parameters and models examined in the sensitivity analysis of the reference scenario described in section 4.3, as summarized in Table 4.4. The Table 4.5 shows the chronologies of the main events for the reference case in the sensitivity analysis and the new reference case for the reflooding study. The results calculated for the reflooding scenarios will be compared with that one without HPI systems injection (NR case), in order to underline the water injection effect.

Table 4.4: Models adopted in the new reference case for reflooding study

Reflooding calculations	ASTEC
Oxidation correlation	Urbanic-Heidrick
Clad failure criteria	$T_{\text{clad}} > 2350 \text{ K}$ and $ZrO_2$ thickness $< 100 \mu\text{m}$
UO <sub>2</sub> -ZrO <sub>2</sub> melting point	UO <sub>2</sub> -ZrO <sub>2</sub> = 2800 K
Debris formation criteria	Dislocation Fuel temperature 3100 K
Vessel failure criteria	Creep criteria

Table 4.5: Chronology of the main events

EVENT	Old reference case (Windows)	New reference case (Windows)
Break opening and total loss of main feedwater	0	0
Pressurizer PORV opens ( $P > 15.56 \text{ MPa}$ )	16.20	16.2
Reactor scram ( $P > 16.30 \text{ MPa}$ )	19.79	19.79
Pressurizer PORV closes ( $P < 14.96 \text{ MPa}$ )	24.36	24.35
Full steam generator dryout	25.29	25.29
Startup of auxiliary feedwater	100.00	100.29
Pressurizer is empty	142.29	145.29
Stop of primary pumps (primary mass (liquid + steam) $< 85000 \text{ kg}$ )	2907.29	2908
First fuel rod clad perforation/burst	4646.00	4669
Total mass of degraded core materials (M-tco) = 5 tons	5270.00	5400
Total mass of degraded core materials (M-tco) = 30 tons	5573.00	6100
First clad melting and dislocation	5131.30	4670
First ceramic melting and dislocation	5150.00	5259
First molten material slumping in the lower plenum	5613.00	6547
Vessel failure	11887.20	15146

 <b>Ricerca Sistema Elettrico</b>	<b>Sigla di identificazione</b>	<b>Rev.</b>	<b>Distrib.</b>	<b>Pag.</b>	<b>di</b>
	ADPFISS-LP1-054	0	L	72	106

#### 4.4.1 Calculation results

The simulations for the reflooding cases have been performed on Windows platform, and some remark on the dependency of the code on the platform are compulsory and will be discussed in the following section 4.5. In this paragraph, the calculated results for the three cases simulated case: R1 reflooding at 5400 s, R2 reflooding at 6400 s and NR no reflooding, will be compared and discussed. The front-end phase results are the same for the three cases until the intervention of the HPI systems, Fig. 4.12 and Fig. 4.13 show the evolution of water and steam discharged through the break during the transient.

The water injection in the case R1 leads to an increase of pressure in the RCS (see Fig. 4.14) due to the steam production inside the core. This effect is less evident in the R2 case, due to the different degradation state of the core and thus a worst core geometry to be cooled.

The calculated results indicate that when the HPI systems are triggered, the RCS inventory increases up to stabilize at 130000 kg for R1 and R2 cases (Fig. 4.15). The same behavior is observed for the core water collapsed level increases rapidly (Fig. 4.16), but once the water level reaches the top of the fuel the results start showing an instable behavior swinging around at the top height of the core.

These perturbations are due to the coupling problems between ICARE and CESAR module, because when the ICARE module is activated the thermo- hydraulic phase should be almost completed or however negligible in comparison with the degradation phase. Concerning the hydrogen production, the calculations results are not be able to capture the expected effect following a water ingress in the hot core (see Fig. 4.17).

The increase of the steam availability inside the core seems not to have any effect on the hydrogen generation. Observing the Fig. 4.17 immediately after 5400 s and 6400 s (intervention of HPI), the calculated H<sub>2</sub> production shows approximately the same trend for all three cases. It was expected, at least for the R1 case, (where the core still shows a rod-like geometry) but also for R2 one, that the reflood can result in large increases in the hydrogen production, in comparison with the NR case.

For R2 simulation, this lack of the code could be partially due to the models adopted for predicting the thermo-hydraulic within the vessel. The ASTEC code generally use models that predict the flows within predefined patterns and so can predict the general trends associated with the flow patterns in the vessel but have difficulty predicting the effects of change in core geometry. As a result, these models could not predict the flow patterns in the core and the resulting heat-up and melting of the core very accurately.

According to the calculated results, the core degradation is stopped just after the core reflooding starts (Fig. 4.18), in both the cases, even if the total amount of corium material mass involved are completely different 18 t for R1 and 70 t for R2. For the R2 case, a degraded material mass relocation of 15000 kg inside the lower head is predicted after 6400 s (Fig. 4.19). A further difference is observed concerning the maximum temperature calculated (Fig. 4.20), indeed for the R2 case given the large amount of degraded material mass, the

maximum temperature calculated, is the same of the NR case (2500 K), while for the R1 case is around 500 K.

The calculated maximum cladding temperatures at the top of the core show the same tendency (shifted of 1000 s) for R1 and R2 case1, even if in the R2 case the result is due to a complete failure of the claddings, while for the R1 one, is due to an effectiveness cooling (Fig. 4. 21). The core degradation final state is more clearly illustrated in Fig. 4.22 and Fig. 4.23, where for the R1 case, the core turns out to be almost totally intact, and the degraded material is composed mainly by ZrO<sub>2</sub> coming from the Zircaloy cladding oxidation in the upper part of the core.

Concerning the R2 case, the degradation involves a consistent part of the fuel; the code predicts a melting pool formation in the center of the core, which does not cool during the entire transient. Furthermore, the R2 case computes a corium material relocation inside the lower plenum, which has undergone a quenching process, given that the low temperature inside the lower head.

It is important to point out again, that the ASTEC model, for reflooding process, has not been validated, and these results are affected by significant uncertainties in the selection and application of the most applicable correlations.

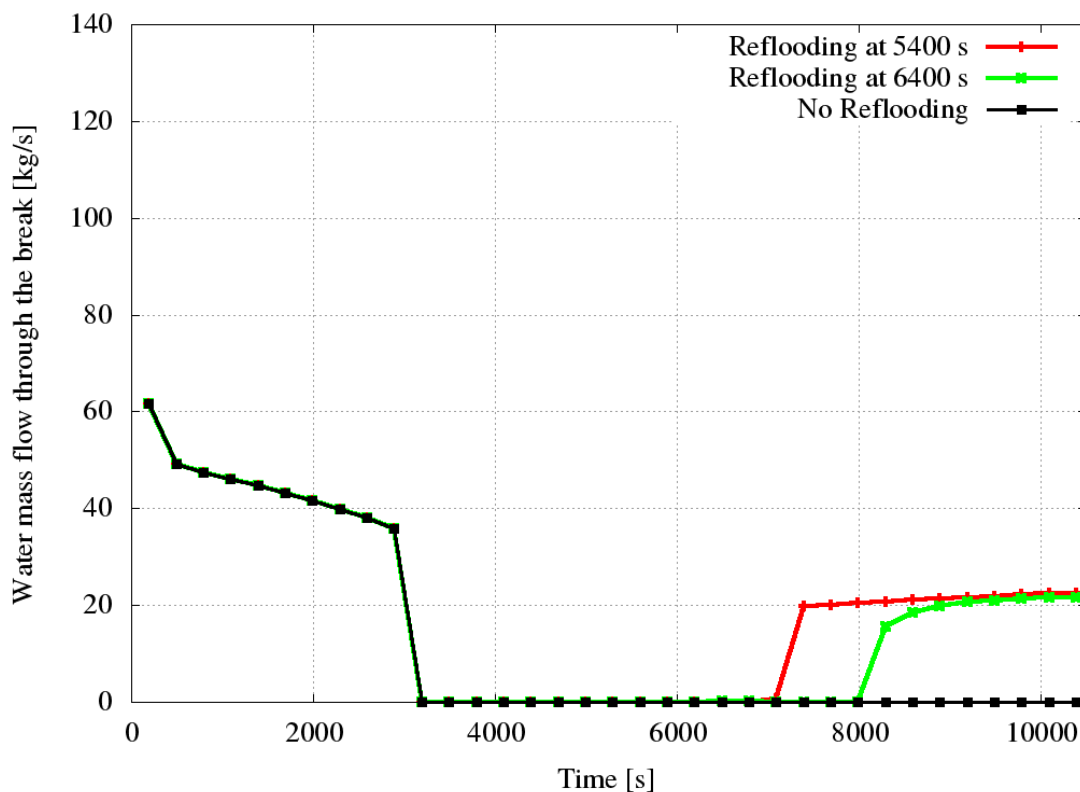


Figure 4.12: Water mass flow through the break

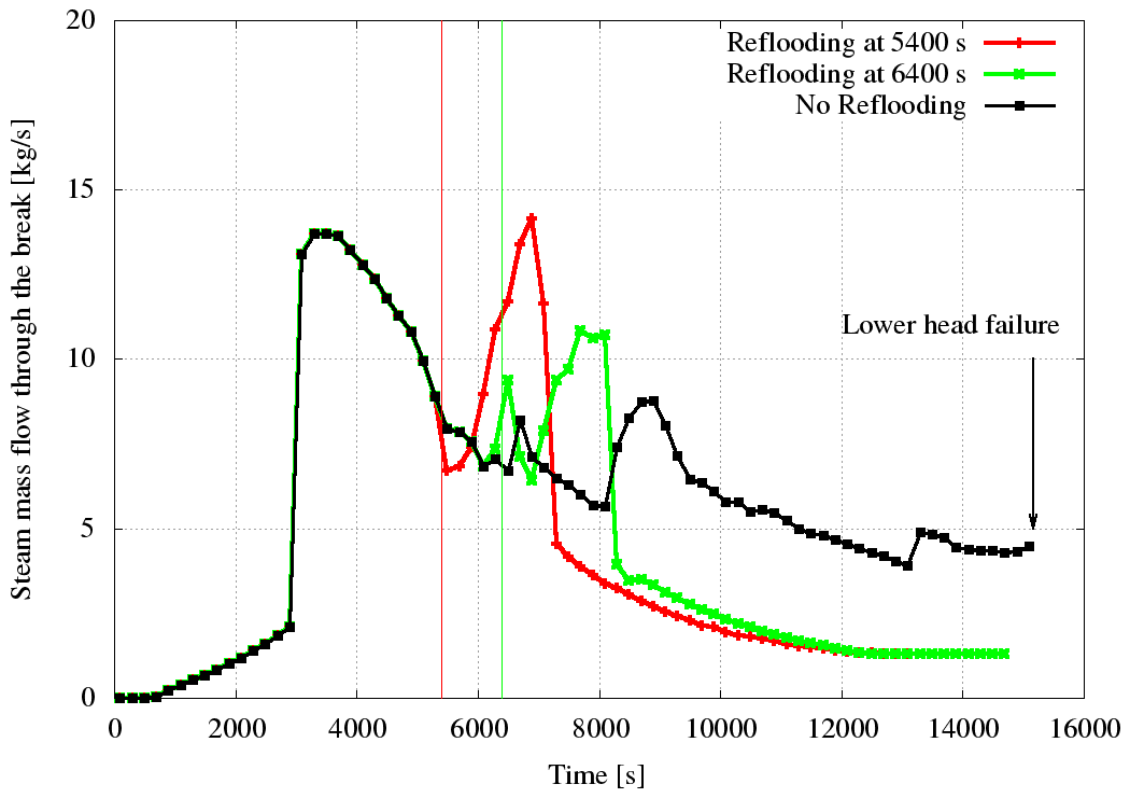


Figure 4.13: Water mass flow through the break

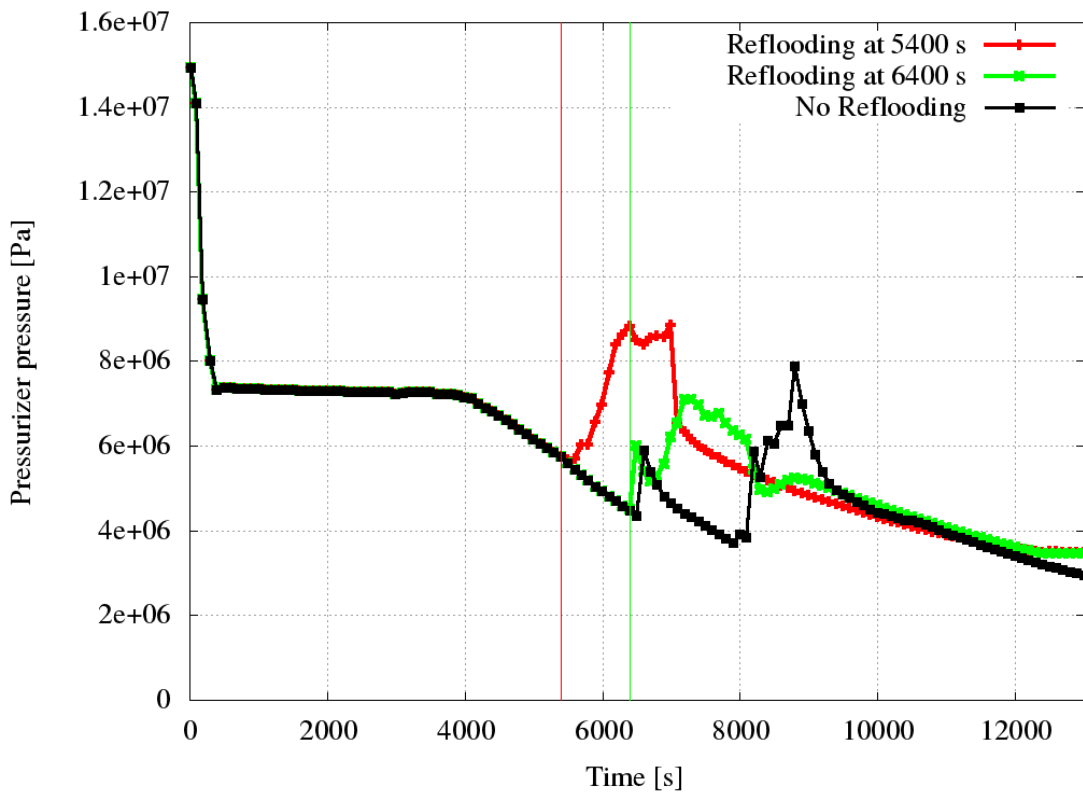


Figure 4.14: Pressurizer pressure



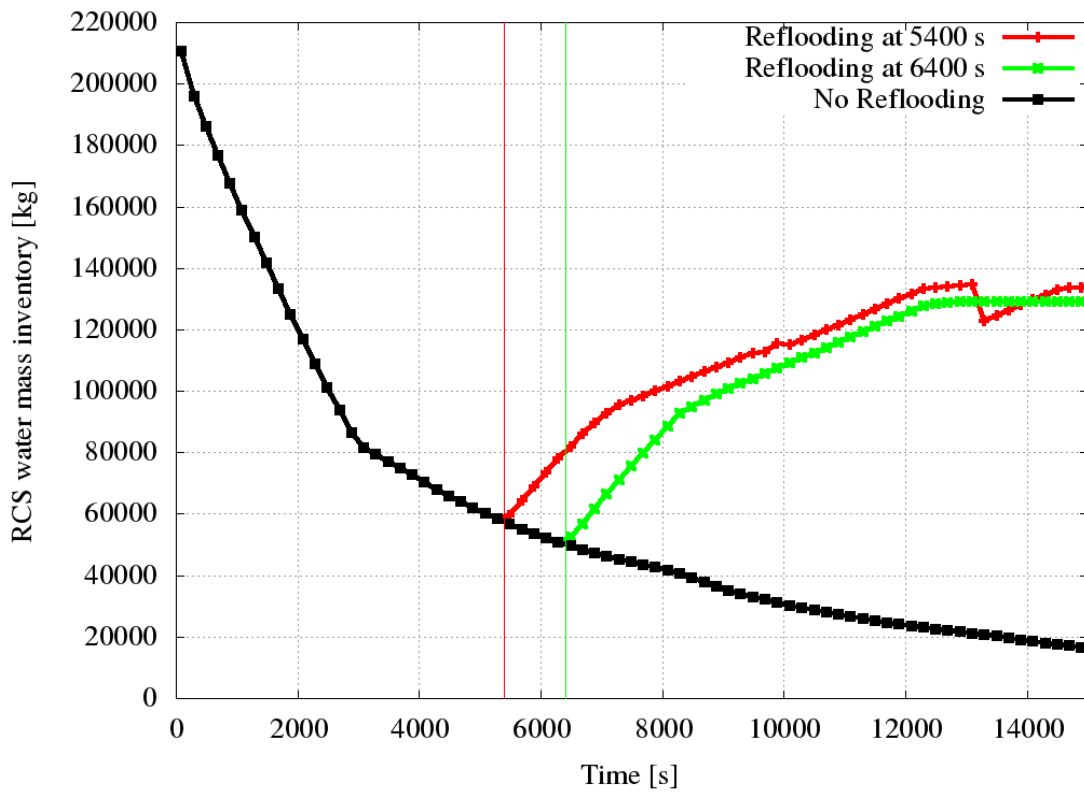


Figure 4.15: RCS water mass inventory

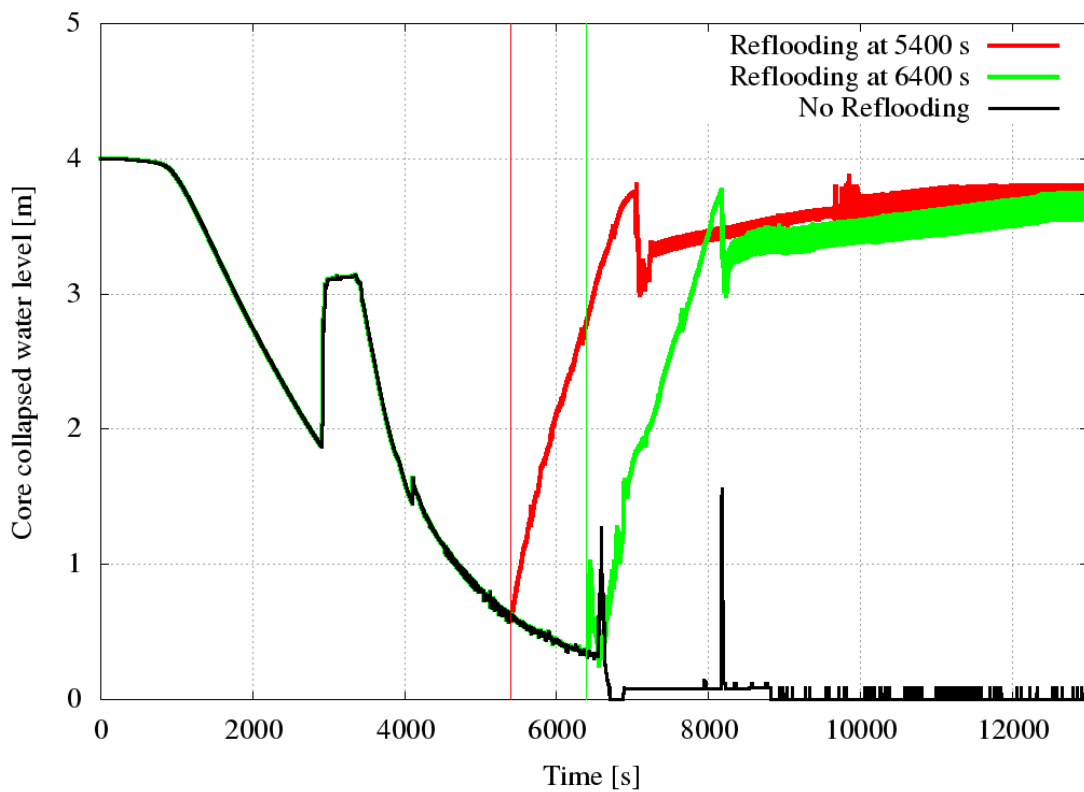


Figure 4.16: Core water collapsed level

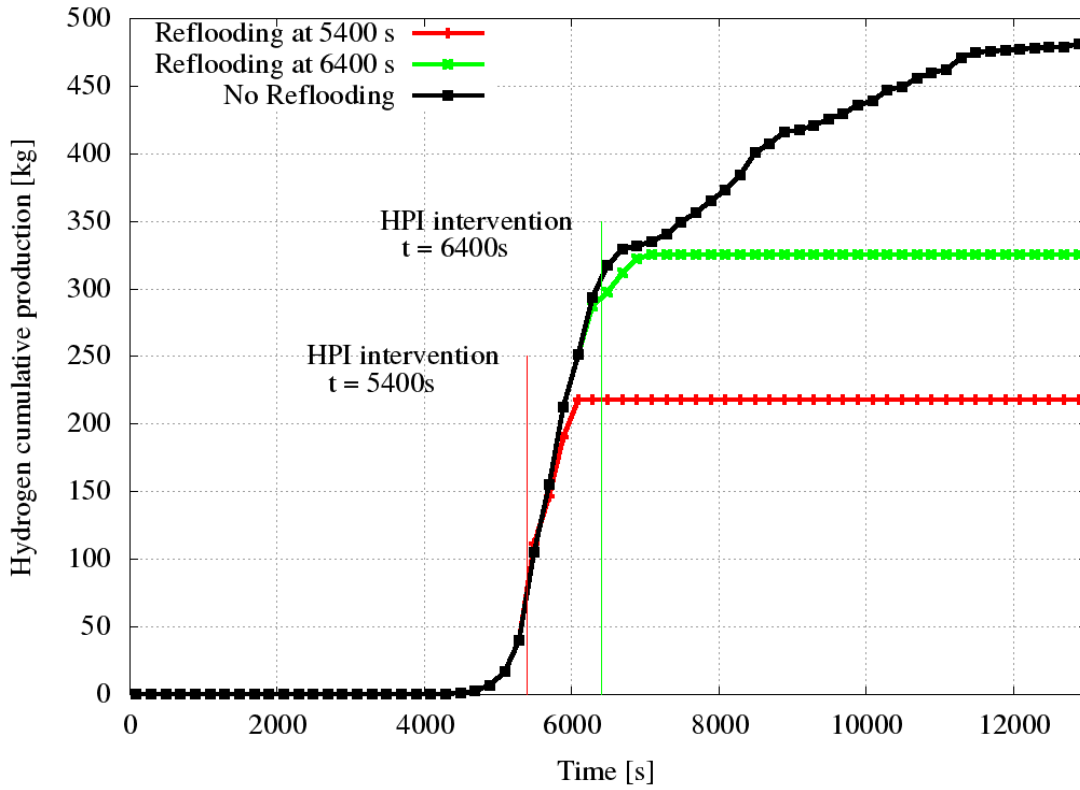


Figure 4.17: Hydrogen cumulative production

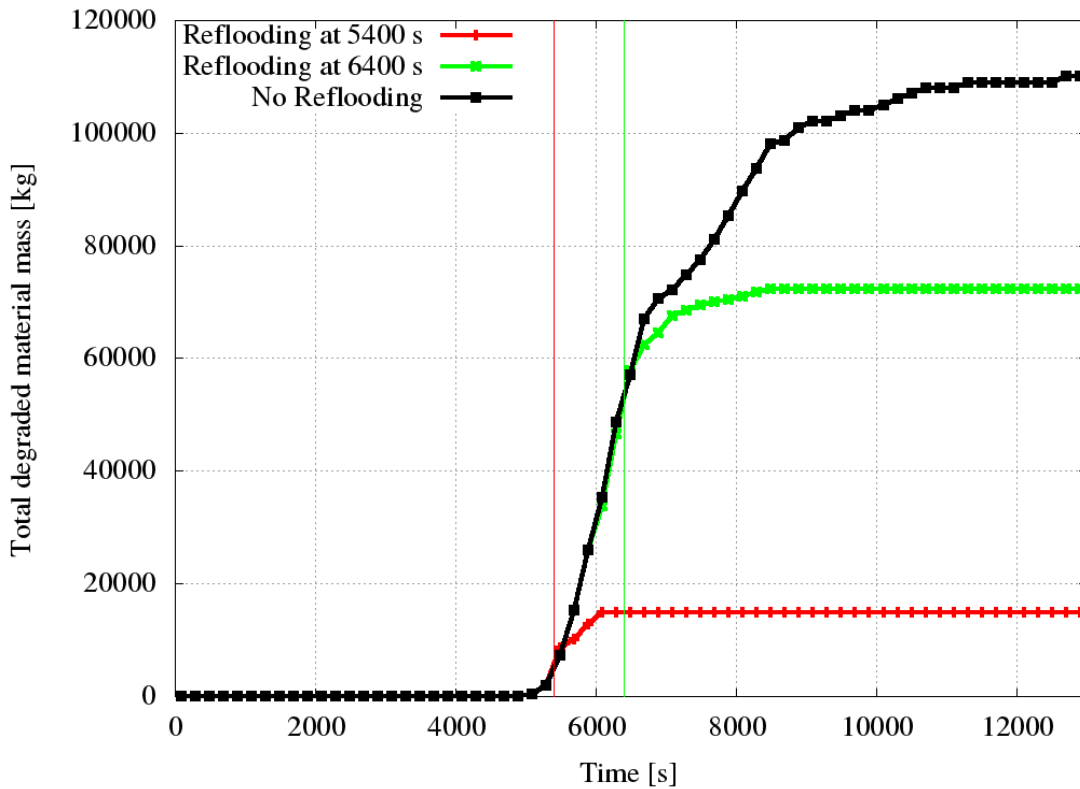


Figure 4.18: Total degraded material mass

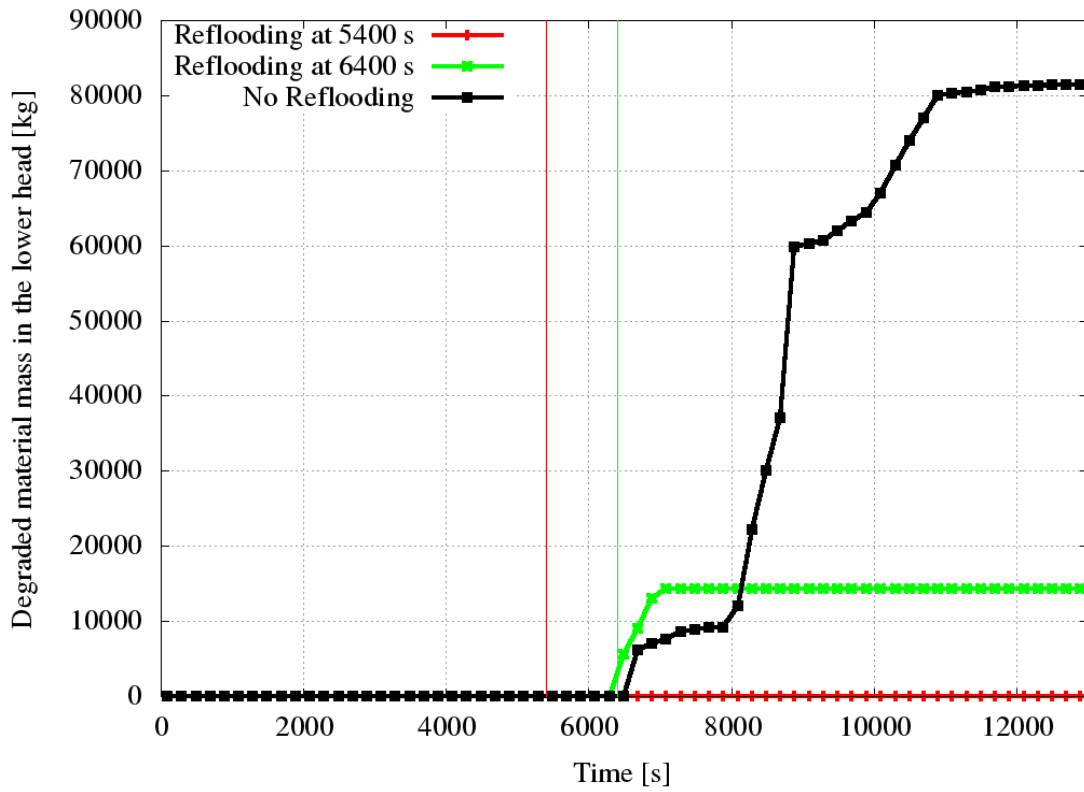


Figure 4.19: Degraded material mass in the lower head

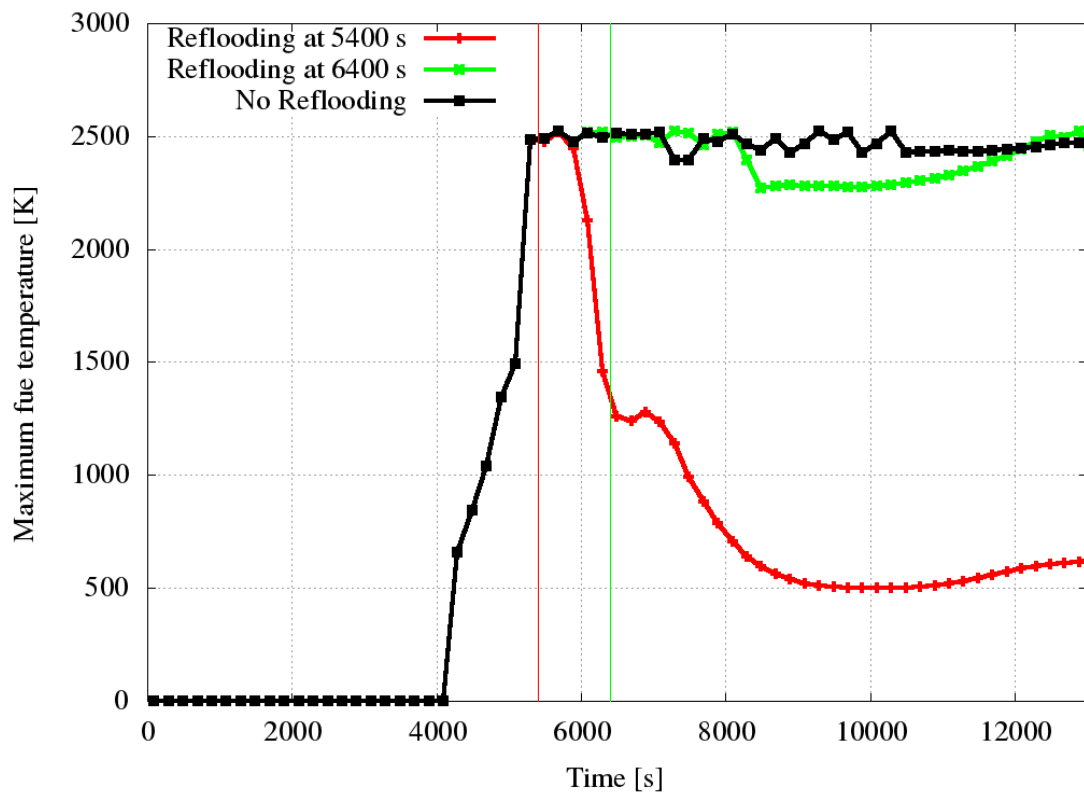


Figure 4.20: Maximum fuel temperature

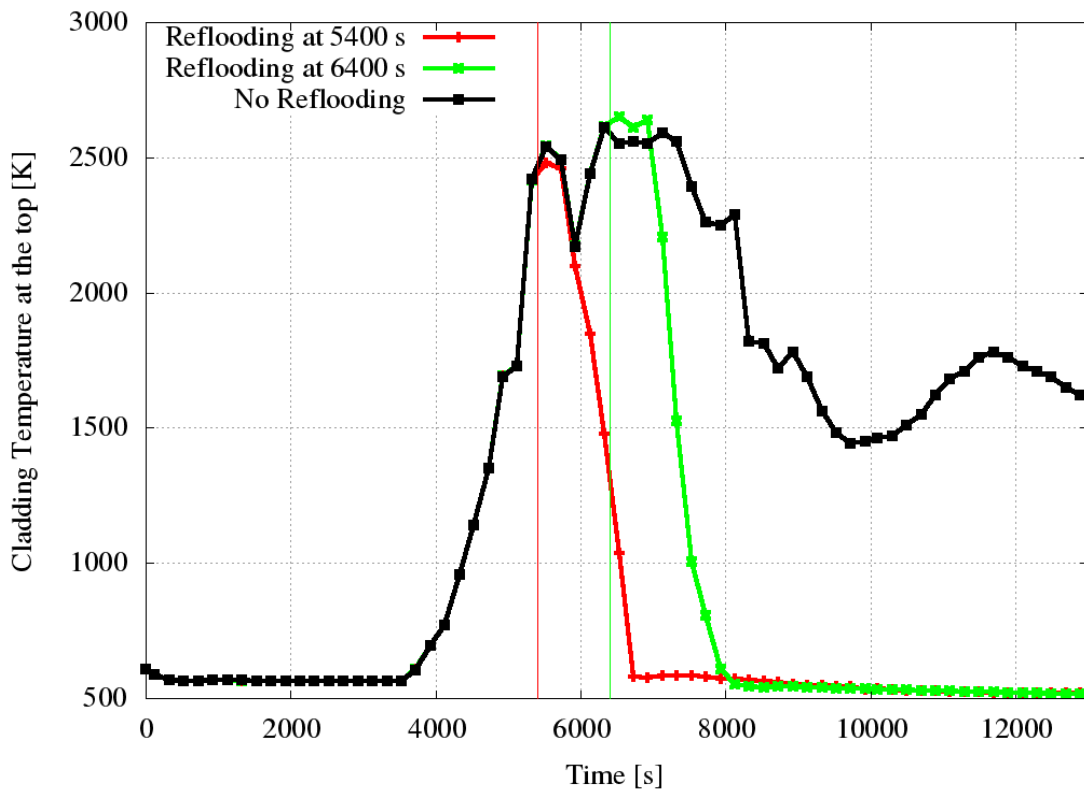


Figure 4.21: Cladding temperature at the core top

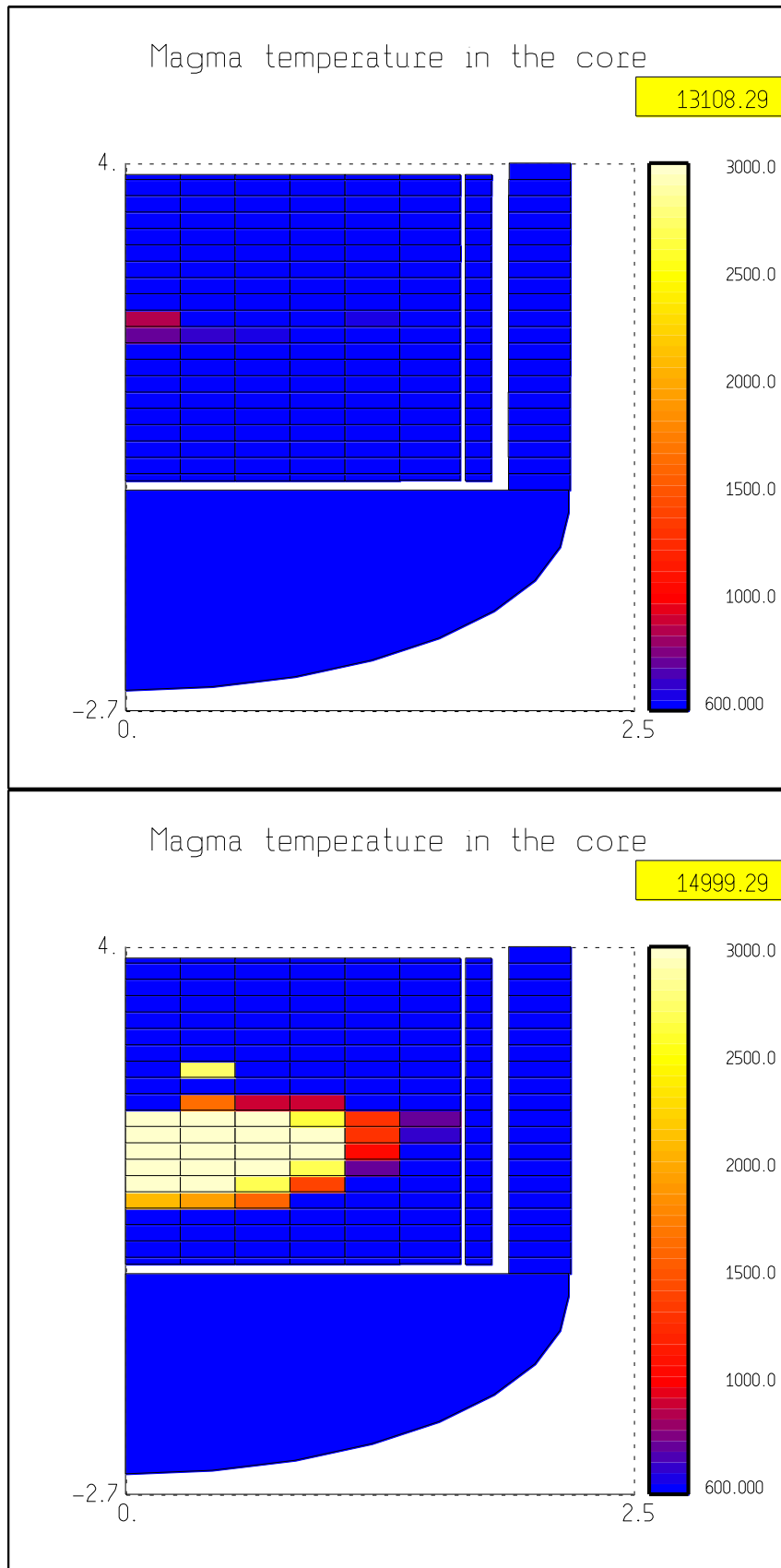


Figure 4.22: Corium temperature [K] for the case R1 (upper) and R2 (lower)

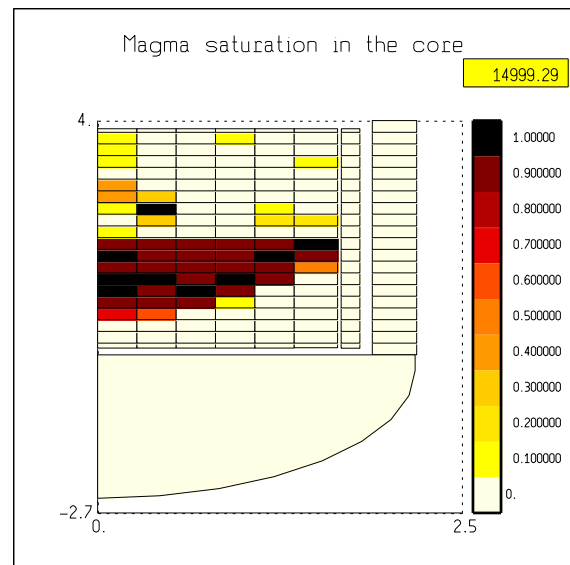
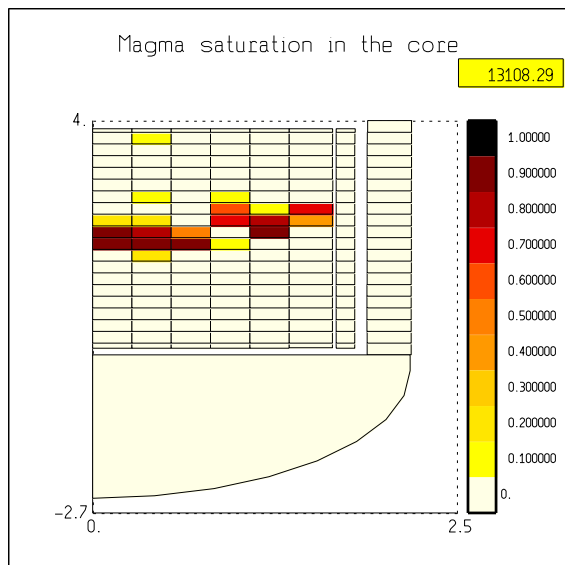
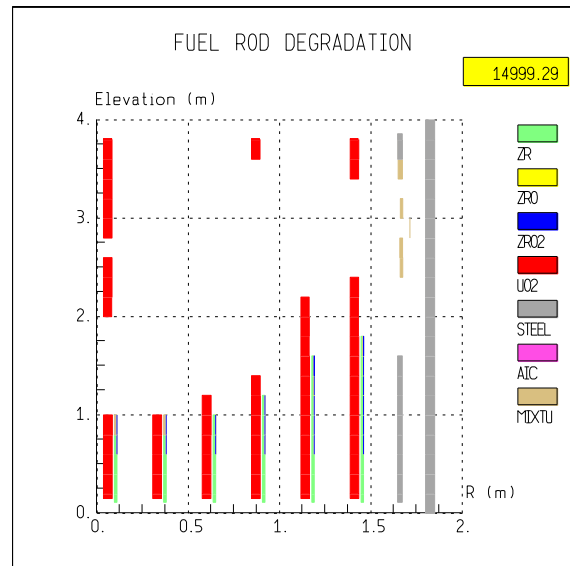
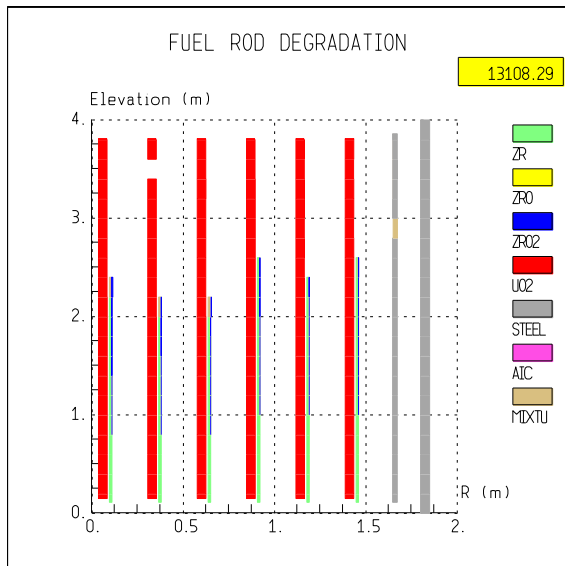
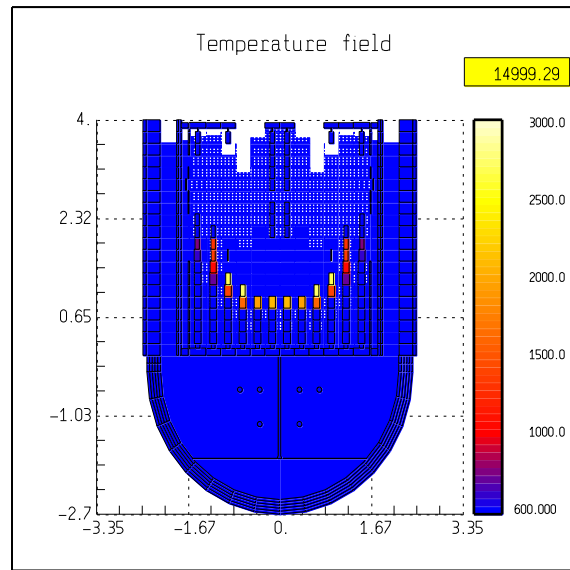
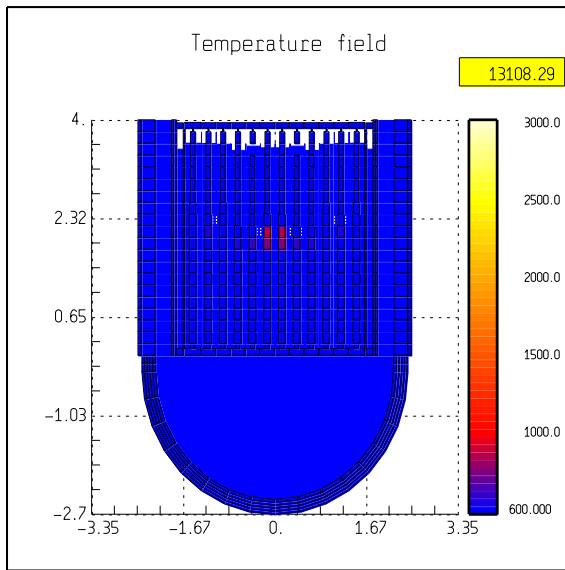


Figure 4.23: Core final degradation state, case R1 (left) and R2 (right)

#### 4.5 Platform dependencies

As previously mentioned, differences between Linux and Windows results were observed both in degradation and relocation material part, leading to different relocation sequences and lower head failure time. The presence of platform dependence has implications on code assessment. The presence of these effects confounds genuine sensitivities arising from parameter variations, and should therefore be mitigated as far as possible, preferably eliminated entirely.

It is not normally clear which, if any, of the results from the same case run on different machines produced the ‘right’ results. Further discussion is beyond the scope of the present document, but it is noted the issue has been addressed for thermal hydraulic codes. It would be beneficial if this study was extended to the severe accident area. In order to point out the platform dependencies of the ASTEC v2r2p2 code, the reference case and case 6 was run on Linux and Windows, and the results compared.

Table 4.6: Chronologies of the main events

EVENT (s)	Windows		Linux	
	Reference	Case 6	Reference	Case 6
Break opening and total loss of main feedwater	0	0	0	0
Pressurizer PORV opens ( $P > 15.56$ MPa)	16.20	16.20	16.20	16.20
Reactor scram ( $P > 16.30$ MPa)	19.79	19.79	19.79	9.79
Pressurizer PORV closes ( $P < 14.96$ MPa)	24.36	24.36	22.02	22.02
Full steam generator dryout	25.29	24.79	24.35	24.79
Startup of auxiliary feedwater	100.00	100.00	100.00	100
Pressurizer is empty	142.29	141.29	141.29	141.29
Stop of primary pumps (primary mass (liquid + steam) $< 85000$ kg)	2907.29	2658.29	2908.29	2658.29
First fuel rod clad perforation/burst	4646.00	4297.00	4651.00	4297.00
Total mass of degraded core materials (M-tco) = 5 tons	5270.00	4878.00	5229.00	4871.29
Total mass of degraded core materials (M-tco) = 30 tons	5573.00	5169.00	5523.00	5188.00
Total H <sub>2</sub> production	501.20	587	433.68	474.84
First ceramic melting and dislocation	5150.00	4771	5143.00	4772.29
First molten material slumping in the lower plenum	5613.00	5517	5826.00	5702
Vessel failure	11887.20	10460	13370	11674

The Table 4.6 shows the chronologies of the main events for the reference and case 6 calculated on Windows and on Linux platform. As is possible to see the thermal-hydraulic

results calculated by the CESAR module (until about 4000 s) do not exhibit any discrepancy, see Fig. 4.24 and Fig. 4.25. When ICARE starts, the discrepancies become more evident. In particular the total hydrogen generation calculated on the Linux platform are lesser of about 20% in comparison with windows one, while the timing of release are the same (Fig. 4.26).

The models of degradation and relocation of core materials are affected by the platform selected to perform the calculations (Fig. 4.27). It is not clear if the discrepancies concerning the timing of the lower head failure depend on the different corium material relocation in the lower head, or on the lower head failure model. In any case, the platform dependencies introduce further uncertainties on the results with a magnitude, which makes difficult to discriminate between the uncertainties due to the models and those due to the platform.

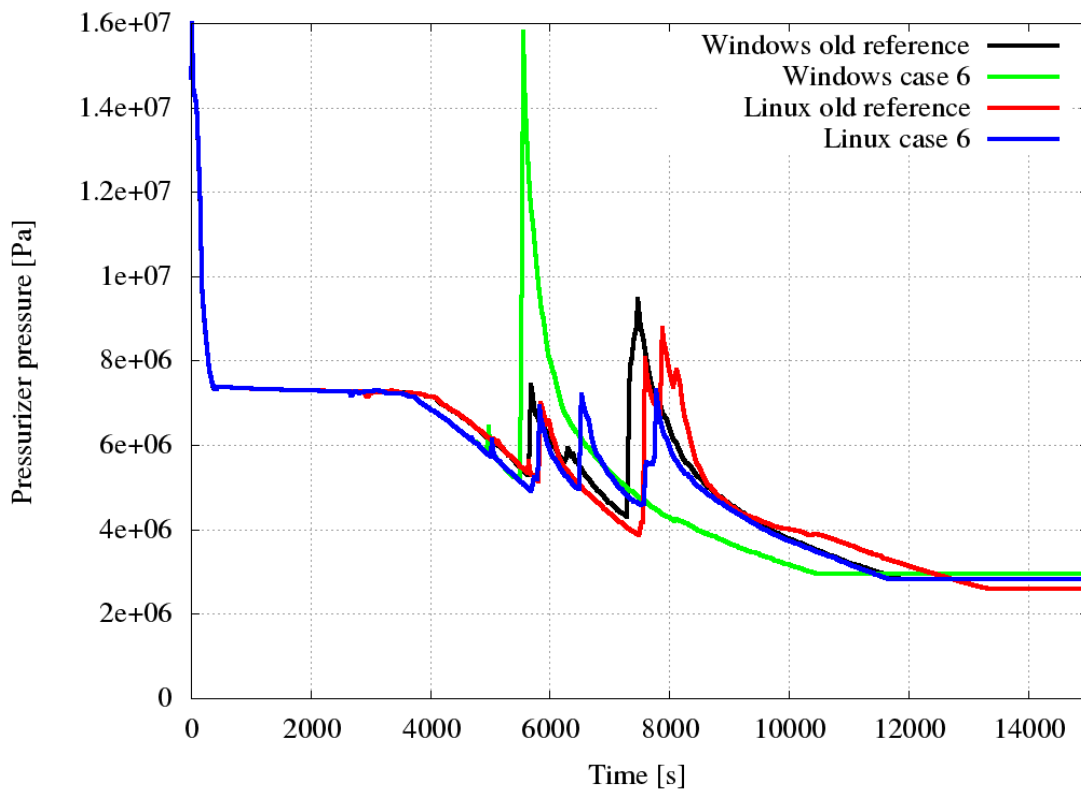


Figure 4.24: Pressurizer pressure



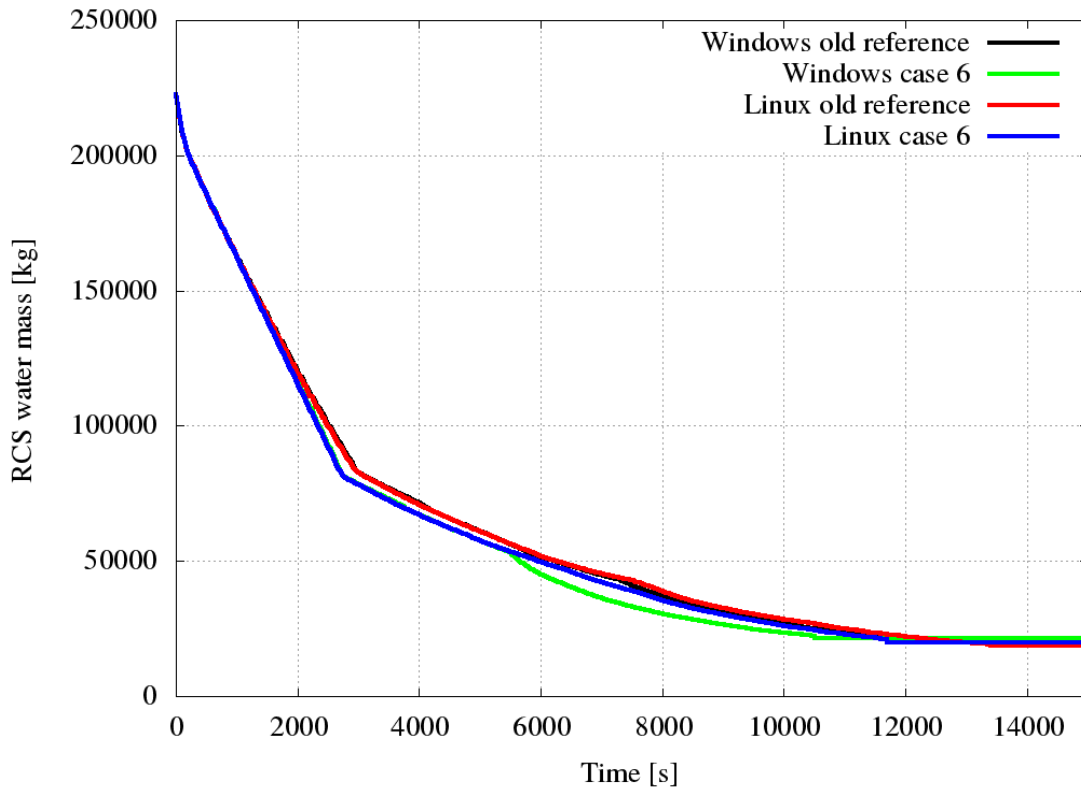


Figure 4.25: RCS water mass inventory

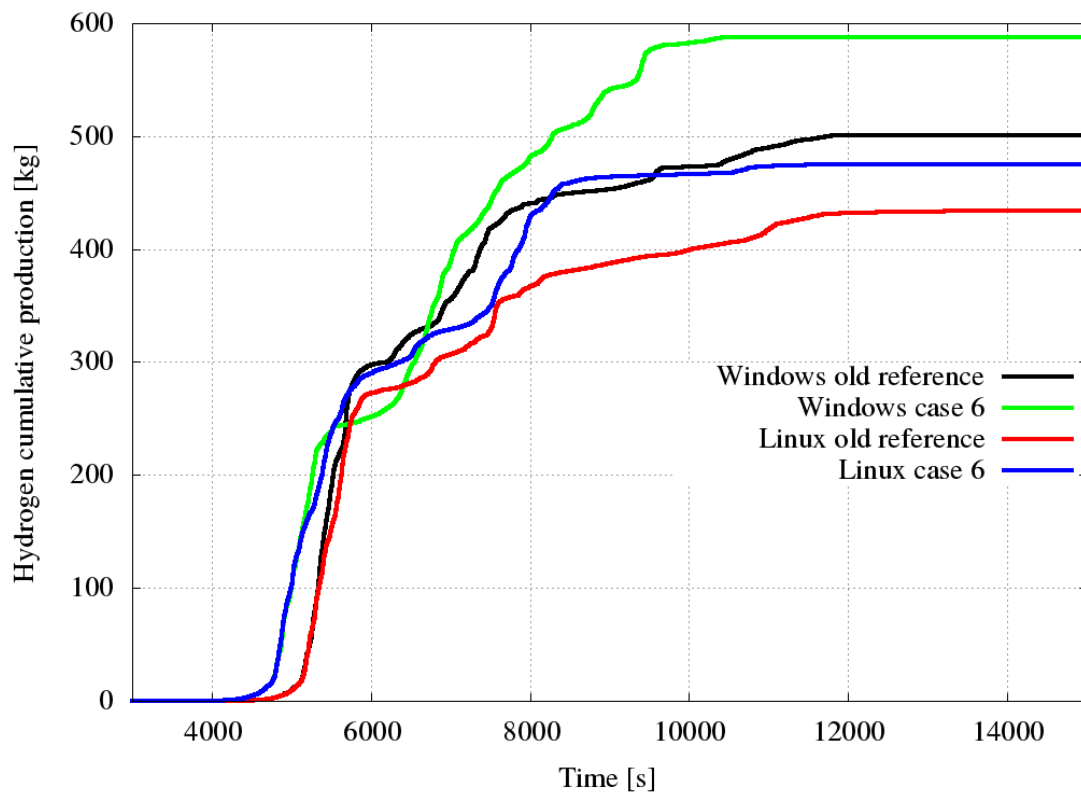


Figure 4.26: Hydrogen cumulative production

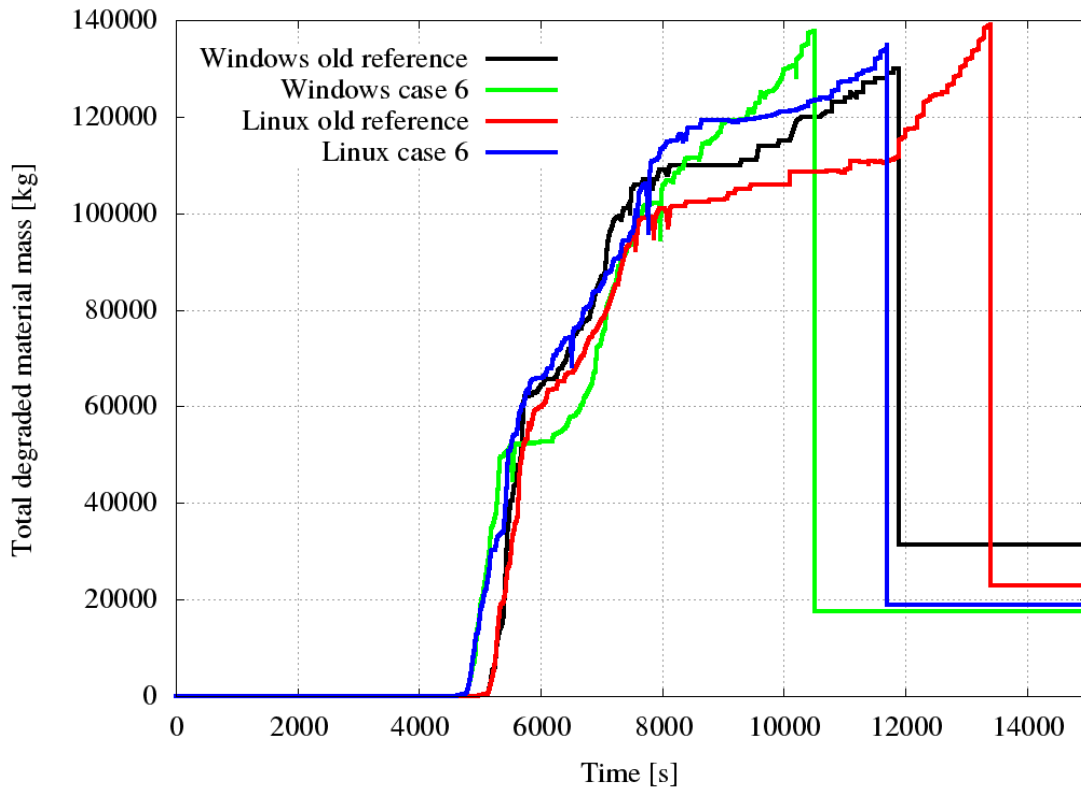



Figure 4.27: Total degraded material mass

#### 4.6 Summary and conclusions

The behavior of a plant during a severe accident is affected by a complex range of thermal, mechanical and physical processes. The consequences of reflooding the reactor core will depend on the state of the core at the time of reflood. Reflooding during the initial stages of an accident, before melting of any rods or structures has occurred, should result in the rapid quench of the core.

Reflooding during the early phases of core degradation can either result in the shattering of fuel rods, in formation of debris or even, if the peak temperature is higher, in an increase of Zircaloy oxidation and rapid heat-up of some parts of the core. The core heat up can lead to the formation of large blockages or even molten pools, and the production of significant quantities of hydrogen. Reflooding during the later stages of the accident, once molten pools have been formed, may be largely ineffective in cooling much of the core.

The exact response associated with reflood is extremely difficult to predict by mean of an integral code like ASTEC. In general, integral codes allow the user to model the reactor coolant system using parametric models that must be tuned by the user. Because these codes were intended to be fast running, modelling accuracy was of less concern than speed. In addition, the users of integrated codes have a strong impact on the overall predicted response of the plant, because of the large number of modelling parameters that must be set. In this

 <b>Ricerca Sistema Elettrico</b>	<b>Sigla di identificazione</b>	<b>Rev.</b>	<b>Distrib.</b>	<b>Pag.</b>	<b>di</b>
	ADPFISS–LP1-054	0	L	85	106

document, to better understand the separate effect of some of these modelling parameters a sensitivity analysis was performed with the ASTEC code.

The sensitivity analysis has shown that the models selected by the user can provide results very different each other. It has been generally concluded that the uncertainties in predicting the early phases of a severe accident are relatively small, while the uncertainties for the later stages are still relatively large. In addition, as discussed in the second part of this document, the uncertainties associated with the reflooding of damaged cores or debris beds are also still relatively large.

It is important to mark, that simplified thermo-hydraulics models adopted by the ASTEC code for reflooding sequence simulations, may predict quenching in almost any case. This is due because, the transient physical process involves, in most cases, thermal and mechanical non-equilibrium, which has to be taken into account in the modelling. The ASTEC code uses a quasi-equilibrium thermal-hydraulic models, whereas detailed codes use non-equilibrium models. For this reason, the ASTEC code may not model all of the features of reflooding of damaged cores in the right way.

As briefly discussed in the last part of these document further uncertainties are introduced by the platform dependencies of the same magnitude of those due to “tunable” parameters. With all these uncertainties due to the modelling parameters and the platform dependencies, it is difficult for the end-user of the integral code to draw quantitative conclusions regarding the overall accuracy of the severe accident codes and models for a full range of accident conditions.

## References

- 4.1. Van-Dorsselaere, J. P., Seropian, C., Chatelard, P., Jacq, F., Fleurot, J., Giordano, P., Reinke, N., Schwinges, B., Allelein, H.J., Luther, W., 2009a. The ASTEC integral code for severe accident simulation. *Nuclear Technology* 165, 293–307.
- 4.2. Trégourès, N., Moal, A., 2007. ASTEC V1 code: CESAR physical and numerical modeling. ASTEC-V1/DOC/07-18.
- 4.3. Trégourès, N., et al., 2008. Validation of CESAR thermal–hydraulic module of ASTEC V1.2 code on BETHSY experiments. *Journal of Power and Energy Systems* 2 (1).
- 4.4. Van-Dorsselaere, J. P., et al., 2009. The ASTEC integral code for severe accident simulations *Nuclear Technology* 165.
- 4.5. Carénini, L., Fleurot, J., Fichot, F., 2014. Validation of ASTEC V2 models for the behavior of corium in the vessel lower head. *Nuclear Engineering and Design* 272, 152–162.

## 5. MELCOR and ASTEC result comparison

One of the main objectives of this activity is to highlight the uncertainties in the calculation of a severe accident sequence by the comparison of different codes. Two of the main integral codes actually employed worldwide for severe accident analysis have been considered: the U.S NRC MELCOR code and the European ASTEC code. The MELCOR calculation has been performed by the University of Pisa, while the ASTEC calculation has been performed by the University of Bologna in the frame of CIRTEN activities.

The main results from the SBLOCA transient analysis for the new reference case, employing similar core degradation parameters/criteria, and the reflooding scenarios described in details in the previous sections are compared and discussed, highlighting and trying to explain the main differences observed in code results.

### 5.1 TMI-2 steady-state conditions at nominal power

The steady-state conditions calculated by the two codes are compared with TMI-2 specification data in Table 5.1 below.

Table 5.1:Nominal TMI-2 steady-state

Parameter	Unit	MELCOR	ASTEC	TMI-2
Reactor core power	MW	2772	2772	2772
Pressurizer pressure (dome)	MPa	14.95	14.93	14.96
Temperature hot leg A	K	591.3	591.28	591.15
Temperature hot leg B	K	591.3	591.28	591.15
Temperature cold leg A	K	561.8	563.23	564.15
Temperature cold leg B	K	561.8	563.23	564.15
Mass flow rate loop A	kg/s	8600	8800	8800
Mass flow rate loop B	kg/s	8600	8800	8800
Pressurizer collapsed level	m	5.56	5.588	5.588
Total primary mass	kg	220300	221559	222808
Steam pressure SG A (outlet nozzle)	MPa	6.41	6.78	6.41
Steam pressure SG B (outlet nozzle)	MPa	6.41	6.78	6.41
Steam temperature SG A	K	570.0	570.8	572.15
Steam temperature SG B	K	570.0	570.8	572.15
SG A collapsed level	m	6.12	3.20	-
SG B collapsed level	m	6.12	3.20	-
Feedwater flow rate SG A	kg/s	761.1	784.4	761.1
Feedwater flow rate SG B	kg/s	761.1	784.4	761.1
Feedwater Temperature SG A & B	K	511.15	511.15	511.15

There is a general good agreement between code results and TMI-2 reference data for the primary system. Some more important deviations are found in the initial conditions of the SG secondary side, but these are not retained very important on the overall thermal-hydraulic behavior of the primary system during the transient phase.

## 5.2 In-vessel core degradation parameters and modelling options

In-vessel core degradation parameters and modelling options used in the new reference calculations to evaluate the core melt progression during both early and late degradation phases of the SBLOCA transient are compared in Table 5.2. As much as possible, similar parameters and model options have been used with MELCOR and ASTEC in order to try to reduce the discrepancies in the results observed in the previous analysis [5.1]. In particular, the same zircaloy clad oxidation kinetics, the same clad and vessel failure criteria, and the same fuel rod melting temperature (UO<sub>2</sub>-ZrO<sub>2</sub>) have been defined in the new calculations with the two codes.

Table 5.2: In-vessel core degradation parameters/criteria

Parameter	MELCOR	ASTEC
Zircaloy oxidation kinetics	Urbanic-Heidrick	Urbanic-Heidrick
Cladding failure criteria	ZrO <sub>2</sub> thickness <100 μm and T <sub>clad</sub> > 2350 K or T <sub>clad</sub> > 2500 K	T <sub>clad</sub> > 2350 K and ZrO <sub>2</sub> thickness < 100 μm
Melting point of UO <sub>2</sub> -ZrO <sub>2</sub> ceramic material	UO <sub>2</sub> T <sub>m</sub> = 2800 K ZrO <sub>2</sub> T <sub>m</sub> = 2800 K	UO <sub>2</sub> -ZrO <sub>2</sub> = 2800 K
Debris formation criteria	For other materials than fuel rods: thickness < 100 μm Fuel rod failure and debris formation when: T <sub>fuel</sub> > 2500 K	Dislocation Fuel temperature = 3100 K
Molten core relocation into the lower plenum	After failure of grid-supported plate that can initially support fuel assemblies and particulate debris above it. Thus, everything resting on that ring of the plate will fall, but the plate will remain in place until it melts (1273 K). This event corresponds to failure of the plate portion with survival of the grid	Baffle melting (relocation through core by-pass) or melting at core bottom (relocation through core support plate)
Reactor pressure vessel failure	Failure of the lower head will occur if creep-rupture failure of a lower head segment occurs, in response to mechanical loading at elevated temperatures	Creep criteria

### 5.3 Chronology of main events for the new reference case

The chronology of main events for the new reference calculations is compared in Table 5.3 below. Good agreement is found for the initial phase of the transient and the stop of primary pumps based on residual water inventory in the primary system. As in the previous analysis [5.1], the ASTEC code predicts an earlier onset of core degradation and melting than with MELCOR, likely due to some natural convection phenomena in the upper plenum of the vessel which are taken into consideration only in the MELCOR simulation. Conversely, the vessel failure is anticipated in the MELCOR calculation by about 2000 s.

Table 5.3: Chronology of main events

Parameter	ASTEC	MELCOR
Break opening and total loss of main feedwater	0 s	0 s
Pressurizer PORV opens ( $P > 15.56$ MPa)	16.20 s	14.00 s
Reactor scram ( $P > 16.30$ MPa)	19.79 s	22.5 s
Pressurizer PORV closes ( $P < 14.96$ MPa)	24.35 s	27.02 s
Start-up of auxiliary feedwater	100 s	100 s
Stop of primary pumps (*)	2908 s	2910 s
First clad melting and dislocation	4670 s	5850 s
First ceramic melting and dislocation	5259 s	6310 s
First molten material slumping in the lower plenum	6547 s	5890 s
Vessel failure	15146 s	13100 s

(\*) Primary mass (liquid + steam) < 85000 kg

(\*\*) Not calculated by MELCOR

### 5.4 Evolution of main parameters

The main parameters investigated for code results comparison are listed in Table 5.4. They concern: the thermal-hydraulic behavior of the primary system, the in-vessel core degradation progression, and the hydrogen production.

Table 5.4: List of main parameters plotted for code result comparison

Parameter	Unit
Pressurizer pressure	Pa
Loop A mass flow rate	kg/s
Break mass flow rate	kg/s
Total primary mass (liquid + steam)	kg

Core collapsed water level	m
Fuel rod clad temperature at core top ( <i>central ring</i> )	K
Instantaneous hydrogen production	kg/s
Cumulated hydrogen production	kg
Total mass of degraded core materials (debris or molten, cumulated value)	kg
Total mass of materials in the lower plenum (cumulated value)	kg

#### 5.4.1 Reference case without reflooding

As already observed in previous calculations [5.1], the differences in the thermal-hydraulics behavior of the primary circuit are reduced thanks to the good harmonization of input decks for the two codes and the use of simple and well defined boundary conditions. A residual difference found in the break mass flow rate calculated by MELCOR with respect to ASTEC has been eliminated through a refinement of the primary legs MELCOR model. As a result, the evolution of break mass flow rate (Fig. 5.1) and total primary mass (Fig. 5.2) calculated by the two codes is in good agreement in the initial phase of the transient before primary pumps stop around  $t = 2900$  s. After this time, the primary pressure is overestimated by MELCOR (see Fig. 5.3) and, as a consequence, the pure steam flow through the break becomes larger with a more pronounced reduction of the total primary mass inventory. There is now a very good agreement in the instant of primary pump stop, as confirmed in Fig. 5.4 which shows the evolution of mass flow rate in the primary loop.

Despite the discrepancies in core collapsed level calculated by the two codes before primary pump stop (see Fig. 5.5), which come from a different void distribution inside the vessel, there is a good agreement in the onset of core uncover and core heatup at the core top (Fig. 5.6). Total core uncover is predicted by the two codes during the transient, but with some delay with ASTEC with respect to MELCOR. The clad heatup rate is larger with ASTEC and then temperature escalation at the core top is reached earlier with ASTEC than with MELCOR. This difference in core heatup behavior seems mainly dependent on natural convection phenomena in the vessel upper plenum which are taken into account in the MELCOR simulation only. After the clad reaches dislocation or melting temperature values around  $t = 7000$  s, the clad temperature values plotted become unreliable.

In spite of similar core degradation parameters/criteria used in the present analysis, there are still significant differences in the evolution of core degradation mass (Fig. 5.7) and corium mass relocated in the lower plenum (Fig. 5.8). A more accelerated core melting and relocation is predicted by ASTEC with respect to MELCOR; the largest difference is in the timing of massive core slumping into the lower plenum, mainly due to different assumptions in the corium relocation path, through the side, after core baffle failure in ASTEC, or through the bottom, after core support plate failure in MELCOR. Despite the smaller amount of relocated material in MELCOR and the later core slumping, an earlier vessel failure is

calculated by this code, likely due to different assumptions on corium fragmentation and oxidic metallic phases separation into the lower head, since similar creep failure criteria has been used to predict vessel wall rupture.

In both code calculations, most of the hydrogen is produced by zircaloy clad oxidation during the early degradation phase. Despite the difference in timing, due to difference in the onset of core heatup, the total amount of hydrogen produced is in rather good agreement between the two codes. The ASTEC code predicts the release of some more hydrogen by oxidation of relocated mixtures in the late transient phase.

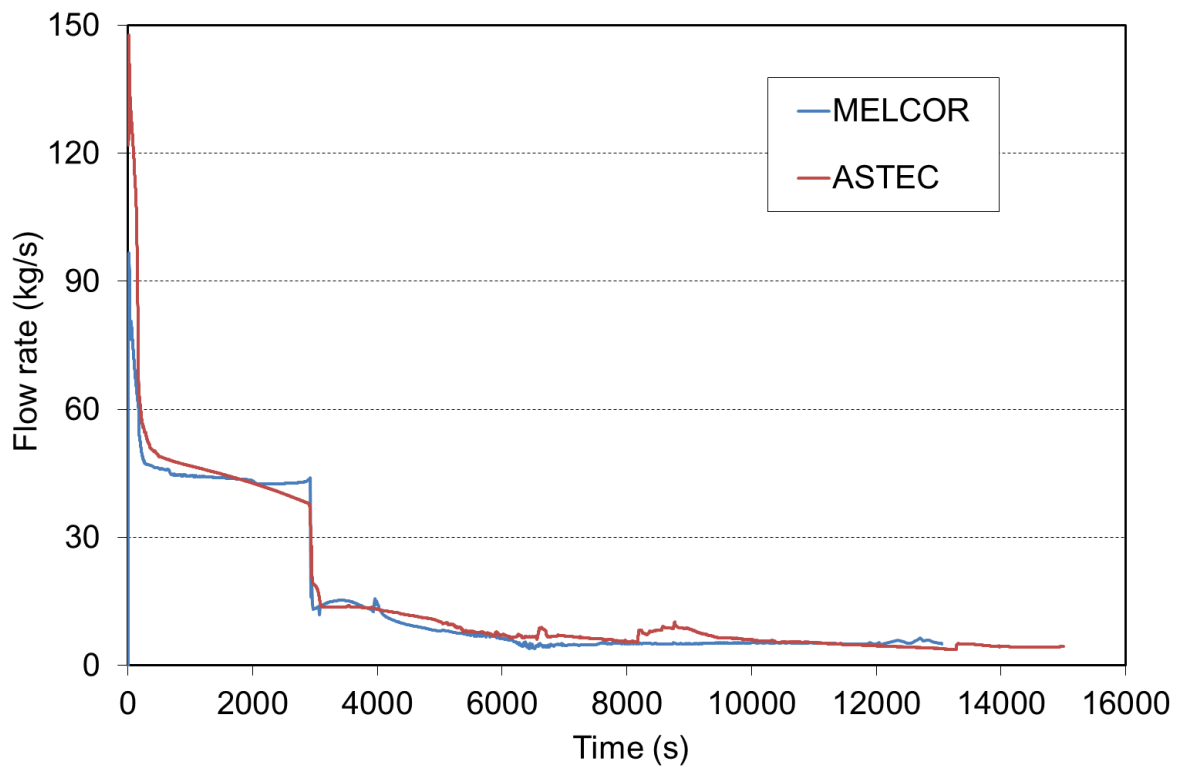


Figure 5.1: Break mass flow rate



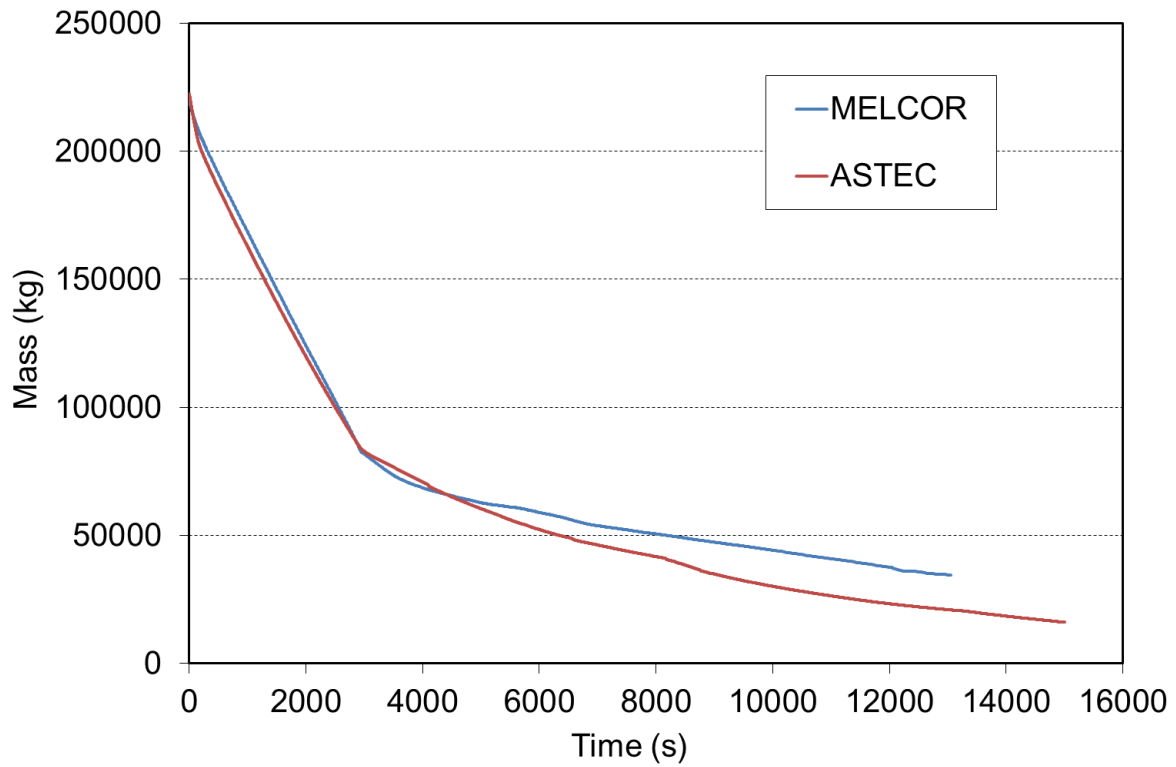


Figure 5.2: Total primary mass (liquid + steam)

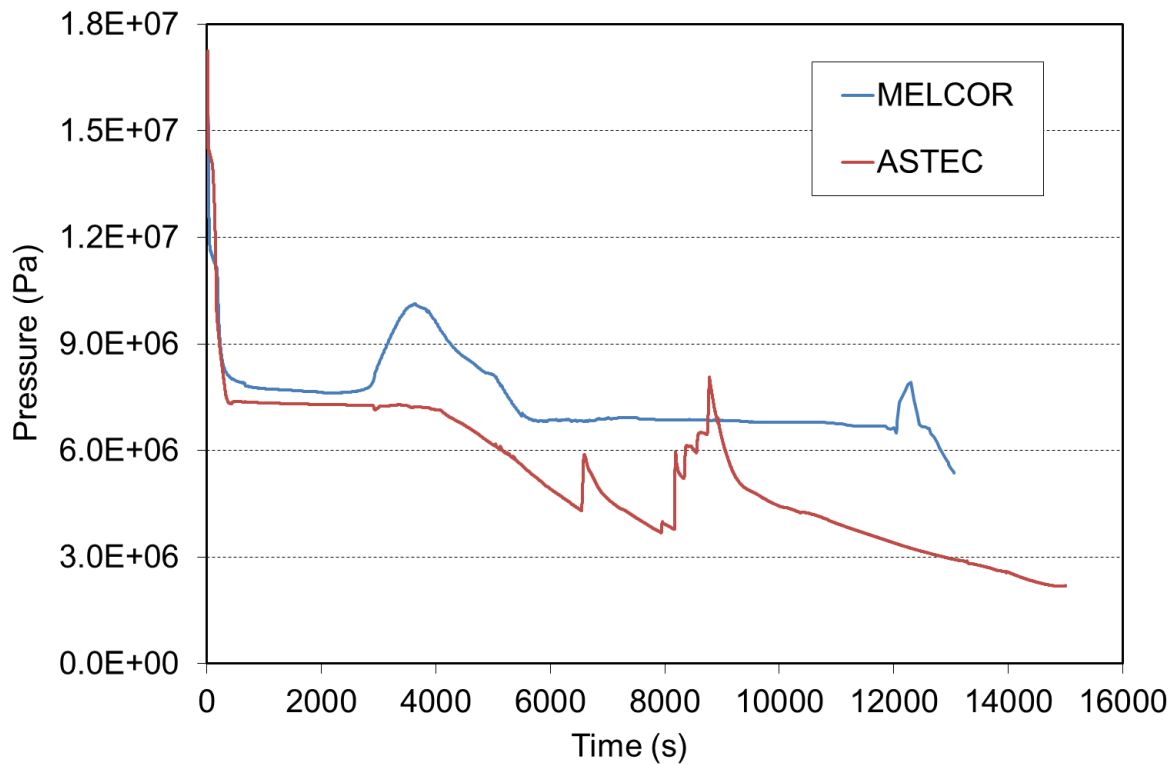


Figure 5.3: Pressurizer pressure

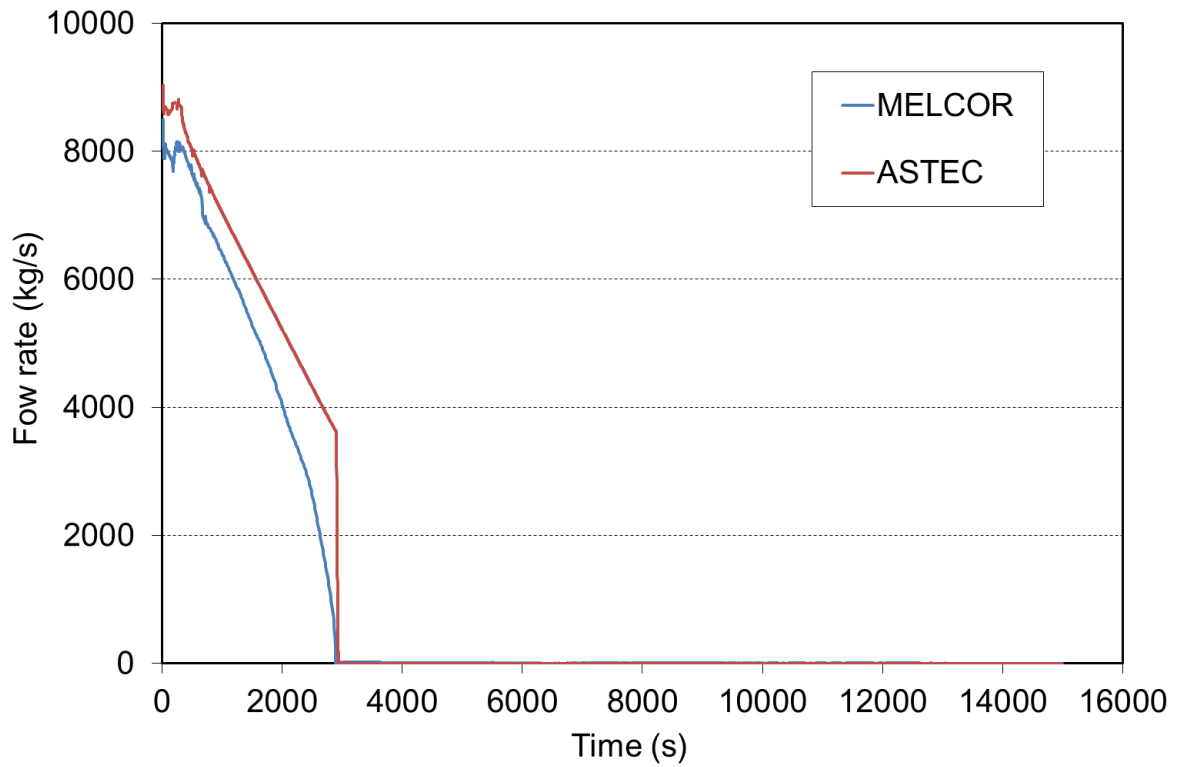


Figure 5.4: Loop A mass flow rate

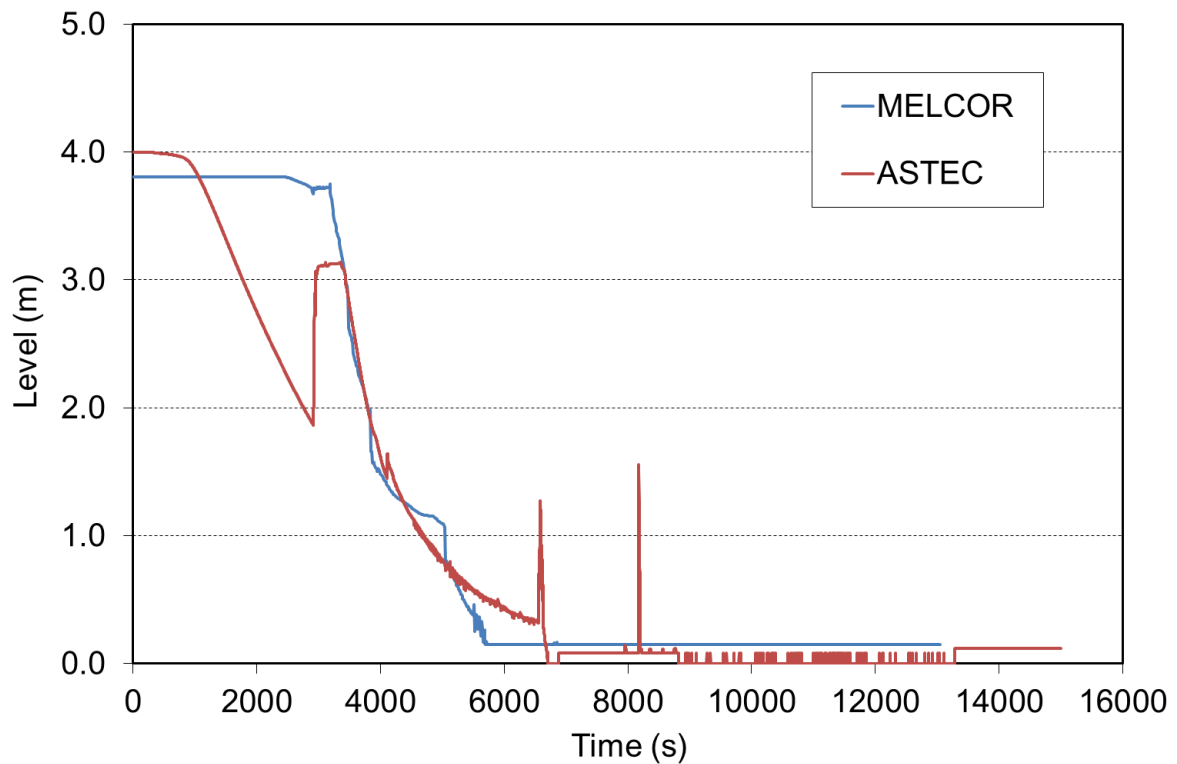


Figure 5.5: Core collapsed water level

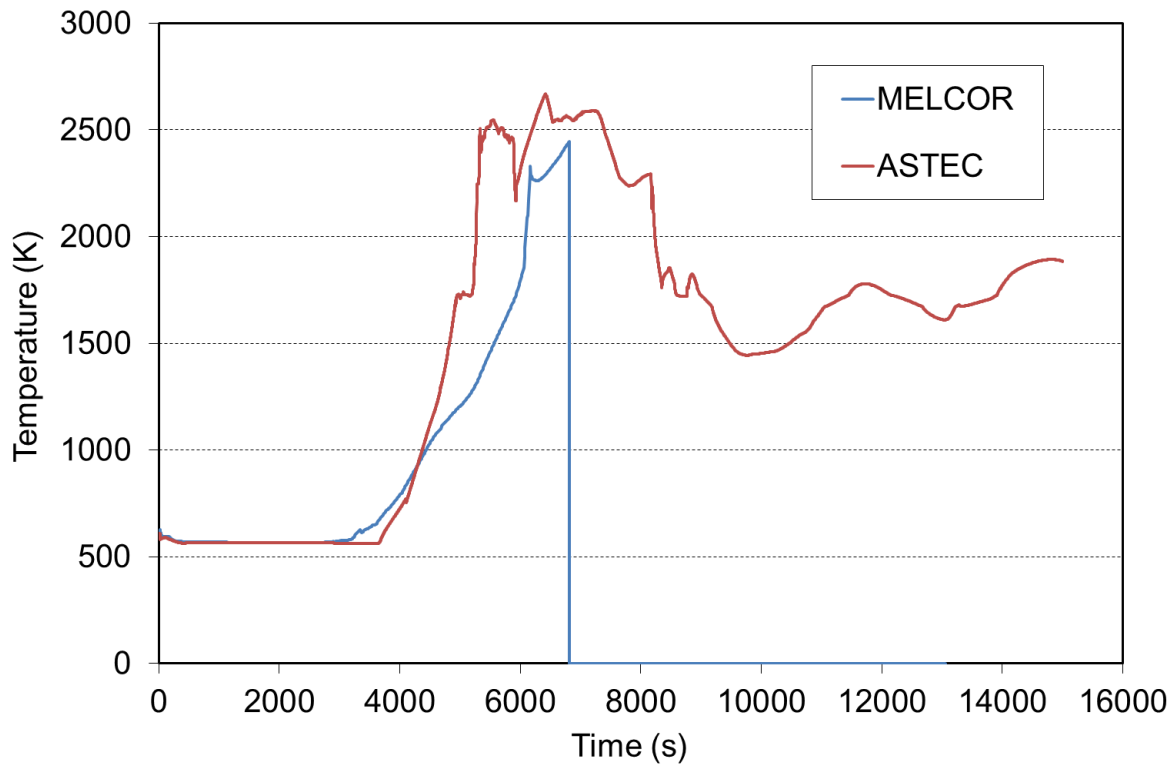


Figure 5.6: Fuel rod clad temperature at core top (central ring)

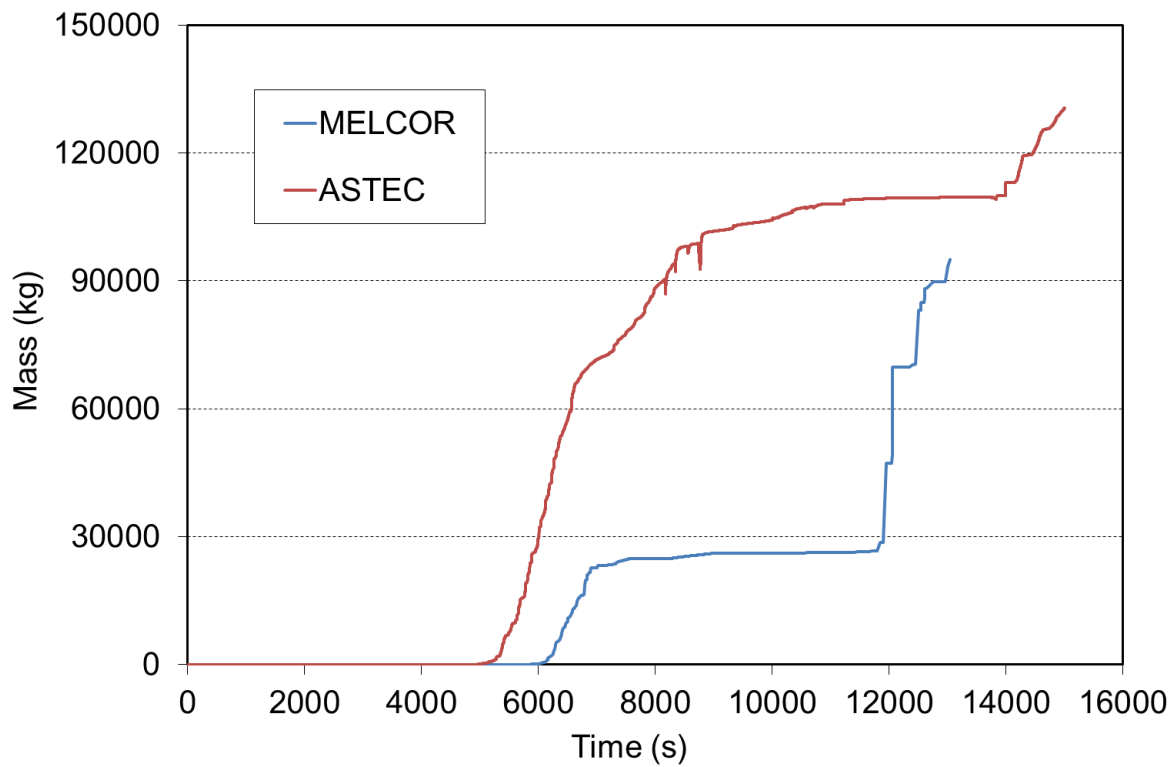


Figure 5.7: Total mass of degraded core materials (debris or molten, cumulated value)

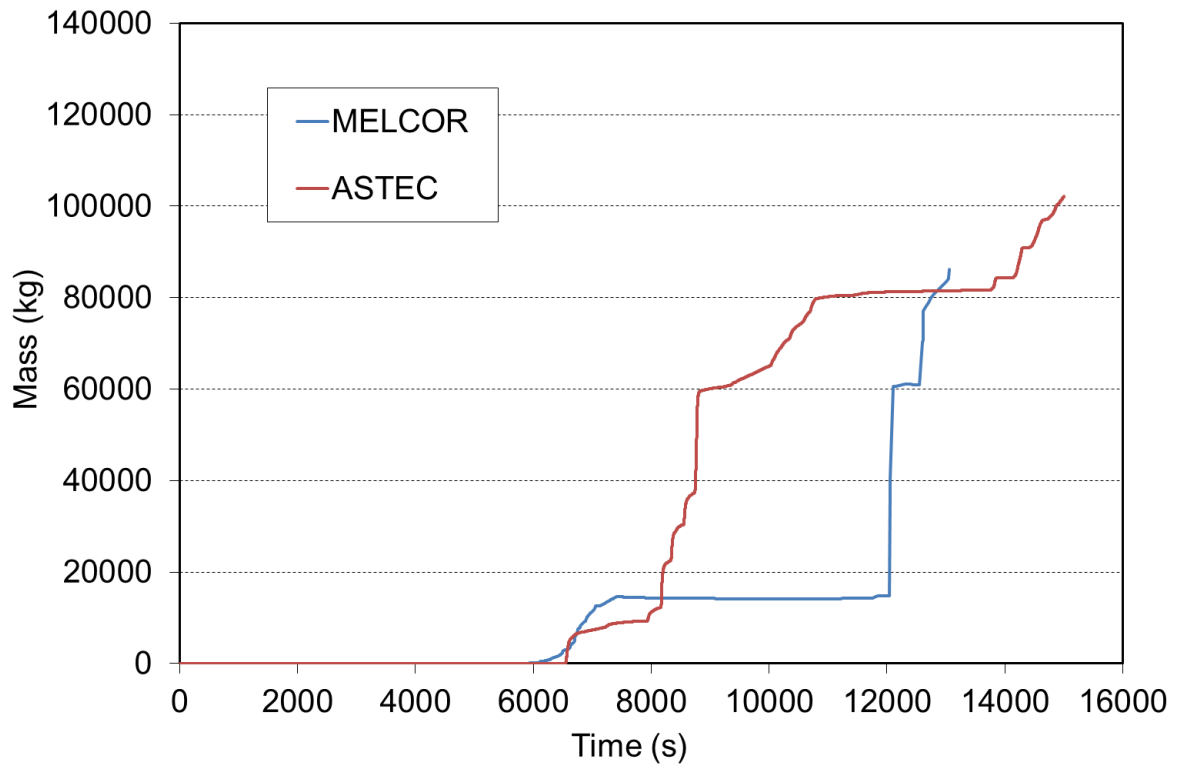


Figure 5.8: Total mass of materials in the lower plenum (cumulated value)

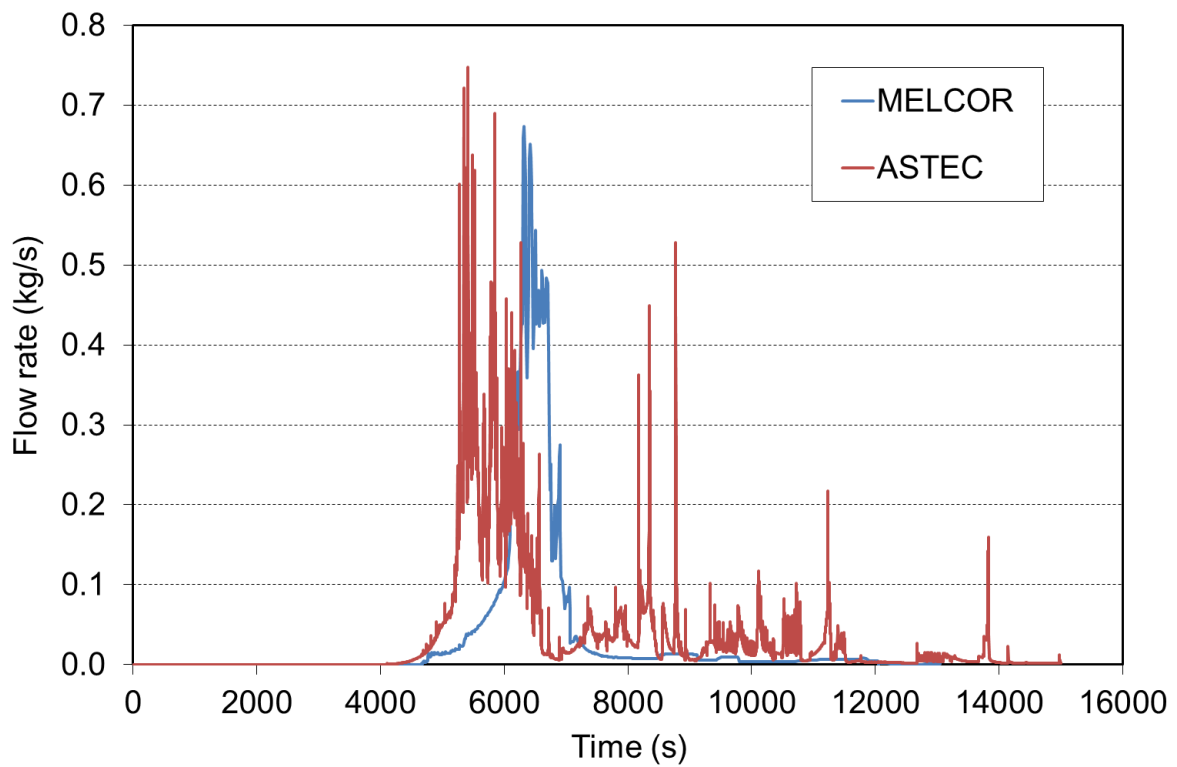


Figure 5.9: Instantaneous hydrogen production

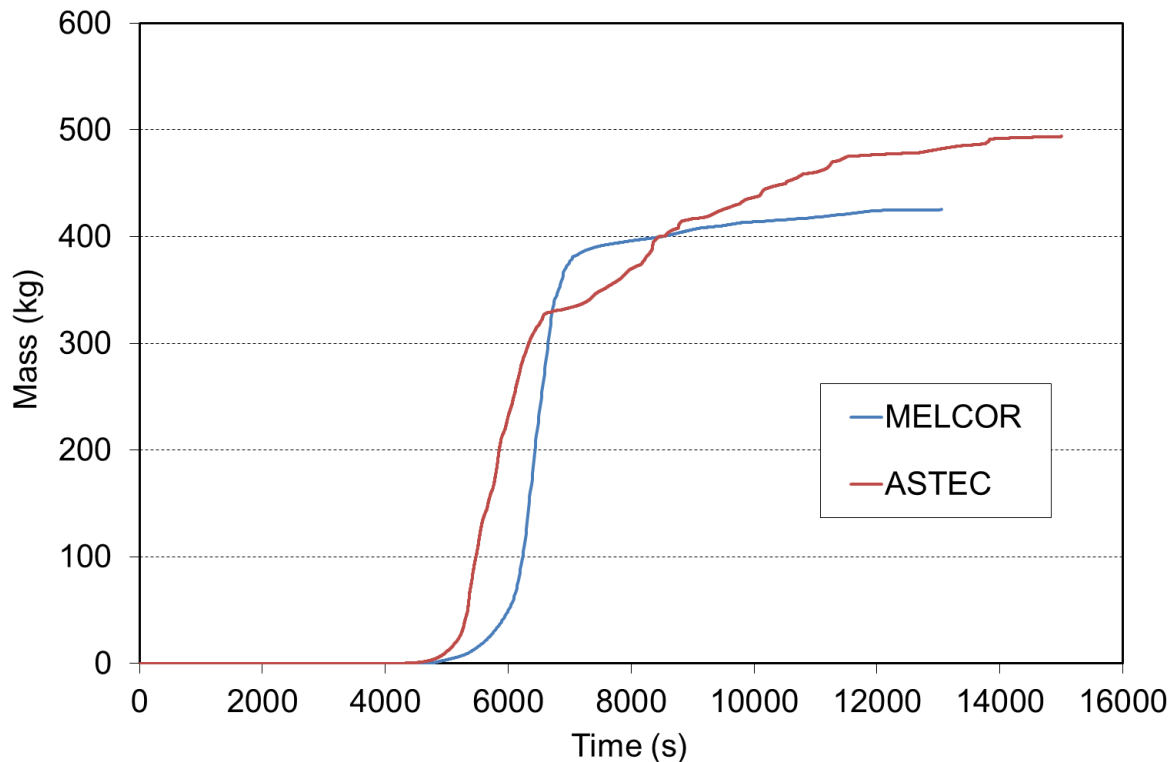


Figure 5.10: Cumulated hydrogen production

#### 5.4.2 Reflooding of a slightly degraded core

In this calculation the reflooding of the core is simulated by the activation of HPI injection at the rate of 30 kg/s in the cold legs at the beginning of the core degradation phase, when the total core degraded materials amount to about 5 tons. This means that the HPI injection is not started at the same instant with the two codes, but with a delay of about 1000 s in MELCOR calculation due to delayed core heatup and onset of degradation. The primary coolant mass inventory is then restored (Fig. 5.11) until a nearly constant value is reached above 100 tons, due to renewed loss through the break (Fig. 5.12). Both codes calculate enhanced primary pressure rise at the onset of core reflood (Fig. 5.13), mainly due to strong water vaporization in contact with the hot structures of the core.

The reflood of the core is shown in Fig. 5.14 through the evolution vs. time of the collapsed water level: both codes predict complete core recovery after HPI actuation. ASTEC predicts fast core quenching at core top (Fig. 5.15), while in MELCOR calculation, clad failure and relocation cannot be avoided at core top, due to delayed core quenching, since in this case the HPI actuation starts when the water level has already dropped below the core bottom (see Fig. 5.14). The delayed core quenching in MELCOR leads also to enhanced hydrogen production during the reflood phase (Fig. 5.16). In the ASTEC calculation the core degradation process is stopped early during the reflood phase (Fig. 5.17) and no molten core material is relocated in the lower head (Fig. 5.18). Conversely, in the MELCOR calculation, the core degradation continues and a large fraction of core materials is relocated in the lower head. While the absence of vessel failure in ASTEC calculation is obvious, vessel failure is

not predicted also in this MELCOR reflow calculation due to successful quenching of debris in the lower head flooded by water.

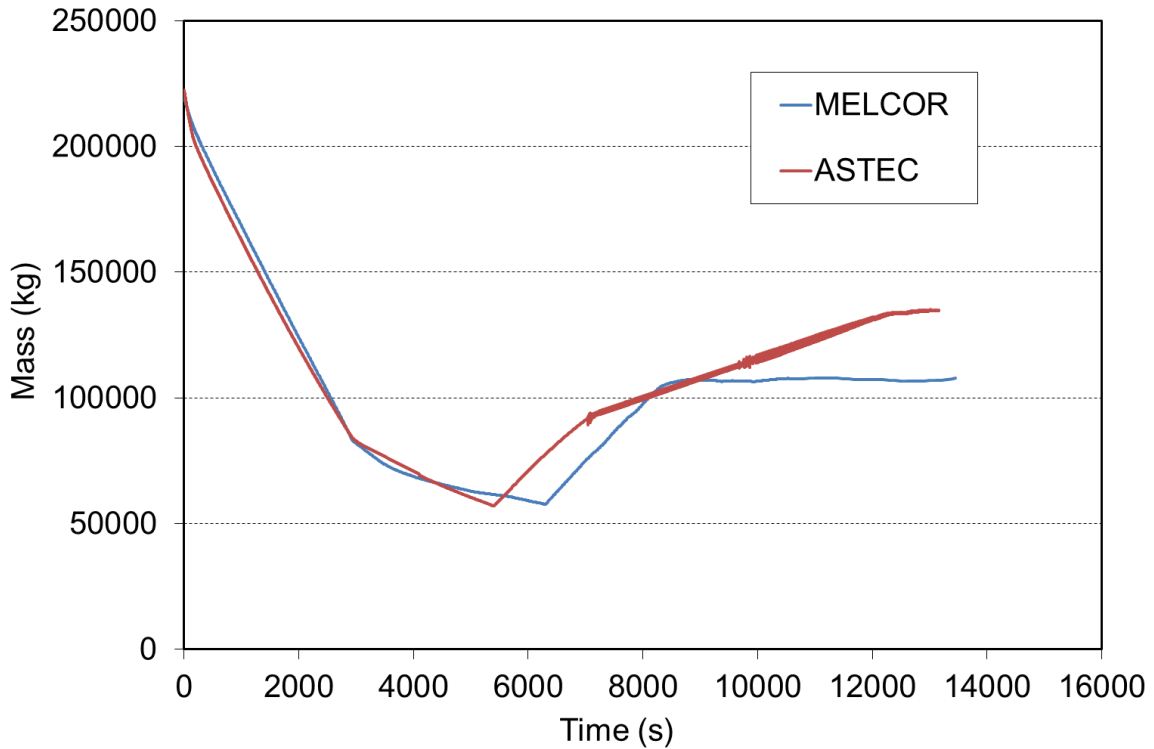


Figure 5.11: Total primary mass (liquid + steam)

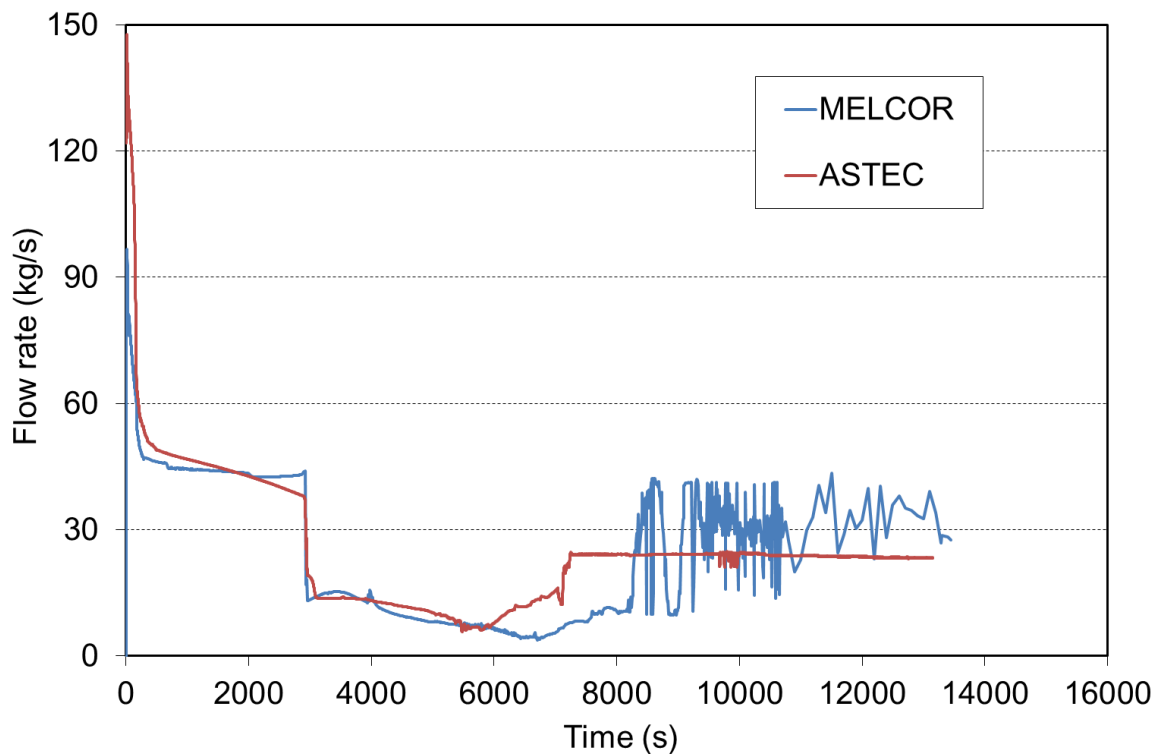


Figure 5.12: Break mass flow rate

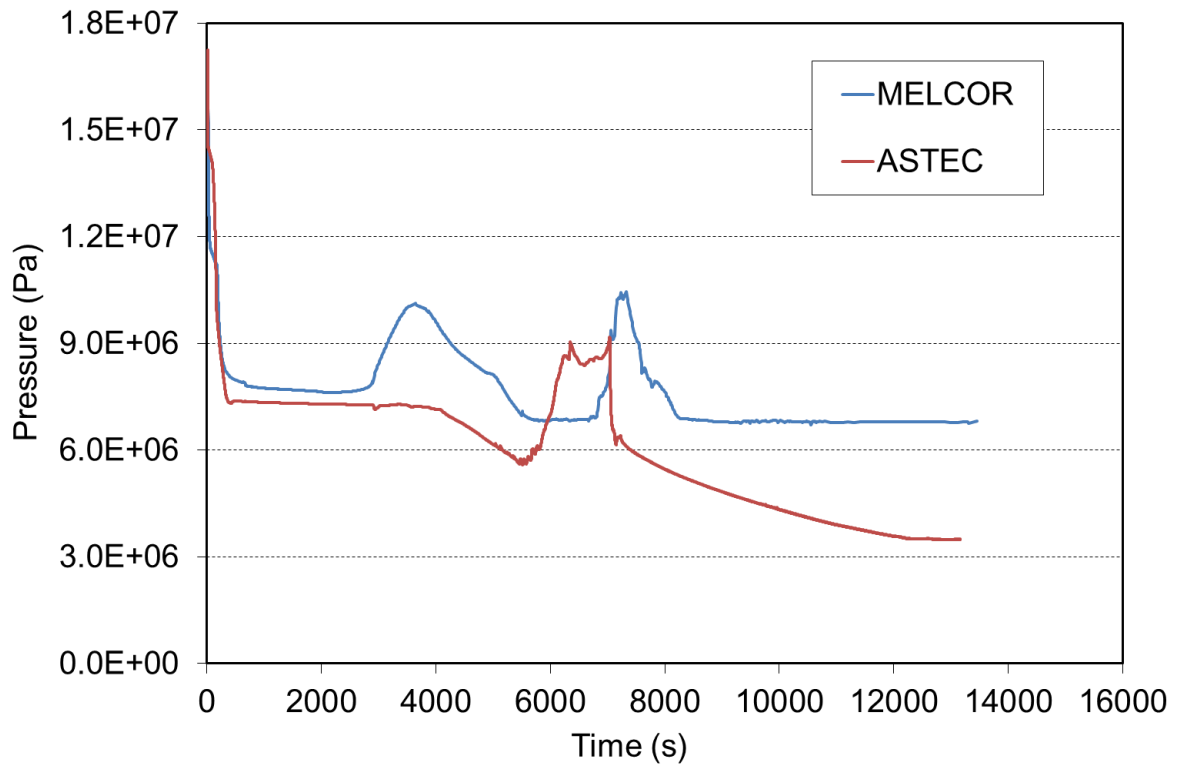


Figure 5.13: Pressurizer pressure

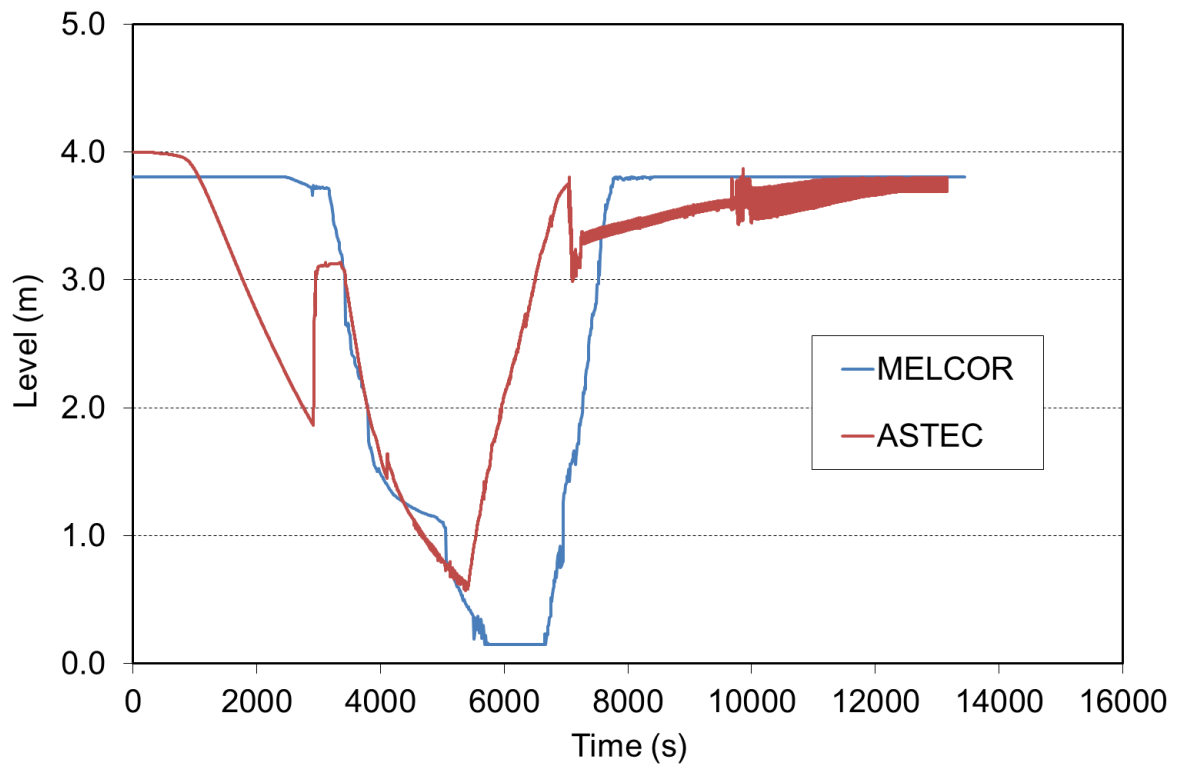


Figure 5.14: Core collapsed water level

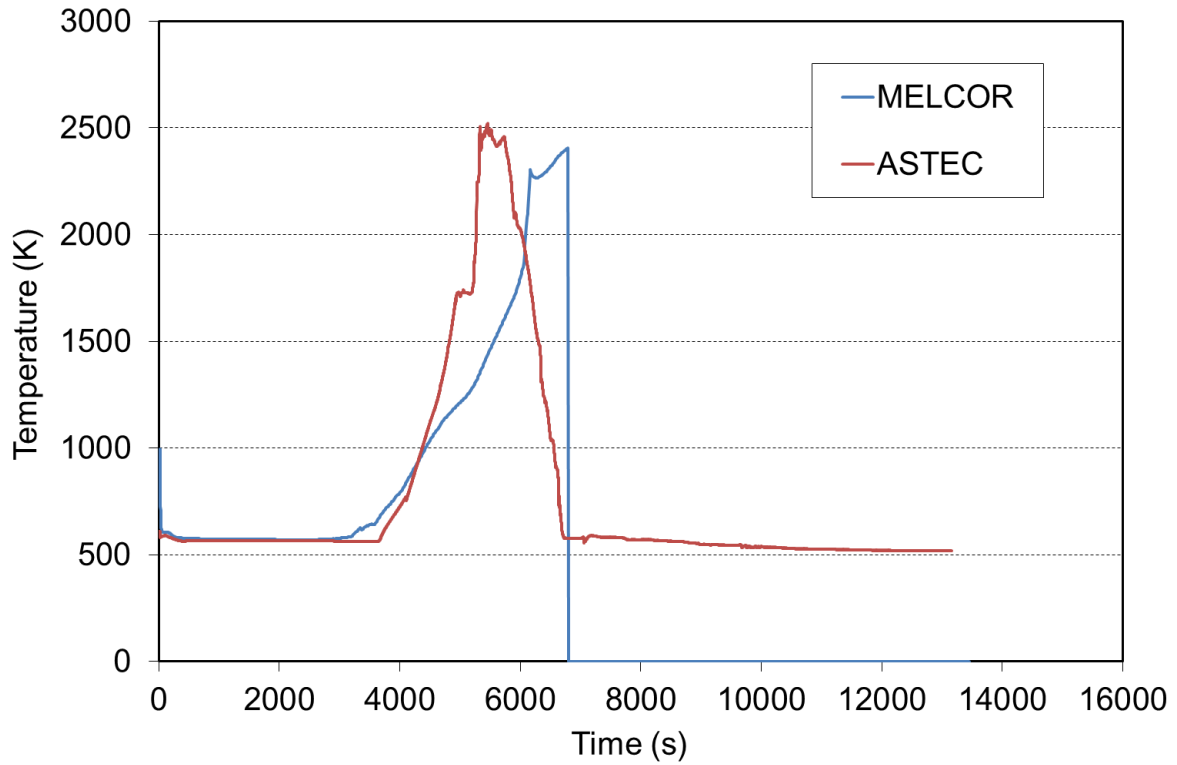


Figure 5.15: Fuel rod clad temperature at core top (central ring)

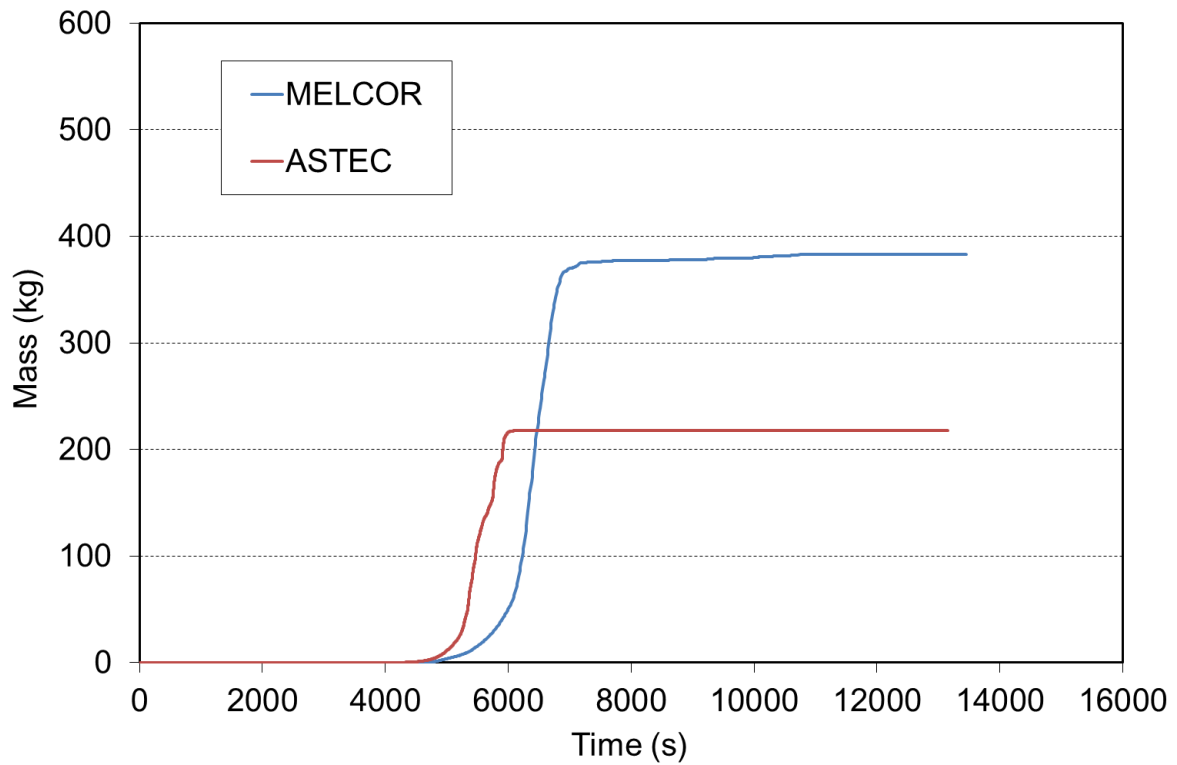


Figure 5.16: Cumulated hydrogen production



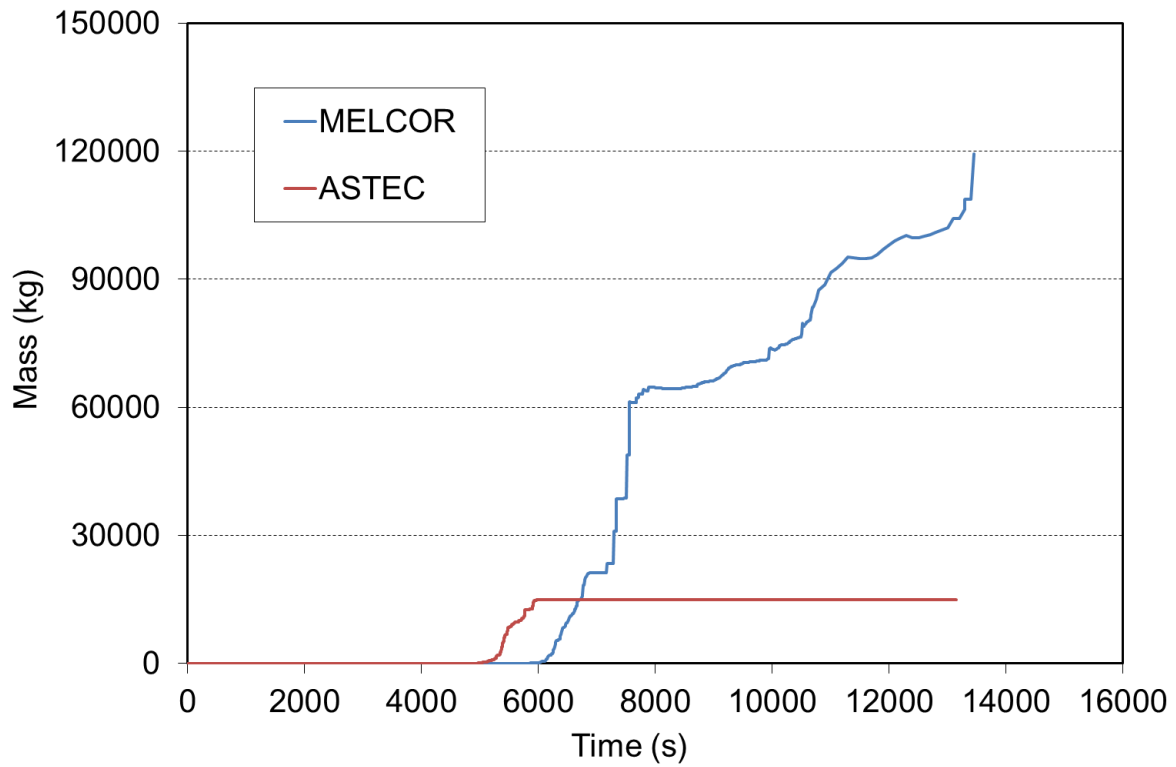


Figure 5.17: Total mass of degraded core materials (debris or molten, cumulated value)

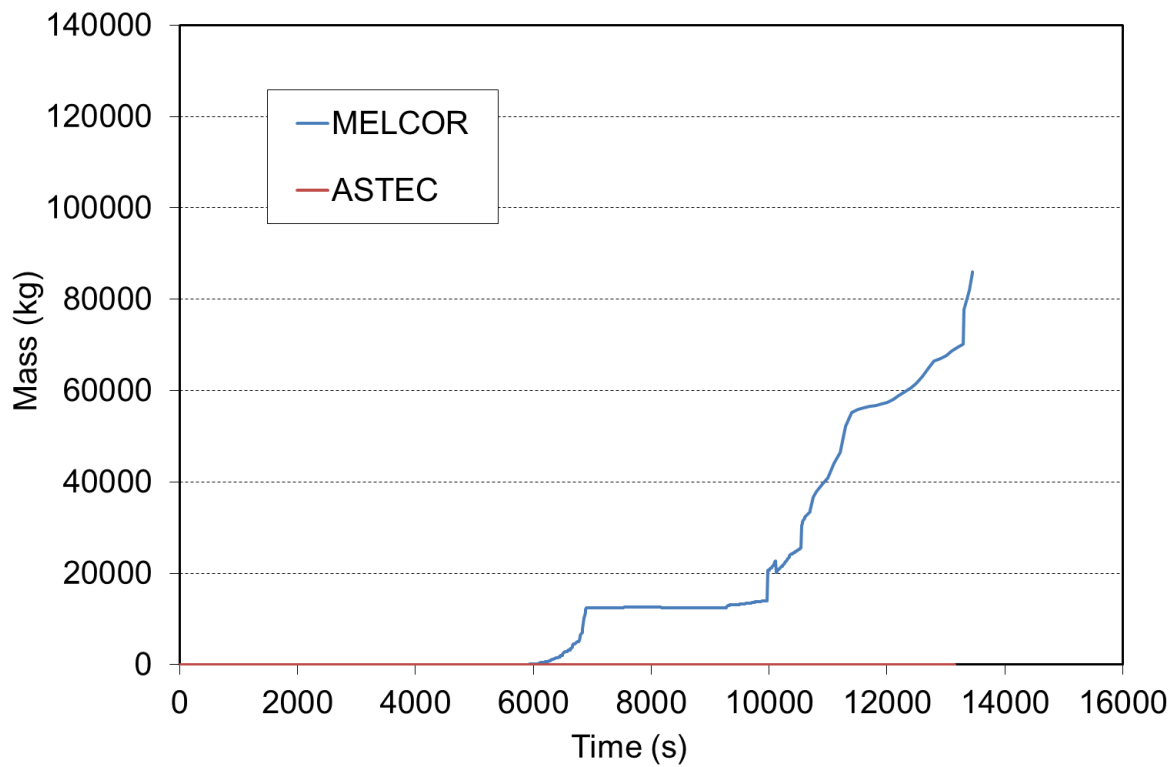


Figure 5.18: Total mass of materials in the lower plenum (cumulated value)

### 5.4.3 Reflooding of a highly degraded core

Differently from the previous core reflooding scenario, the HPI actuation is started with a delay of 1000 s, that is when the degradation amounts to several tens of tons of core materials. The results of calculations are compared from Fig. 5.19 to Fig. 5.26 like for the previous scenario.

Except for the delay in the start of core reflow, the MELCOR results are similar to the ones of the previous scenario. Also in this case the core degradation and corium relocation cannot be stopped, but the successful quenching of the corium in the lower head can prevent the vessel from failure in the late phase. In the ASTEC calculation, the hydrogen generation and core degradation are stopped at higher values than in the previous scenario during the reflow phase, and only a relatively small amount of corium is relocated and quenched in the lower head, without vessel failure.

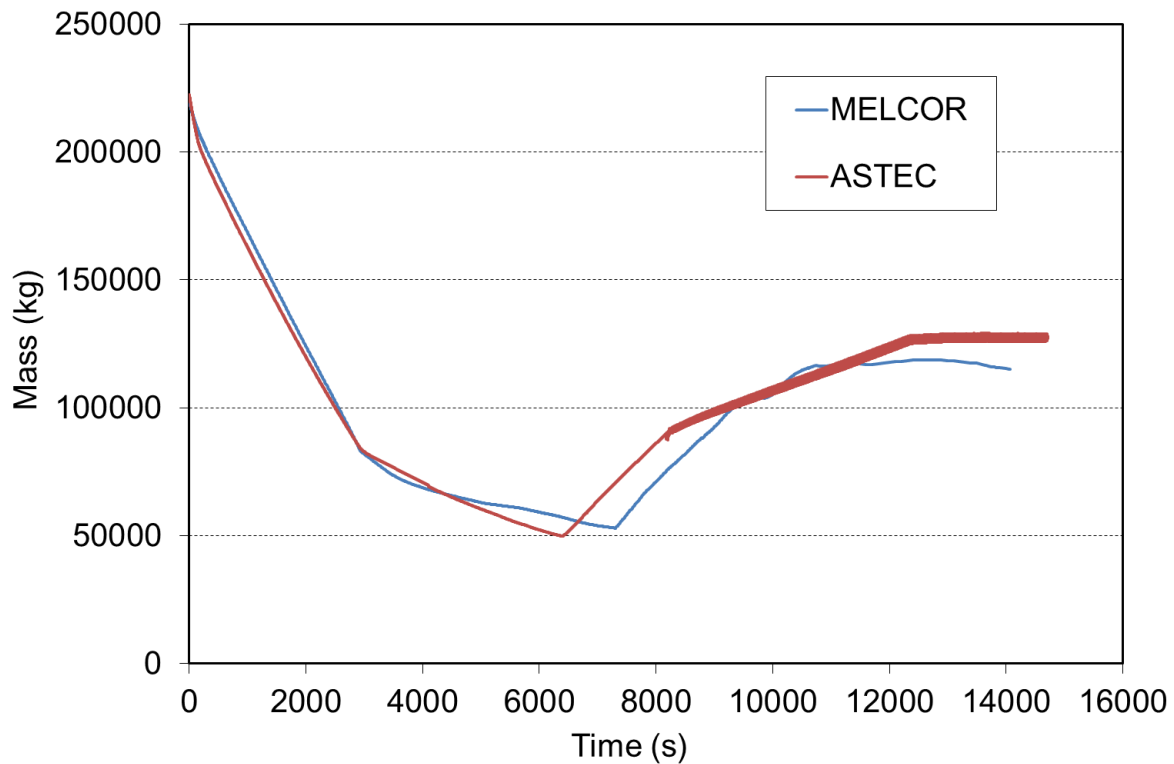


Figure 5.19: Total primary mass (liquid + steam)

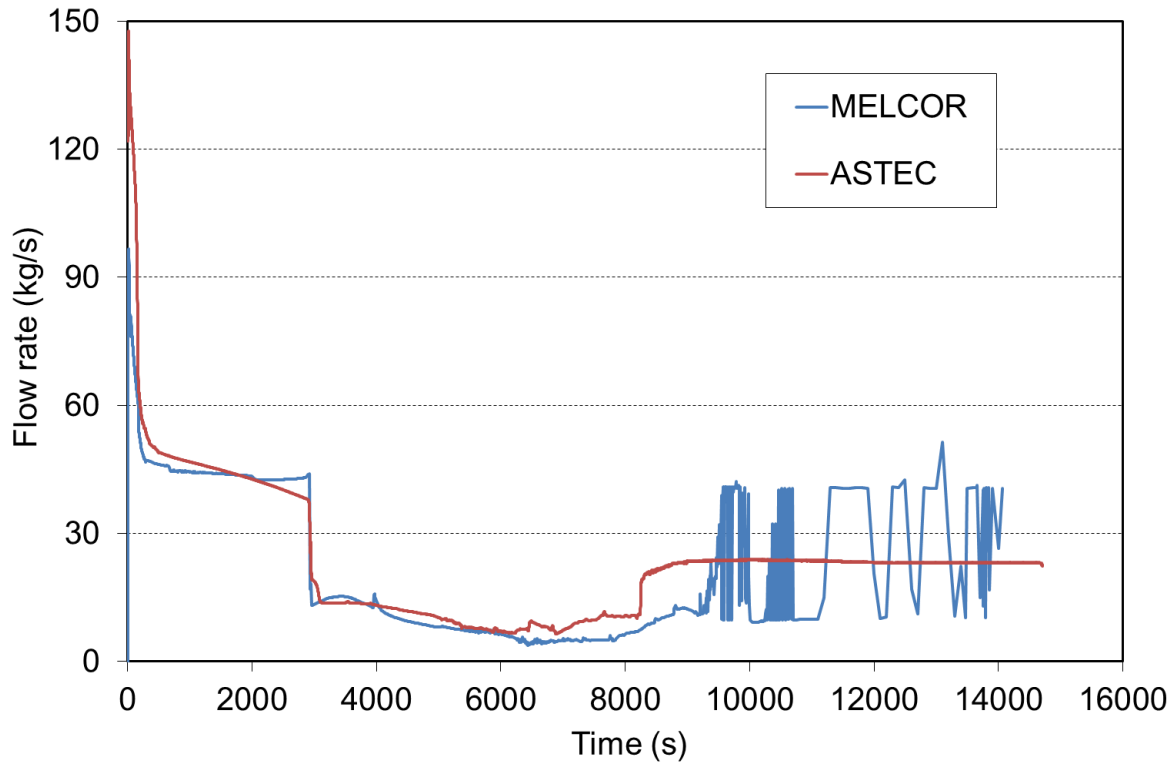


Figure 5.20: Break mass flow rate

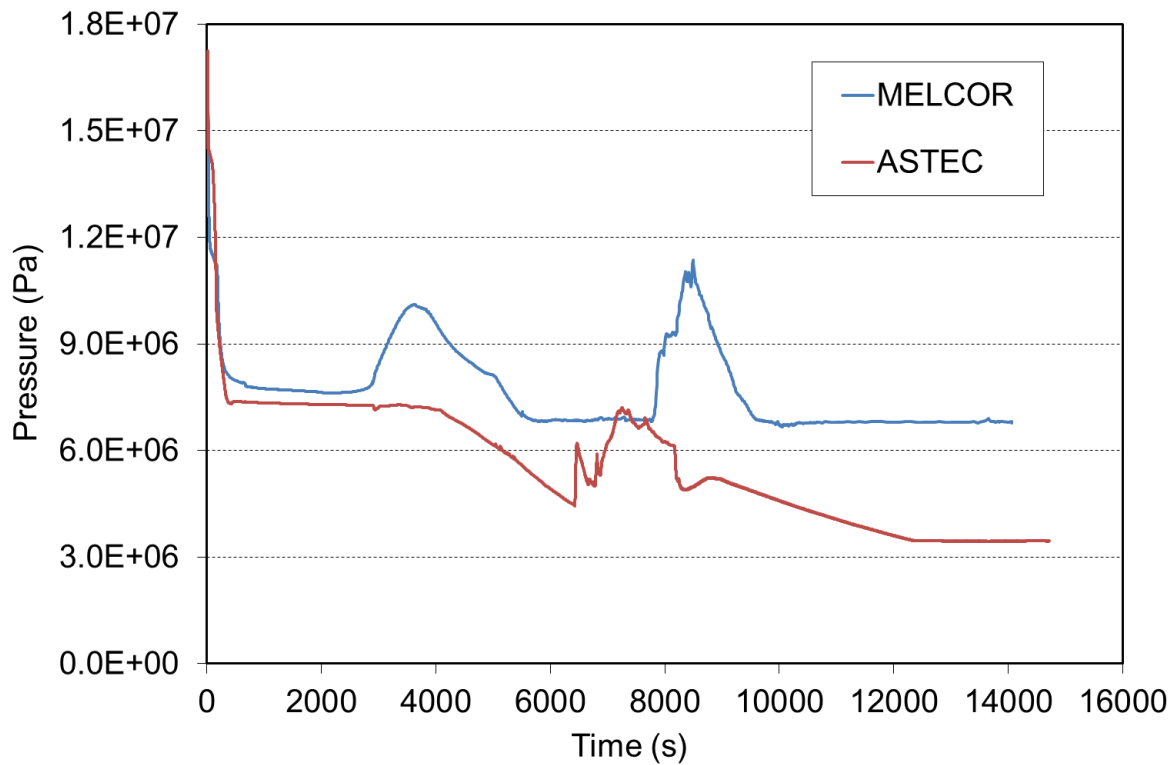


Figure 5.21: Pressurizer pressure

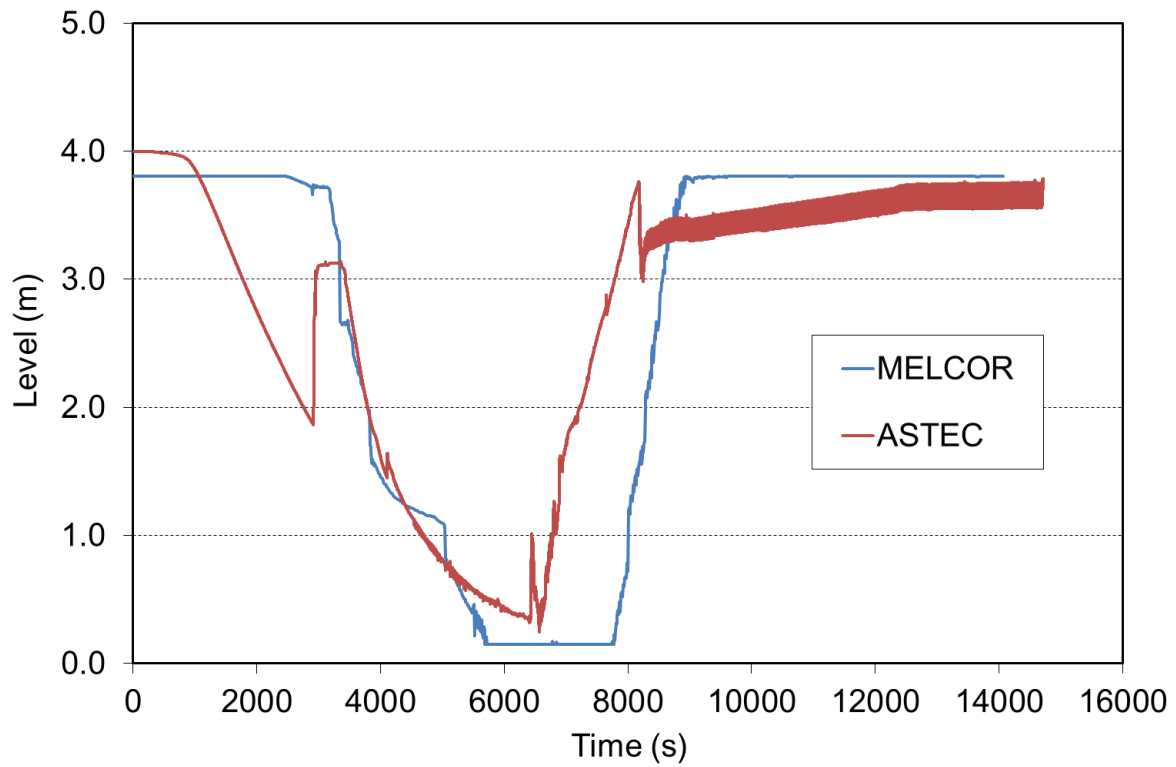


Figure 5.22: Core collapsed water level

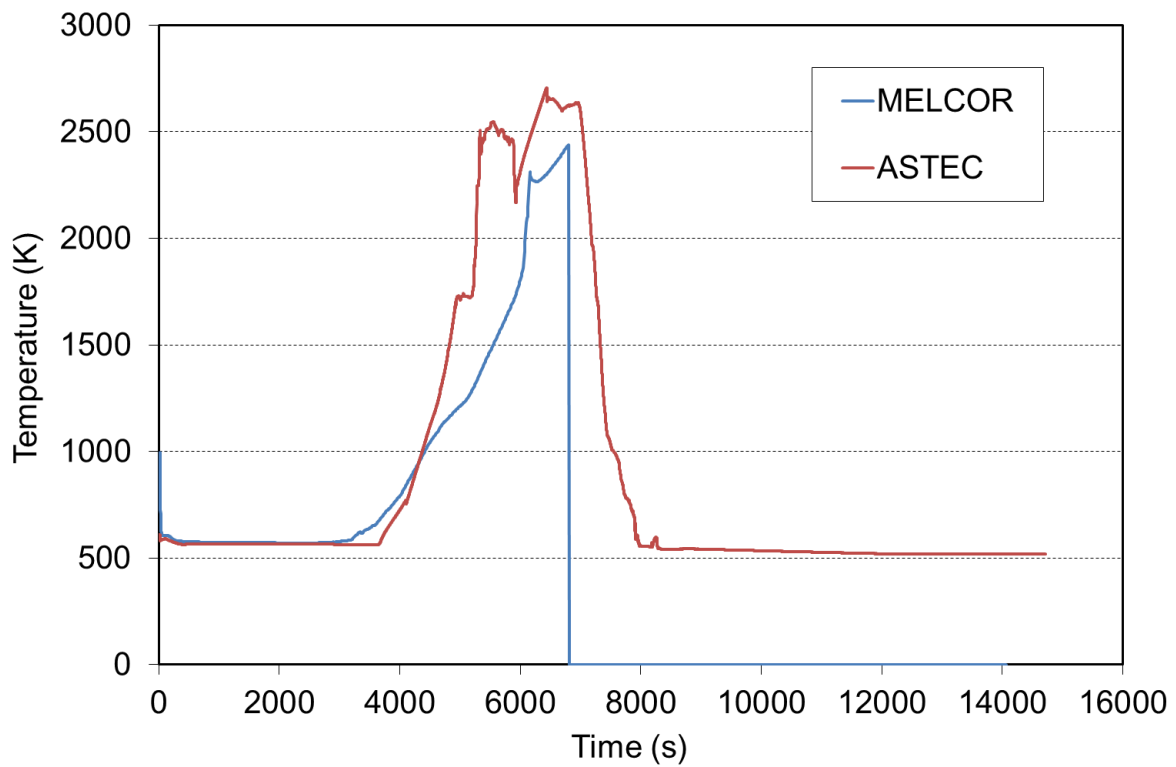


Figure 5.23: Fuel rod clad temperature at core top (central ring)

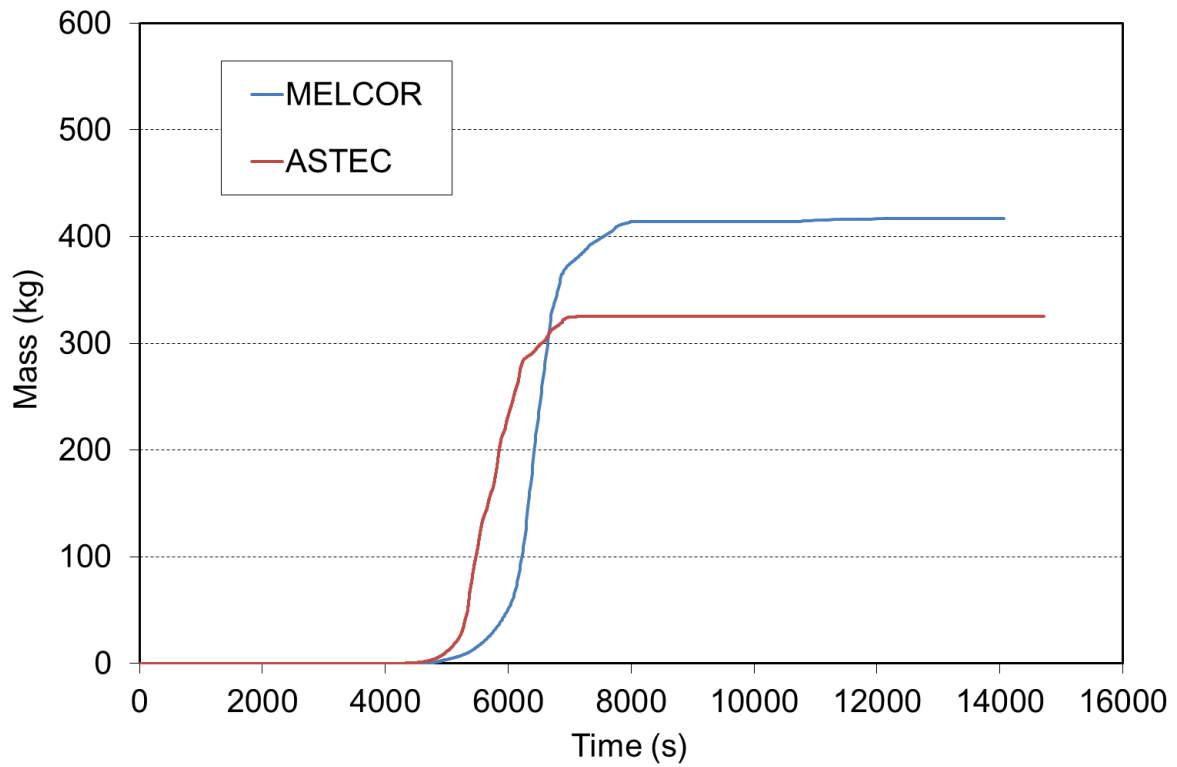


Figure 5.24: Cumulated hydrogen production

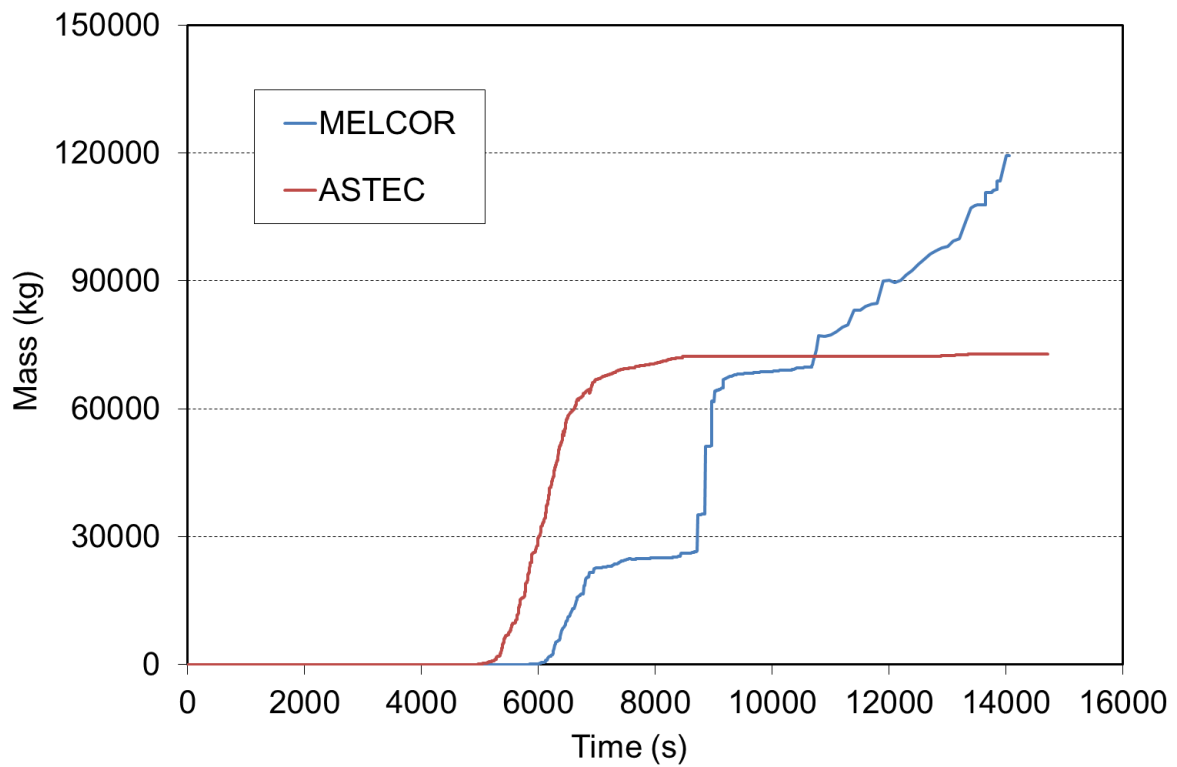


Figure 5.25: Total mass of degraded core materials (debris or molten, cumulated value)

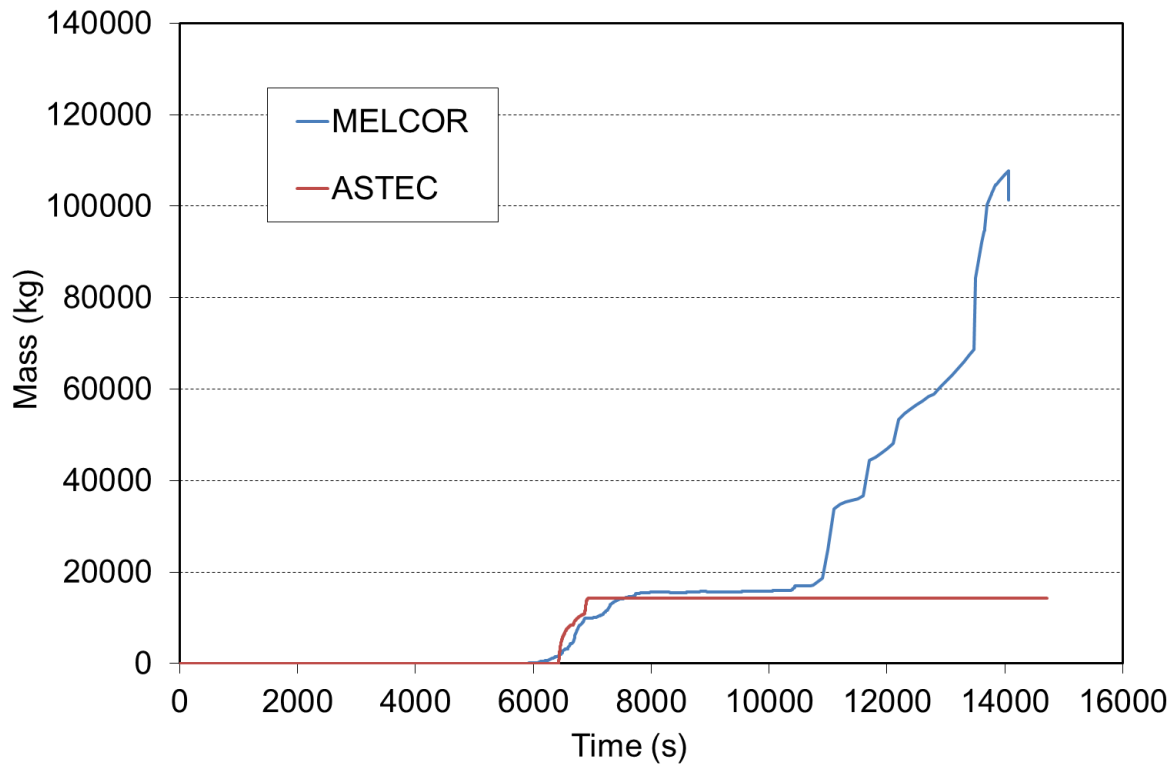



Figure 5.26: Total mass of materials in the lower plenum (cumulated value)

## References

- 5.1. G. Bandini, M. Di Giuli, M. Sumini, A. Manfredini, W. Ambrosini – Lessons Learned from the Result Comparison of a Reference Severe Accident Sequence on a TMI2-like Reactor of 900 MWe Power with the Integral Codes ASTEC and MELCOR – ENEA - ADPFISS - LP1 – 032 – Settembre 2014.

 <b>Ricerca Sistema Elettrico</b>	<b>Sigla di identificazione</b>	<b>Rev.</b>	<b>Distrib.</b>	<b>Pag.</b>	<b>di</b>
	ADPFISS–LP1-054	0	L	105	106


## 6. Conclusions and recommendations

The integral codes ASTEC and MELCOR have been applied, by the University of Bologna and the University of Pisa respectively, for the calculation of a reference severe accident sequence (SBLOCA) and some core reflooding scenarios on the TMI-2 plant (PWR of 900 MWe). Similar core degradation parameters/criteria have been used with the two codes to try to reduce the differences observed in previous analyses (PAR2013). Furthermore, sensitivity studies on important and uncertain core degradation parameters/criteria have been performed to investigate their influence on code results.

The sensitivity analysis on core degradation parameters and modelling options performed with the ASTEC code has highlighted their influence on core melt progression and the hydrogen source. Furthermore, another important source of uncertainty in the results is the use of the code under different computer operating systems (Windows, Linux). These differences are quite small for the early phase degradation, but the deviations in the results can significantly enlarge once entering the late degradation phase with enhanced core melting and relocation in the lower plenum.

The use of similar core degradation parameters and modelling in the two codes does not seem to reduce significantly the discrepancies observed in code results regarding the late phase. Phenomena, such as partial or total blockages, which might occur during core melting and relocation, could lead to different core configuration, which on its turn may alter the subsequent degraded core structure thermal behavior and melt progression. The prediction of the above mentioned flow blockages remains a difficult challenge for severe accident codes and small differences on code's input can result in very large discrepancies on blockages formation and location. Sensitivity and uncertainty analysis is then recommended in order to identify and quantify the range of uncertainty of code results.

Large uncertainties still exist in the analysis of core reflooding scenarios. In spite of the large differences observed in code results, both codes have confirmed the ability of emergency core cooling systems to stop the core degradation and prevent vessel failure in the late phase of a severe accident. However, code modelling for the reflood phase is still incomplete and not enough validated, and thus the consequences of core reflood, such as observed in several integral tests and the real TMI-2 accident, could be significantly underestimated. Therefore, further development and validation is recommended regarding code models to more precisely investigate the core reflood phase.

 <b>Ricerca Sistema Elettrico</b>	<b>Sigla di identificazione</b>	<b>Rev.</b>	<b>Distrib.</b>	<b>Pag.</b>	<b>di</b>
	ADPFISS-LP1-054	0	L	106	106

### CIRTEN Authors CV

**Dr. Mirco Di Giuli:** degree in Chemical Engineering in 2007 at University of Bologna, Master in Design and Management in Advanced Nuclear Systems at University of Bologna in 2009, SIET Company Consultant for the core design of the ALFRED LCR prototype (in the framework of the European Research Program LEADER), PhD in Nuclear and Energy Engineering and Environmental Control at University of Bologna with, a Thesis on the study of severe accidents in SMR

**Prof. Marco Sumini:** Nuclear Engineer, Associate Professor in Nuclear Reactor Physics at University of Bologna since 1987; research activities on Reactor Physics, Core Design and on Neutral and Charged Particle Transport. Experimental activities on Pulsed Power Plasma Devices.

**Dr. Antonio Manfredini:** degree in Nuclear Engineering in 1989 at University of Pisa, PhD in Nuclear Engineering – Safety of Nuclear Power Plants in 1992. Research activities on BDBA and Severe Accidents phenomena on nuclear power plants.

**Prof. Walter Ambrosini:** degree in Nuclear Engineering in 1985 at University of Pisa, PhD in Nuclear Engineering – Safety of Nuclear Power Plants in 1989. Research activities on Nuclear Safety, Researcher at University of Pisa since 1992, Associate Professor in Nuclear Plants since 2000.